UNIVERSITY OF OKLAHOMA

GRADUATE COLLEGE

DEVELOPMENT OF NANOSTRUCTURED ENZYMATIC BIOFUEL CELLS

A DISSERTATION

SUBMITTED TO THE GRADUATE FACULTY

in partial fulfillment of the requirements for the

Degree of

DOCTOR OF PHILOSOPHY

By

JIE CHEN
Norman, Oklahoma
2014

Downloaded from SHAREOK. Persistent Handle URL: https://hdl.handle.net/11244/13858

DEVELOPMENT OF NANOSTRUCTURED ENZYMATIC BIOFUEL CELLS

A DISSERTATION APPROVED FOR THE
DEPARTMENT OF CHEMICAL, BIOLOGICAL AND MATERIALS ENGINEERING

BY

_____
Dr. Steven Crossley, Chair

_____
Dr. David Schmidtke

_____
Dr. Daniel Glatzhofer

_____
Dr. Edgar O'Rear III

_____
Dr. Roger Harrison

© Copyright by JIE CHEN 2014
All Rights Reserved.

ACKNOWLEDGEMENTS

I would like to take this opportunity to thank everyone who helped, inspired me in my studies and research. I would like to thank Dr. Schmidtke for giving me the opportunity to work on this project, for his guidance and support throughout my research in his lab. He provided me with many thoughtful suggestions, helped me overcome challenges, and gave me opportunities to think and learn from research problems. He has mentored me not only on specific projects but also on being a better researcher and thinker. I would like to thank Dr. Crossley for being my chair in my last semester. He guided me with his broad knowledge and insightful suggestions, which helped me a lot in overcoming obstacles in my research. I would like to give special thanks to Dr. Glatzhofer for his valuable advice during the numerous discussions, which not only helped me improve my research project, but also increased my knowledge and gave me new perspectives. I would also like to thank Dr. O'Rear, Dr. Harrison and Dr. Starly for taking time on my committee and advice both in the classroom and in this dissertation.

I would like to thank all of my colleagues in the Schmidtke lab: Tu O. Tran, Emily Lammert, Christopher Lewis, Kevin Lam and Etienne Bendjebbar, for their help over the years. I would also like to thank everyone I have worked with in the Glatzhofer, Crossley, and Johnson labs: Dr. David Hickey, Nick Godman, Dan Bamper, Nicholas Briggs, Brandon Bonk, Michael T. Ray, Daniel B. Brunski, and Joel C. Keay for their collaborative work.

Last but not the least, I would like to thank my husband, Ming Xie, my daughter, Evelyn Xie, and my son, Evans Xie, for their support and love all along these years. They brighten my life in the difficult and challenging times, encourage

and give me confidence to focus on important things in my life. Also, I would like to give special thanks to my parents, my parents in law, my grandparents in law, my sister and her husband. All of these family members provided me with tremendous support and encouragement.

TABLE OF CONTENTS

Acknowledgements....iv

List of tables....xi

List of figures....xii

Abstract....xvii

Chapter 1:Introduction and background information....1

Introduction....1

Purpose of the work....4

Background....6

Enzymatic biofuel cell....6

Redox enzyme type....9

Key performance characteristics....13

Project background....25

Overview....27

Chapter 2:Effect of surfactant type, redox polymer type and nanotube loading on single-walled carbon nanotube modified electrodes....30

Introduction....30

Experimental section....32

Chemicals and solutions....32

Uv-vis spectrophotometry....33

Enzyme sensor construction....34

Electrochemical measurements....35

Characterization of SWNTs films 35
Calculation and statistics 36
Results and diccusion 36
SWNTs dispersion properties 36
Electrochemical response is surfactant and redox polymer dependent 38
Enzymatic response is surfactant dependent 42
SEM imaging of SWNTs films 45
Effect of SWNTs films on diffusional mediators 46
Effect of nanotube loading on the performance of electrodes 48
Conclusions 51
Chapter 3:Development of fructose dehydrogenase-ferrocene redox polymer films for biofuel cell anodes 54
Introduction 54
Experimental section 56
Chemicals and solutions 56
Fructose dehydrogenase electrodes 56
Laccase electrodes 57
Electrochemical measurement 57
Eesults and discussion 58
Effect of enzyme solution pH on electrochemical and enzymatic response 58
Effect of Fc-C_6-lpei redox polymer solution with different pH 60
Effect of incorporating SWNTs film into FDH/ Fc-C_6-lpei electrodes 63

Effect of incorporating SWNTs on the performance of PVP-OS/laccase cathode electrodes 65

Fructose/O_2 biofuel cells 66

Conclusions 69

Chapter 4:Single wall carbon nanotube (7,6) film modified ferrocene-modified linear poly(ethylenimine) hydrogel film for biofuel cell 71

Introduction 71

Experimental section 72

Chemicals and solutions 72

Anodic enzyme electrodes 73

Cathodic enzyme electrodes 73

Electrochemical and spectroscopic measurement 74

Calculation and statistics 74

Results and discussion 75

Effect of different swnts on the performance of $FcMe_2$- C_3-LPEI /GOx electrodes 75

Effect of swnts (7,6) film loading on the performance of $FcMe_2$- C_3-LPEI /GOx electrodes 77

Effect of redox hydrogel loading on the performance of $FcMe_2$- C_3-LPEI /GOx electrodes 79

Swnts (7,6) film modified Cl-Fc-LPEI/laccase cathode electrode 82

Glucose/O_2 biofuel cell 84

Conclusions 88

Chapter 5:effect of SWNTs (7,6) incorporating method on the ferrocene-modified linear poly(ethylenimine) hydrogel film for biofuel cell 91

Introduction 91

Experimental section 92

Chemicals and solutions 92

Enzyme electrode construction 93

Anodic enzyme electrodes: 93

Control anode electrodes 93

Type A anode electrodes 93

Type B anode electrodes 94

Cathodic enzyme electrodes: 95

Electrochemical and spectroscopic measurement 95

Calculation and statistics 96

Results and discussion 96

Effect of swnts incorporating methods on the performance of $FcMe_2$- C_3-LPEI /GOx electrodes 96

Effect of incorporating SWNTs (7,6) onto Cl-Fc-LPEI/laccase cathode 101

Glucose /O_2 biofuel cell 102

Fructose/O_2 biofuel cell 107

Conclusions 109

Chapter 6:Vertically-aligned MWCNTs forest based ferrocene redox polymer for glucose sensing.....112

Introduction.....112

Experimental section.....113

Chemicals and solutions.....113

Enzyme electrode construction.....114

Electrochemical measurement.....115

Characterization of MWCNTs forest.....116

Calculation and statistics.....116

Results and discussion.....116

Conclusions.....124

Chapter 7:Conclusions and recommendations for future work.....125

Conclusions.....125

Recommendations for future work.....125

Biblography.....131

LIST OF TABLES

Table 1.1 Implantable medical devices applications and power consumption…… …….. .8

Table 1.2 The redox potential of redox enzyme applied in biofuel cell and the corresponding chemical reactions……21

Table 2.1 Resonance Ratio for the Various Surfactant Suspensions…….…….43

Table 2.2 Effect of SWNT Films on Peak-to-Peak Separation Potential ΔEp (mV) ……..46

Table 3.1 Comparison of the Enzymatic Response of Various Fructose Sensors Based on Redox Polymer-Fructose Dehydrogenase Films ……..…….....59

Table 4.1 Summary of biofuel cells without and with SWNTs(7,6) film at 25 ^{o}C and 37 ^{o}C…….93

Table 5.1 Summary of biofuel cells without and with SWNTs at 25 ^{o}C and 37 ^{o}C……...111

LIST OF FIGURES

Figure 1.1 Approximate power output of electrochemical devices including biofuel cell, conventional fuel cell, battery etc…….....9

Figure 1.2 Schematic of an enzymatic biofuel cell without and with mediator. Redox mediator I shuttle the electron from enzyme to the electrode surface at anode, and redox mediator II mediated the electron transfer at the cathode. ……14

Figure 1.3 Schematic of a glucose/O_2 EBFCs that use GOx and laccase as enzymatic catalysts on the anode and cathode……...15

Figure 1.4 Schematic of three different groups of redox enzyme described by Heller et al. ……....16

Figure 1.5 Electron-transfer steps in the elctrooxidation of glucose on a wired glucose oxidase electrodes suggested by Adam Heller et al…….18

Figure 1.6 Schematic of the six enzyme oxidation pathway of glucose proposed by Shuai Xu et al……...21

Figure 1.7 Schematic of construction of SWNTs incorporated redox hydrogel sensor…….....30

Figure 1.8 Effect of SWNTs incorporation method on electrochemical and enzymatic response of electrodes. ……....31

Figure 1.9 Electron transfer mechanism for enzymatic electrodes without (left) and with SWNTs (right). ……32

Figure 2.1 Chemical structure of the surfactants used to disperse single-walled carbon nanotubes in this study…….38

Figure 2.2 Schematic of the construction of redox polymer/enzyme biosensors incorporated with SWNTs film……39

Figure 2.3 Optical images of SWNTs in different aqueous solutions on day 0 and day 7……41

Figure 2.4 UV-VIS spectra of SWNTs solutions dispersed by different surfactants (TX, TW, SC and NaDDBS). ……..43

Figure 2.5 Effect of redox polymer and surfactant type on the electrochemical behavior of SWNT composite films. ……...44

Figure 2.6 Glucose calibration curves for three different polymers (A) PVP-Os, (B) Fc-C_6-LPEI, (C) Fc-C_3-LPEI based electrodes incorporated with different SWNTs film. ……48

Figure 2.7 Differential interference contrast (DIC) and SEM images of electrodes coated with SWNT solutions with: no surfactant, non-ionic Triton 100 and Tween 20 surfactants, and ionic sodium cholate and NaDDBS surfactants. ……..50

Figure 2.8 Electrochemical response of diffusional mediators on different SWNT films. ……51

Figure 2.9 (A) Effect of the SWNTs film loading on electrochemical performance of PVP-OS/GOx based biosensors……...53

Figure.2.10 Glucose response for PVP-OS /GO_X based electrodes incorporated with different SWNTs film loading. T=25℃, E=0.5 V vs SCE……..55

Figure 2.11 Effect of SWNTs films on the enzymatic stability of PVP-OS/GO_X biosensors. ……...55

Figure 3.1 Effect of enzyme solution pH on sensor performance. ……65

Figure 3.2 Effect of redox polymer solution pH on sensor performance. ……..66

Figure 3.3 Effect of SWNT films on the electrochemical and enzymatic response of Fc-C_6-LPEI/FDH modified electrodes. ……...68

Figure 3.4 Effect of SWNT films on the electrochemical and enzymatic response of PVP-Os/Laccase modified electrodes……..70

Figure 3.5 Fructose/O_2 Biofuel cell schematic with Fc-C_6-LPEI mediated fructose anode electrodes and PVP-OS mediated laccase cathode electrodes. …….71

Figure 3.6 Effect of SWNT films on Bioanode and Biocathode Response**.** ……..…71

Figure 3.7 Effect of incorporating SWNTs on the biofuel cell performance. …….. 73

Figure 4.1 Effect of SWNTs conductivity on the performance of nanotube film incorporated $FcMe_2$-C_3-LPEI /GOX based electrodes…….80

Figure 4.2 (A) and (B) Effect of SWNTs(7,6) film loading on electrochemistry of $FcMe_2$-C_3-LPEI /GOX based electrodes……..83

Figure 4.3 (A) and (B) Glucose calibration curves for $FcMe_2$-C_3-LPEI /GOX based electrodes modified with different SWNTs loading in sodium phosphate buffer. ….84

Figure.4.4 Effect of redox polymer and enzyme solution loading on the electrochemical performance of electrodes. ……85

Figure 4.6 Effect of SWNTs(7,6) film on the enzymatic stability of $FcMe_2$-C_3-LPEI /GOX electrodes. …….86

Figure 4.7 Effect of incorporating SWNTs films on the electrochemical and enzymatic response of Cl-Fc-LPEI/Laccase cathode electrodes……..87

Figure 4.8 Polarization curves of $FcMe_2$-C_3-LPEI /GOX anode and Cl-Fc-LPEI/Laccase cathode without (A) and with SWNTs film (B). …….91

Figure 4.9 Effect of incorporating SWNTs on the performance of biofuel cell performance. ……93

Figure 4.10 Biofuel cell stability. Biofuel cell with and without SWNTs were continuously operated at maximum power for 12 h at 25 ^{o}C. …….95

Figure 5.1 Schematic of the construction of redox polymer hydrogel film with the incorporation of SWNTs by different method: two layer method (procedure A) and mixing/two layer method (Procedure B)……102

Figure.5.2 Cyclic voltammograms (A) and Glucose response (B) of GCE with redox polymer/enzyme film alone (control), type A electrodes, and type B electrodes….105

Figure 5.3 Glucose calibration curves of control electrodes (▲) and Type B electrodes (■) at 25◦C (No fill) and 37◦C (Solid filled). ……...107

Figure 5.4 Enzymatic stabilities of $FcMe_2$-C_3-LPEI /GO_X electrodes without and with SWNTs (type B electrodes). ……..108

Figure 5.5 (A) Effect of incorporating SWNTs(7,6) on cyclic voltammetry curves of Cl-Fc-LPEI/Laccase electrodes without and with SWNTs. ……109

Figure 5.6 Polarization curves of $FcMe_2$-C_3-LPEI /GOX anode and Cl-Fc-LPEI/Laccase cathode without (A) and with SWNTs (B). ……..110

Figure 5.7 Effect of incorporating SWNTs on the performance of biofuel cell……112

Figure 5.8 Biofuel cell stability. …….…….114

Figure.5.9 Cyclic voltammograms (A) and Glucose response (B) of $FcMe_2$-C_3-LPEI/FDH electrodes without SWNTs and with SWNTs (type B electodes…….114

Figure 5.10 Biofuel cell Performance without SWNTs and with SWNTs. …….....116

Figure 6.1 Schematic of MWCNTs array electrode……..124

Figure 6.2 (A) Cyclic voltammograms and glucose calibration curves (B) of GCEs and MWCNTs array electrodes modified with $FcMe_2$-C_3-LPEI and GOx hydrogel film. ……...125

Figure 6.3 Scanning microscope image (SEM) of vertically alligned MWCNTs forest before (A) and after oil burn off (B). (C) Magnified SEM images of MWCNTs forest electrodes……127

Figure 6.4 (A) Cyclic voltammograms and glucose calibration curves (B) of unburned and burned MWCNTs array electrodes modified with $FcMe_2$-C_3-LPEI and GOx hydrogel film……129

Figure 6.5 Optical images of burned MWCNTs forest electrodes without (A) and with the modification of 1% Triton X-100 (B) with the addition of redox polymer hydrogel solution. (C) and (D) are optical images of burned MWCNTs forest without and with the modification of 1% Triton X-100, when the redox hydrogel solutions get dried……129

Figure 6.6 (A) Cyclic voltammograms and glucose calibration curves (C) of burned MWCNTs array electrodes without and with the modification of Triton X-100 surfactant, followed by $FcMe_2$-C_3-LPEI and GOx hydrogel film ……130

ABSTRACT

Nanostructured enzymatic biofuel cells with high power density output and prolonged lifetime were developed by the incorporation of carbon nanotubes into redox polymer-enzyme films. The performance of the enzymatic biofuel cells was optimized by dispersing carbon nanotubes with different surfactants, modifying the method of nanotube incorporation, and varying the nanotube type and loading. The first part of this work focused on fabricating high surface area of single walled carbon nanotubes (SWNTs) for construction of redox polymer-enzyme based electrodes. It was demonstrated that the deposition of SWNTs(6,5) films onto glassy carbon electrodes from suspensions of the non-ionic surfactant Triton X-100 resulted in the highest response to glucose, producing current densities of ~1.7–2.1 mA/cm^2. In contrast the formation of SWNTs networks from anionic surfactant suspensions (i.e. sodium cholate and NaDDBS) showed a decrease in the glucose response.

To demonstrate that these SWNTs networks could be applied to anodic films that contained enzymes other than glucose oxidase, we constructed redox polymer-enzyme films both with and without SWNTs but with the enzyme fructose dehydrogenase (FDH). We demonstrated that the electrochemical and enzymatic properties of FDH/redox polymer electrodes were highly dependent on both the pH of the enzyme solution and the redox polymer solution. The maximum current density of Fc-C_6-LPEI/FDH electrodes was 245 $\mu A/cm^2$. Modification of GCEs with SWNTs (6, 5) films prior to coating of the Fc-C_6-LPEI/FDH films resulted in an increase in the fructose response to ~ 1 mA/cm^2. Fabrication of enzymatic biofuel cells based on these films produced a power density of 29 $\mu W/cm^2$ in response to fructose.

The role of SWNTs conductivity was investigated by comparing the performance of electrodes coated with SWNTs networks made from dispersions of

conductive SWNTs(7,6) and semiconducting SWNTs(6,5). It was demonstrated that network of SWNTs(7,6) showed higher glucose response than networks of SWNTs(6,5) when coated with a mixture of the ferrocene redox polymer ($FcMe_2$-C_3-LPEI) and the enzyme (GOx). Optimizing the composition of SWNTs(7, 6) networks resulted in a maximum current density response to glucose of 11.2 mA/cm^2. Furthermore, a novel method (mixing/ two layer method) was developed by incorporating carbon nanotubes into redox polymer-enzyme hydrogel films that were deposited onto the SWNTs networks. This mixing/two layer method resulted in a further increase in the response to glucose to 16.2 mA/cm^2 at 37 ^oC. In addition, the stability of $FcMe_2$-C_3-LPEI / GOx electrodes increased with the incorporation of SWNTs. Applying the optimized SWNTs method to cathodes that were coated with a chloro-ferrocene redox polymer (Cl-Fc-LPEI) and the enzyme laccase generated biofuel cells that produced a maximum power density of 802 $\mu W/cm^2$ at 355 mV and at 37 ^oC.

Finally, we evaluated the potential of high surface area vertically aligned multiwalled carbon nanotubes (MWCNTs) forests as an electrode platform. Coating of these MWCNTs platforms with a mixture of ferrocene redox polymer ($FcMe_2$-C_3-LPEI) and the enzyme glucose oxidase produced electrodes that were responsive to glucose despite the fact that a majority of the MWCNTs (>99%) were electrochemically inaccessible.

Chapter 1:

Introduction and Background Information

INTRODUCTION

Enzymatic biofuel cells (EBFCs) are devices capable of generating electrical energy directly from chemical energy via electrochemical reactions using renewable biocatalysts (enzymes) [1, 2, 3, 4]. The first enzyme based glucose/O_2 biofuel cell was reported by A.T.ahiro et al in 1964[5]. In their system, a flavoprotein (glucose oxidase or D-amino acid oxidase) anode, coupled with an O_2 cathode generated voltages between 175 mv and 350 mv. Since then, considerable attention has been drawn to the development and improvement of EBFCs due to the great advantages conferred by the biological catalysts. The presence of a biocatalyst (redox enzyme) endows some unique properties to the enzymatic biofuel cell, which differ from conventional fuel cells typically requiring expensive inorganic catalysts such as platinum. EBFCs tend to operate under mild conditions (25-40 ^oC, and near neutral pH), while conventional biofuel cells operate under harshly acidic conditions and high temperatures exceeding 80 ^oC. The high specificity of an immobilized enzyme in a biofuel cell to a particular substance eliminates the need to separate the anode and cathode compartments by a membrane; this allows for construction of compartment-less enzymatic biofuel cells. Meanwhile, the variety of natural mass able to be transformed by enzymes provides a wide selection of fuel substances. Substrates such as glucose[6, 7, 8], fructose[9, 10], ethanol[11, 12], glycerol[13] and pyruvate[14] have been investigated as possible fuel sources for EBFCs. Among these options, glucose, used to construct glucose/O_2 biofuel cells, gains the most attention due to the natural presence of both components in the blood serum of humans with a concentration of 5 mM (glucose) and 0.1 mM (O_2), respectively. Glucose/O_2 enzymatic biofuel cells could utilize the fuel glucose or O_2

directly from the blood flow, potentially providing a long term power supply for implantable medical devices (IMDs). Table 1.1 shows the applications, power requirements, and current battery sources for some IMDs. The power requirements of implantable medical devices are relatively low, in the range of a hundred microwatts to several milliwatts. For example, cardiac pace makers only require ~100μW of electrical power consumption, while hearing aids require less than 50 μW of power.

Table 1.1 Implantable medical devices applications and power consumption[15]

Application	**IMD**	**Power requirement**	**Current battery system**	**Nominal voltage**	**Battery lifetime**
Bradycardia	pacemaker	30-100 μW	Li/I_2	2.8 V	5-12 years
Tachycardia fibrillation	Cardioverter defibrillator	30-100 μW(pacing) +10 w for defibrillation	Li/SVO $Li/Ag_2V_4O_{11}$	3.1 V	4-7 years
Chronic pain, deep brain stimulation	Spinal cord stimulator; Deep brain stimulator	300 μW to 50 mW	$Li/SOCl_2$	3.5 V	3-6 years
Bladder control	Sacral nerve stimulation	300 μW to 50 mW	Li/SVO $Li/SOCl_2$	3.5 V	3-5 years
Hearing loss	Cochlear Implant	200 μW to 50 mW	Zinc-Air	1.35-1.4 V	10-60 hours
Spasticity	Drug pump	100 μW to 2mW	$Li/SOCl_2$	3.5 V	4-8 years

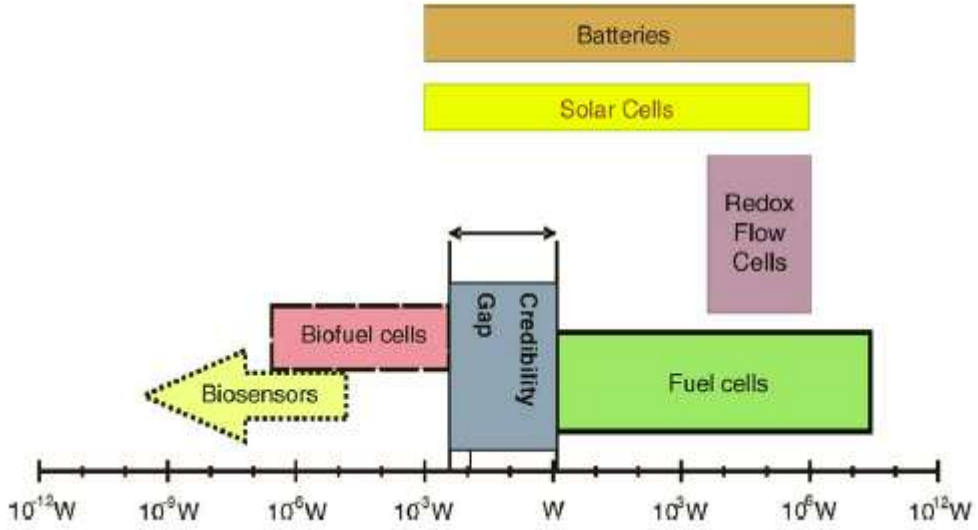


Figure 1.1 Approximate power output of electrochemical devices including biofuel cell, conventional fuel cell, battery etc (from ref 16).

Although EBFCs show exciting potential, some obstacles, such as low power density, low operation potential, and poor stability, must be overcome for practical applications[16]. Currently, EBFCs have been shown to produce a few hundred microwatts of power density whereas conventional fuel cells generate power ranging from a few watts to several hundreds of megawatts. The graph shown in Figure 1.1 (R.A.Bullen et al.[17]) compares the power output of biofuel cells with conventional fuel cells and other electrochemical devices, and suggests that a credibility gap between biofuel cells and conventional fuel cells need to be filled to achieve real world application. The lifespan of current EBFCs are short due to the inherent instability of enzymes, typically on the order of 7-10 days. Moreover, most implantable medical devices in Table 1.1 require a minimum voltage of 1.3 V or higher to operate, whereas the cell voltage of enzymatic biofuel cells is limited to around 0.88 V on the high end[18]. Compared to battery systems for implantable medical devices, current glucose/O_2 biofuel cells cannot compete with (i) the Li/I_2 battery in cardiac pacemakers due to shorter lifetime, and (ii) Li/$SOCl_2$ battery in nerve, cord, or deep brain stimulator and drug pumps, because of lower potential

output. Therefore, in order to achieve the application of EBFCs, research needs to focus on several areas including: (i) increasing the power output; (ii) increasing the operation potential; and (iii) increasing the lifespan. The combination of the attractive application prospects of EMBCs and demand for improvements in the function of EMBCs provides the motivation for this research.

PURPOSE OF THE WORK

The purpose of this work is to design and fabricate nanostructured enzymatic biofuel cells with the incorporation of carbon nanotubes in an attempt to improve the power density output and cell lifetime. The excellent electronic properties of carbon nanotubes, along with their extraordinary chemical structure, make them favorable electrode materials for construction of enzymatic biofuel cells[7, 19]. Several nanotube configurations have been developed including carbon nanotube arrays[20, 21], fibers[22, 23], films[24], paper[25, 26], and yarns[23]. The properties of these nanostructures are highly dependent on the carbon nanotube type (e.g. single-walled vs. multi-walled), nanotube conductivity, incorporation method, as well as the degree of nanotube bundling. In previous studies, our group has demonstrated that the incorporation of single wall carbon nanotubes (SWNTs) into a redox polymer/enzyme hydrogel film by a novel mixing method dramatically increased both the electrochemical and enzymatic response of the sensors[27]. The incorporation of SWNTs into cross-linked films of glucose oxidase (GO_X) and a ferrocene redox polymer film resulted in a 4-5 fold increase in the oxidation and reduction peak currents during cyclic voltammetry, while the glucose electro-oxidation current increased 5-fold, reaching 2 mA/cm^2. Furthermore, the enzymatic stability of the electrodes was also improved with the incorporation of nanotubes. Similar effects were also observed when SWNTs were integrated into films of GO_X and an osmium based redox polymer,

poly[(vinylpyridine)Os(bipyridyl)$_2$Cl$^{2+/3+}$] (PVP-Os), which showed a 3-fold increase in the glucose response[28]. The high current densities of redox polymer mediated enzyme electrodes obtained with the incorporation of nanotubes in the previous studies led us to investigate the possibility of constructing a nanostructured biofuel cell with high power density output and long lifetime. ***Since electrodes bio-catalytically modified with enzymes are the key component of the biofuel cell, the effect of nanotube de-bundling degree, nanotube incorporation method, nanotube type, and redox polymer/enzyme hydrogel loading on the performance of enzymatic electrodes was systematically studied and optimized.*** I propose to test the following hypotheses:

(i) Providing a high surface area network of nanotubes, by direct solution casting of well dispersed nanotube solution onto electrodes, will increase the electrochemical and enzymatic performance of enzyme electrode;

(ii) Incorporating different type of single walled carbon nanotubes (7,6) film in the redox polymer/enzyme electrode would affect the electrochemical and enzymatic property of electrodes.

(iii) The nanotube loading and redox polymer/enzyme solution loading are important factors affecting the electrochemical and enzymatic performance of electrodes;

(iv) The incorporation of nanotubes into the redox polymer/enzyme hydrogel film on nanotube modified electrodes could further enhance the electrochemical and enzymatic performance of electrodes;

(v) The incorporation of carbon nanotubes into redox polymer-enzyme hydrogel electrodes might be applicable to construct various enzymatic electrodes with improved electrochemical and enzymatic performance.

Finally, novel enzymatic biofuel cells will be constructed based on the optimized nanotube-enzymatic electrodes and be evaluated for their stability, power density output, and operating potential. The remainder of this chapter will provide concise background information necessary for understanding the work presented in the subsequent chapters.

BACKGROUND

Enzymatic biofuel cell

Enzymatic biofuel cells (EBFCs) are capable of utilizing biological species (enzymes) to directly generate power from chemical energy via electrochemical reactions. Redox enzymes are attractive catalysts for constructing biofuel cells due to their high catalytic activity and selectivity. Redox enzymes can either be dissolved or suspended in solution within the anodic or cathodic compartment of the cell, or they can alternatively be immobilized at the electrode surface. Immobilization of enzyme onto electrodes is normally preferred in order to achieve effective electron communication to the electrode surface and to eliminate the need for membranes to separate the anode and cathode. In addition, the stability of enzymes is generally improved when they are immobilized[29, 30]. The use of redox enzymes in biofuel cells endows some unique properties to enzymatic biofuel cells, in contrast to conventional biofuel cells, such as operating under mild temperature of (20-40°C) and physiological pH condition, and eliminating the need for membranes due to the high selectivity. A schematic of an enzymatic biofuel cell configuration is shown in Figure

1.2. When a proper fuel is introduced, it can be either partially or totally oxidized at the anode, releasing electrons. The electrons from this process transfer to the electrode, via direct electron transfer (DET) or by the introduction of a redox mediator I via mediated electron transfer (MET), then flow through the external circuit to reduce oxygen to water at the cathode either directly or facilitated by mediator II.

In DET, electrons from enzyme active sites are directly transported to the electrode surface. The distance between enzyme active sites and an electrode surface, as well as redox enzyme orientation, is an important factor affecting the electron transfer process. Theoretical and experimental research has shown that the electron transfer rate between molecules decays exponentially with the distance between the involved centers[31, 32]. For redox enzymes, the electron transfer rate decreases by 10^4 when the distance between an electron donor and an acceptor increases from 8 to 17Å[33]. Enzymes like laccase [34, 35] or fructose dehydrogenase[9, 36] can achieve direct electron transfer between their active sites and electrode surface. However, the direct electrode transfer between the active sites of most enzymes and electrodes is not possible since the presence of thick insulating protein layers that surround the enzyme's redox centers makes them inaccessible. Taking glucose oxidase (GOx) for example[37], the glycoprotein shell around the $FADH_2$ active centers inhibits electrons transferring from the redox centers of reduced GOx to most electrode surfaces. Therefore, redox mediators are commonly employed to facilitate electron transport, in a process termed as mediated electron transfer. Mediators allow for the shuttling of electrons from the enzyme active sites to the electrodes, regardless of the orientation or proximity of the enzyme active sites to electrodes. The choice of mediator type is affected by the specific design parameters and potential application of the biofuel cell. In order to construct a single compartment biofuel cell, immobilization of the enzyme

and the redox mediator onto the electrode surface are normally necessary to avoid any crosstalk reactions between the anode and cathode, and an electrical short in electron transfer routes. If high current and power outputs are the only requirements, a high concentration of the dissolved mediator in separate compartments can be effective[4].

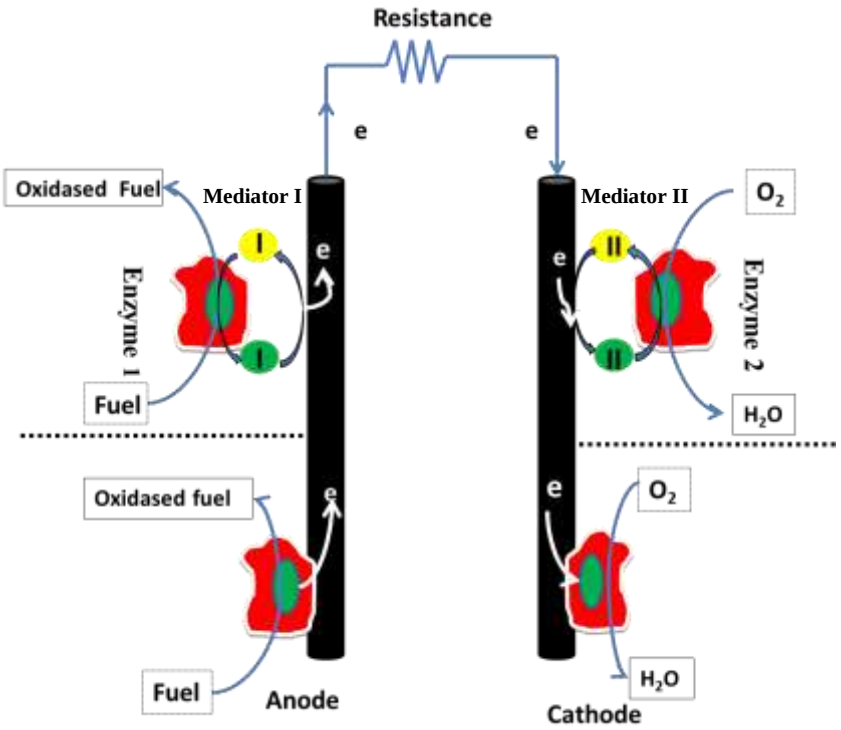


Figure 1.2 Schematic of an enzymatic biofuel cell without and with mediator. Redox mediator I shuttles the electron from enzyme to the electrode surface at anode, and redox mediator II mediated the electron transfer at the cathode. Greed color of mediator I and II represents the oxidized status, while the yellow color is the reduced status

There is a wide range of available substrates such as glucose, fructose, ethanol, pyruvate, alcohols, fatty acids, or even waste materials being used as possible fuel for EBFCs. Among these, glucose gains the most attention to construct glucose/O_2 biofuel cells as an alternative energy source for implantable medical devices due to the presence of glucose and oxygen in human blood serum with concentrations of 5 mM and 0.1 mM, respectively. Meanwhile, the products produced in the anode and cathodes are naturally occurring metabolites, in low concentration. The enzyme applied to construct enzyme electrodes is selected based on the type of substrate and

the reaction mechanism. For a glucose/O_2 biofuel cell, glucose oxidase and glucose dehydrogenase have been widely studied as the biocatalysts in the anode to oxidize glucose to gluconolactone, while blue copper-containing oxidases such as laccase or bilirubin oxidase (BOD) have been applied to reduce oxygen into water at the cathode. The schematic of a glucose/O_2 biofuel cell, using glucose oxidase and laccase as the enzymatic catalyst in the anode and cathode, is shown below in Figure 1.3. The half reaction on the anode and cathode, as well as total reaction of the glucose/O_2 biofuel cell is shown below:

Anode: $Glucose \rightarrow gluconolactone + 2H^+ + 2e^-$ (1) E^{Θ}=-0.25V vs. Ag/AgCl

Cathode: $\frac{1}{2}O_2 + 2H^+ + 2e^- \rightarrow H_2O$ (2) E^{Θ}=+0.75V vs. Ag/AgCl

Cell: $Glucose + \frac{1}{2}O_2 \rightarrow gluconolactone + H_2O$ (3) E^{Θ}=1 V vs. Ag/AgCl

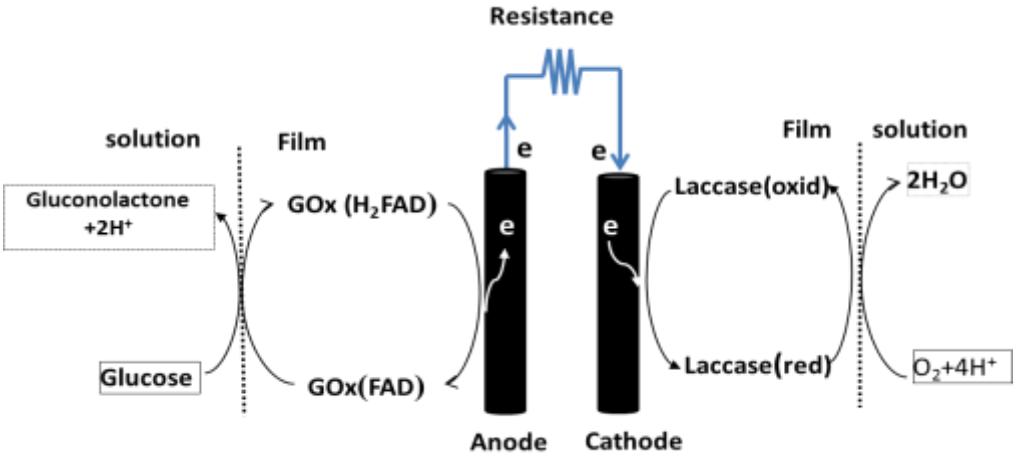


Figure 1.3 Schematic of a glucose/O_2 EBFC that uses GOx and laccase as enzymatic catalysts on the anode and cathode.

Redox Enzyme type

Various types of enzymes may be applied to construct the anode and cathode of EBFCs, depending on the type of substrate and the reaction mechanism. Redox enzymes applied in biofuel cells are of the oxidoreductase family, which are able to

catalyze oxidation and reduction reactions[38]. For convenience in establishing electron transfer between enzymes and electrode surface, Heller et al reported [39] that redox enzymes can be divided into three groups based on the location of enzyme active centers and method used to establish electron transfer between enzymes and electrodes, as shown in Figure 1.4.

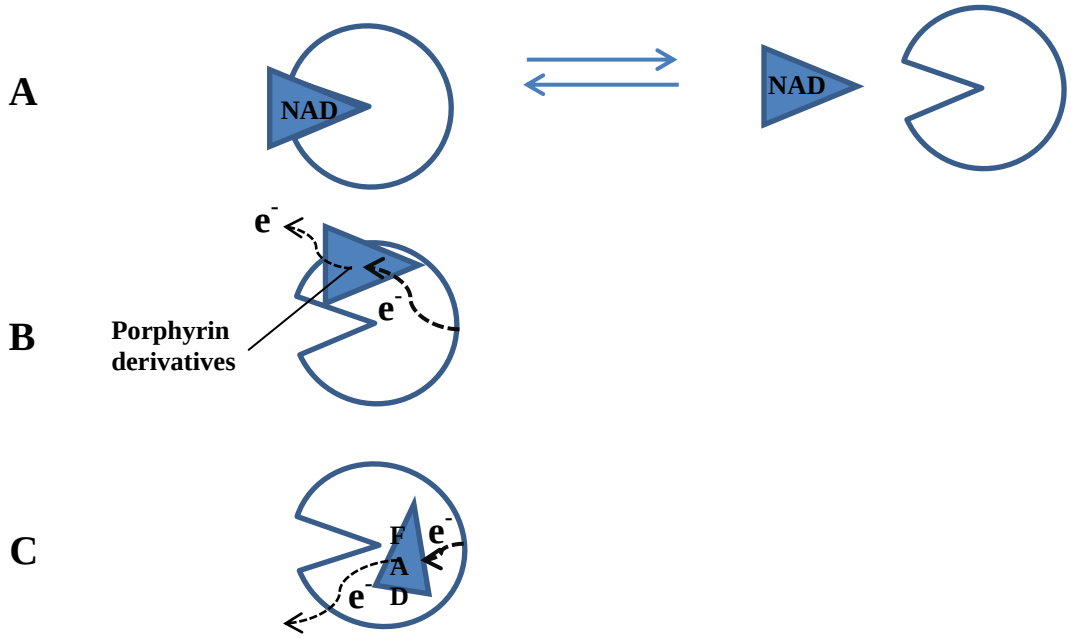


Figure 1.4 Schematic of three different groups of redox enzyme described by Heller et al. (A) type I redox enzyme with diffusive active center, (B) type I redox enzyme with active centers located on the periphery of the enzyme, (C) Type III enzyme with strongly bound and deep buried redox centers.

The first group is characterized by redox enzymes that contain NADH/NAD^+ or NADPH/$NADP^+$ as their redox center, such as glucose dehydrogenase and AlcDH. In this type of enzyme, the redox centers are weakly bound to the protein of the enzyme, and could work as a diffusion redox mediator shuttling electrons between different redox biomolecules[17]. However, there are some issues in the preparation of NADH/NAD^+ or NADPH/$NADP^+$ electrodes, such as loss of the redox center when exposed to substrate. The out-diffusion of redox centers out of the enzyme could be prevented by covalently attaching redox centers to the enzyme protein via a flexible

spacer chain, allowing for the wiggling of the centers between enzyme and electrode surface.

The second group of redox enzyme contains redox centers, usually porphyrin derivatives, located at or near the periphery of the protein shell. One example is glucose dehydrogenase[40]. These enzymes can transfer or accept electrons on contact, thus allowing for the construction of enzyme electrodes via direct electrical communication. The rate of electron transfer varies depending on their orientation on the electrode surface. The third group of redox enzymes are the flavoenzymes, which contain a strongly bound flavin adenine dinucleotide (FAD) redox cofactor buried deep inside the protein structure. Direct electrochemical response between the FAD active site of the flavoprotein enzyme and electrode surface is normally extremely difficult.

Anodic enzymes

The most extensively studied anodic enzyme in the glucose/O_2 biofuel cell, glucose oxidase, is a dimeric flavoenzyme with a molecular weight of 160 kDa, containing one FAD cofactor per monomer. Some reports have suggested that it is possible to achieve direct electron transfer between the FAD active sites of glucose oxidase with the electrode surface with the aid of nanomaterials such as gold nanoparticles[41] or single wall carbon nanotubes[40, 42, 43]. Anthony Guiseppi et al reported that both glucose oxidase (GOx) and FAD spontaneously adsorbed onto unannealed carbon nanotubes, displaying direct electron transfer between the FAD active sites of GOx and SWNTs[44]. Equations (4) and (5) show the widely accepted glucose oxidation and oxygen reduction in the GOx catalyzed redox reaction,

$$Glucose + GOx(FAD) \rightarrow gluconolactone + GOx(FADH_2) \quad (4)$$

$$GOx(FADH_2) + O_2 \rightarrow GOx(FAD) + H_2O_2 \quad (5)$$

The production of H_2O_2 by the enzymatic reduction of oxygen by glucose oxidase is undesirable in an enzymatic biofuel cell, because the production of H_2O_2 might compete with electron transfer to the electrode, lowering the performance of a biofuel cell[45]. Introducing a redox mediator is of interest to construct mediated glucose oxidase electrodes due to the high current density output it might provide. Meanwhile, the competition of oxygen for electron transfer from the active sites of GOx to produce H_2O_2 can be minimized if the rate of electron transfer via the mediator is higher than the rate of the enzyme reaction with oxygen. The mediated electron transfer schematic is shown as follows:

$$Glucose + GOx(FAD) \rightarrow gluconolactone + GOx(FADH_2) \quad (6)$$

$$GOx(FADH_2) + 2M_{(ox)} \rightarrow GOx(FAD) + 2M_{(red)} \quad (7)$$

$$2M_{(red)} \rightarrow 2M_{(ox)} + 2e^- \quad (8)$$

Where $M_{(ox)}$ and $M_{(red)}$ are the oxidized and reduced forms of the mediator.

As an alternative enzyme, glucose dehydrogenase (GDH), with different cofactors including pyrroloquinoline quinone (PQQ)[46], nicotinamide adenine dinucleotide (NAD) [47], or flavin adenime dinucleotide (FAD) [48], has recently gained some attention to construct glucose anode electrodes[49]. Compared with glucose oxidase, the main advantage of using glucose dehydrogenase is its insensitivity to oxygen. However, there are some disadvantages of GDH associated with the different cofactors, which limit their application in EBFCs. For example, PQQ-GDH has a low selectivity due to the oxidation of saccharides such as mannose, maltose, lactose etc., and it showed a poor stability under continuous operation[50]. Similarly, the preparation of FAD dependent GDH is complicated and costly[51]. For the NAD cofactor dependent GDH, an artificial electron transfer mediator needs to be introduced into the system, due to the poor electrochemical reversibility of both the oxidized (NAD^+) and reduced

form (NADH). Besides, NAD dependent GDH exhibits a lower turnover frequency ($75s^{-1}$) than that of FAD bounded GOx ($1900\ s^{-1}$) at room temperature[52].

Cathodic Enzymes

Laccase and bilirubin oxidase (BOD) are the two common enzymes applied to reduce oxygen into water in the cathode of biofuel cell. Both of them belong to the multi-copper oxidase family of enzymes, due to the presence of coordinated copper centers (T1, T2 and T3) that catalyze the oxidation of substrates with phenolic structures and reduction of oxygen to water. A general mechanism for this process is that the T1 copper site, located close to the surface of enzyme, accepts electrons from the substrate, then passes them to the T2/T3 tricopper cluster through a His-Cys-His chain, in which O_2 is coordinated and reduced to water[53, 54]. Although the oxygen reduction catalytic mechanisms for laccase and BOD are similar, there are some differences in their properties. Laccase prefers to operate in the pH range between 4 and 5, and is inhibited by halide ion such as Cl- and F-, whereas the optimal pH of BOD is at 7 and is tolerant to halide ions when immobilized in cross-linked redox polymer films. The T1 site of laccase exhibits a higher redox potential than that of BOD, which might result in the high catalytic efficiency (k_{cat}/k_M) of laccase to the majority of the aromatic reducing substrates.

Key Performance characteristics

Similar to a conventional biofuel cell, the parameters used to evaluate the enzymatic biofuel cells include the cell voltage, power density, and stability. These parameters can be estimated through electrochemical measurements, such as polarization curves, power curves, and constant potential tests. The power extracted from EBFCs (P_{cell}) is the product of cell voltage (E_{cell}) and the cell current (I_{cell}), as described in the following equation (9),

$$P_{cell} = E_{cell} \times I_{cell} \quad (9)$$

Thus, the increase in power density output of EBFCs can be achieved by either increasing cell voltage or cell current. In principle, the cell voltage (E_{cell}) of direct electron transfer based biofuel cell has an upper limit, which is the difference between the formal redox potential of substrates in the anode and cathode. When mediators are immobilized on the enzymatic electrodes, the thermodynamic potential of the biofuel cell is the difference between the formal potentials of the mediators in the anode and cathode compartments[4].

In practice, the actual cell voltage of biofuel cells is lower than the thermodynamic potential, due to the presence of irreversible loss in potential (termed as over-potential) when the cell is operated. There are three main types of irreversible losses of potential, termed as activation loss, ohmic loss, and mass transport loss[38, 55]. The activation loss results from the low kinetics of electron transfer from the enzyme or mediator to the electrode, whereas the ohmic loss arises from the resistance of charge transport through different components in the cell, including contact, ionic, and electronic resistances. Mass transport losses are due to diffusion limitations from the bulk solution to the electrode surface at high current, which can be reduced by mixing the solution well to increase the mass flux of substrate. Taking all these factors into account, the cell voltage of a biofuel cell can be expressed as follows in equation 10:

$$E_{cell} = E_{cathode} - E_{anode} - E_{over} \quad (10)$$

Therefore in order to obtain an optimal cell voltage for a biofuel cell, it is desirable to maximize the potential difference between the cathode and anode, while minimizing the irreversible potential loss in the cell. Taking a glucose/O_2 biofuel cell as an

example, the redox potential of the redox enzyme applied in the anode and cathode and the corresponding chemical reactions are shown in Table 1.2.

Table 1.2 The redox potential of redox enzyme applied in biofuel cell and the corresponding chemical reactions

Electrodes	**Redox enzyme (active sites)**	**Redox potential vs. SCE**
Anode	Glucose oxidase (FAD)	-0.36V
	Glucose dehydrogenase (PQQ)	-0.16 V
	Glucose dehydrogenase (NADH)	-0.57 V
Cathode	Bilirubin oxidase T-1 Cu(II)/Cu(I)	0.48 V
	Laccase T-1 Cu(II)/Cu(I)	0.539 V
Anode reaction	$Glucose \rightarrow gluconolactone + 2H^+ + 2e^-$	E^{Θ}=-0.69V
Cathode reaction	$\frac{1}{2}O_2 + 2H^+ + 2e^- \rightarrow H_2O$	E^{Θ}=+0.82V

Several strategies have been developed to increase the cell potential of biofuel cells, such as preparing direct electron transfer based enzymatic electrodes, choosing proper redox enzymes and redox polymers, changing the geometry of the cell, etc. Frederic Briere et al[56] compared the performance of laccase electrodes mediated by different redox polymers including an osmium based redox polymer with a standard potential of 0.4V and a ruthenium based redox polymer with a potential of 0.63 V. Their results indicated that the osmium polymer showed a promise for use in a compartment-less biofuel cell. In contrast, negligible current was observed with the ruthenium polymer, as its high redox potential is too high (0.585V vs Ag/AgCl) to allow laccase to oxidize them appreciably. Therefore, they suggested that a compromise might need to be made between the choice of mediator with a high redox potential to achieve a large cell potential, and a mediator possessing a low redox potential to ensure a high catalytic current.

Another important factor affecting the power density output of biofuel cells is the current density, which is dependent upon by the electron transfer rate between the active sites of the enzyme and electrode surface. In addition, the current density is also related to the degree of oxidation completion of the substrate. How to achieve efficient electron communication between enzyme and electrode surface is still a critical issue in developing an enzymatic biofuel cell with high power density output. Several strategies have been developed to increase the current density output of enzymatic electrodes, such as introducing redox mediators into the system[56, 57], using enzyme cascades[58] to completely oxidase the substrates[13, 59], or incorporating nanotubes into the system[60]. Each strategy will be discussed in the following content.

Redox mediator to enhance electron transfer

Introducing a redox mediator has proven to be an effective and easy method to shuttle electrons from the active sites of an enzyme to the electrodes, regardless of the orientation of the enzyme active sites relative to the electrodes. Numerous effective mediators have been developed, including diffusion and non-diffusion mediators. The choice of mediator type is dependent on the specific design parameters and potential application of the biofuel cell. In order to a construct a single compartment biofuel, immobilization of enzyme and redox mediators onto electrode surfaces are normally necessary. If high current and power output are the only requirement, high concentration of dissolved mediator in separate compartments can be effective.

Diffusion mediators are dissolved in solution, where they can accept electrons from the enzyme and diffuse to the electrode surface and subsequently become oxidized. Various diffusion mediators have been developed, such as monomeric ferrocenes[57, 61], ferricyanide[62], osmium bipyridine complexes[63], $NAD(P)^+$ [47], etc. To be applied to enzymatic biofuel cells, the introduction of diffusion mediators into the

anode and cathode may require the assembly of a membrane to separate these two compartments to inhibit the cross-talk reaction and electrical short in electron transfer routes. Meanwhile, the potential danger of this diffusion mediator escaping into body fluid and its toxicity might limit the application in implantable biosensors and biofuel cells.

Progress in non-diffusional mediated enzymatic electrodes was pioneered by Adam Heller, when his group achieved MET between an enzyme active site and an electrode surface by co-immobilizing an enzyme within a crosslinked redox polymer film[64, 65]. Redox polymers contain redox active species covalently or electro-statically bound to an electrochemically inactive polymer backbone. Long and flexible tethers allow the redox centers to sweep large volume elements, providing a high electron transfer coefficient[66]. When crosslinked with enzymes onto electrodes, the redox polymer penetrates and binds enzymes through multiple lysine amines to form a three dimensional network that attaches to the electrode surface. The crosslinked hydrogel swells in aqueous solution and permits the diffusion of substrate and ions through the film, while eliminating the leaching of mediator molecules into the buffer solution. The three dimensional structure of the swelling redox polymer allows the increase in the number of enzymes that are electrochemically accessible to the electrode surface due to the large volume it might sweep out. The presence of these redox species results in an electron transport mechanism commonly called “electron hopping”, in which the outer sphere electrons from reduced redox species are self-exchanged to neighboring oxidized redox species when the two redox centers collide with each other, and then to the electrode surface.

Different types of redox mediators have been developed and applied to construct enzymatic electrodes, such as osmium based redox polymers[67, 68], ferrocene

based redox polymers[66, 69], 2,2-azinobis, 3-ethylbenzothiazoline-6- sulfonate (ABTS)[70], and ruthenium based redox polymers[71]. Taking the osmium based redox polymer as an example, Adam Heller et al prepared it by covalently attaching an osmium complex onto a poly(vinylpyridine) or poly(vinylimidazole) polymer back bone[72]. Their results suggested that these osmium based redox polymers can effectively mediate electron transfer from the FAD active sites of glucose oxidase to the electrode surface with a limiting current density up to 800 uA/cm^2. The electro-transfer steps in the electrooxidation of glucose on an osmium based redox polymer wired glucose oxidase electrodes is shown in Figure 1.5.

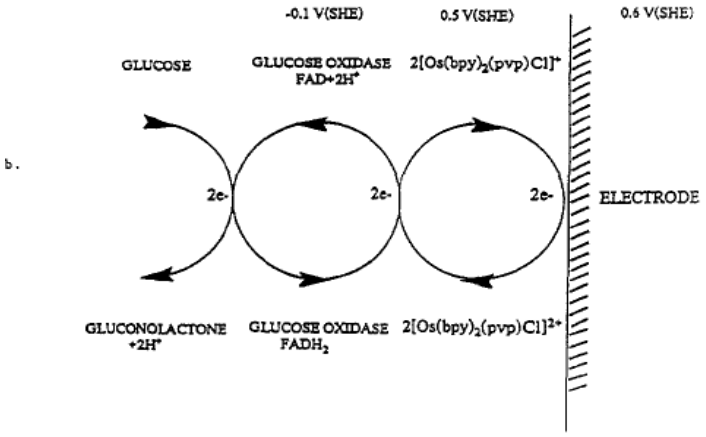


Figure 1.5 Electron-transfer steps in the elctrooxidation of glucose on a wired glucose oxidase electrodes suggested by Adam Heller et al (from ref 71).

Recently, the Schmidtke/Glathofer group has prepared a ferrocene redox polymer by coupling ferrocenecarboxaldehyde to both linear and branched poly(ethylenimine) (PEI) polymer backbones[73]. Initial results suggested that these polymers (Fc-C_1-LPEI) were able to electrically communicate with the FAD redox center of glucose oxidase, with limiting current density up to 1 mA/cm^2. Paul Kavanagh et al [74]compared the performance of osmium based redox polymers with various redox potential mediated laccase cathode electrodes, including [Os(2,20-bipyridine)$_2$(polyvinylimidazole)$_{10}$Cl]$^{+/2+}$ (Polymer I) and [Os(4,40-dichloro-2,20-

bipyridine)$_2$(polyvinylimidazole)$_{10}$Cl]$^{+/2+}$ (Polymer II). Their results showed that polymer I with a redox potential of 0.22 V exhibited much higher current density than polymer II with a potential of 0.35 V. The redox potential of polymer II is more positive than that of T1 site of laccase at pH of 7 (0.26 V), resulting in a thermodynamically unfavorable uphill electron transfer reaction. Therefore, the choice of redox mediator is critical in establishing effective electron wiring between the active sites of the enzyme and electrode surface and determining the current density output of enzymatic electrodes. An ideal mediator would induce a small overpotential, while being capable of transferring electrons at a rate that was approximately equal to, or greater than, the turnover rate of the enzyme used.

Using enzyme cascade

Applying multi-enzyme cascades to completely oxidize a fuel source is actively being pursued by many researchers to construct an enzymatic biofuel cell with high power density outputs. The first example was proposed by Palmore et el for the complete oxidation of methanol to carbon dioxide and water, using 3 enzymes including alcohol dehydrogenase, aldehyde-, and formate-dehydrogenases[75]. Daria et al mimicked the citric acid cycle at the carbon surface electrode using six enzymes to completely oxidize ethanol to CO_2, resulting in an 8.71 fold increase in the power density output and 9.55 fold increase in the current density output compared to single enzyme system[59]. Several enzyme cascades have been studied in biofuel cells to achieve complete oxidation of propanol[76], butanol[77], and glycerol. In the majority of work involving glucose/O_2 biofuel cells, glucose oxidase and glucose dehydrogenases are the two common anodic enzymes to partially oxidize glucose to gluconolactone, generating 2 electrons. However, there is only 1/ 12th of the 24 electrons that can be extracted from glucose with complete oxidation. Therefore, the question of how to

achieve complete oxidation of glucose to extract more electrons is of considerable interest in the construction of glucose/O_2 biofuel cells with high power density output. Normally, in a living system, two main pathways are responsible for the oxidation of glucose: glycolysis and the Kreb's cycle, both of which require multi-step oxidation and various enzymes for inducing chemical reactions. Glycolysis is an enzymatic pathway for breaking glucose to pyruvate, which can then be further oxidized to CO_2 in the Kreb's cycle. During these natural processes, 19 enzymes are utilized to realize the complete oxidization of glucose to CO_2, while only 6 of these enzymes are oxidoreductase enzymes capable of generating electrical energy. The other enzymes are essential for metabolism, but do not produce electrical energy. The high proportion of non-energy producing enzymes in the metabolic process would decrease the power density produced per unit area of electrodes. Meanwhile, the oxidoreductases in the metabolic pathways are NAD and FAD dependent, which require mediators in the enzyme cascade. Moreover, the turnover rate and enzymatic activities of each enzyme in the cascade is different. Therefore, it is challenging to balance the reaction rates of each enzymatic reaction to make sure the enzyme cascade reaction goes smoothly. Shuai Xu et al developed a six-enzyme cascade containing PQQ dependent enzymes from *Gluconobater*, aldolase from *Sulfolobus solfataricus*, and oxalate oxidase from barley to completely oxidize glucose to carbon dioxide through a synthetic minimal metabolic pathway[78]. Coupled with an air-breathing cathode, this glucose enzymatic bio-anode produced a maximum power density of 6.74±1.43 μW/cm^2.The schematic of the six enzyme oxidation pathway of glucose are in Figure 1.6.

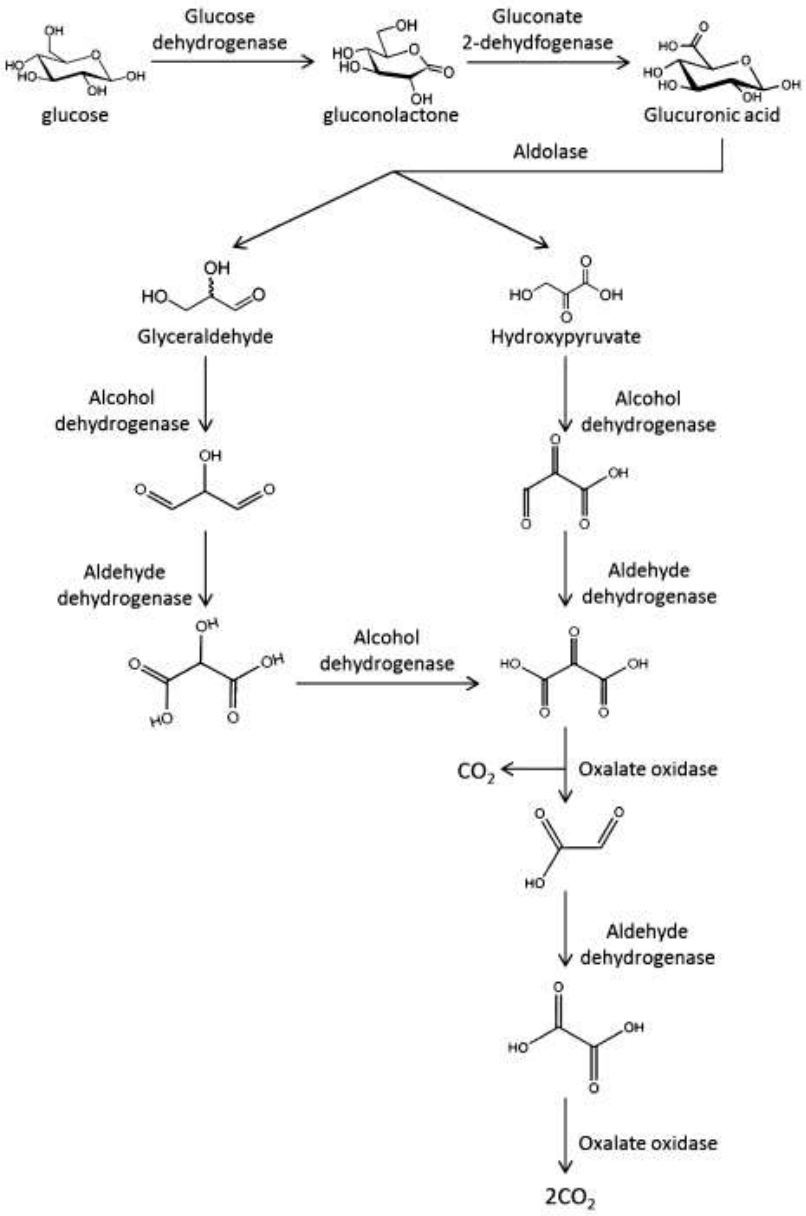


Figure 1.6 Schematic of the six enzyme oxidation pathway of glucose proposed by Shuai Xu et al (from ref 77).

Nanomaterials to enhance electron transfer

Due to their unique structure, high surface area, and excellent electronic properties, nanomaterials have attracted enormous interest in constructing enzymatic electrodes for their applications in biosensors and biofuel cells. The incorporation of carbon nanotubes has proved to be an effective and easy way to enhance the electron communication between the active sites of enzyme and electrode surface. However,

how to maximally explore and take advantage of their superior properties still attracts much attention from researchers. Until now, several nanotube based structures have been developed, including nanotube mat[79, 80] or paper[81, 82], vertically aligned nanotube electrode arrays[83, 84], and enzyme-SWNTs composite electrodes[85, 86].

Preparing nanotube mat or paper for immobilizing enzymes is a common way to provide a high surface area and conductive support for enzyme immobilization. There are some obstacles to prepare robust nanotube mat or paper modified electrodes, such as the insolubility of pristine carbon nanotubes in normal aqueous solutions and nanotube aggregation due to strong van der Waals interactions between tube walls. Many efforts have been made to find ways to solubilize SWNTs in aqueous or organic solutions, such as covalent modification with hydrophilic functionalities or non-covalent modification. Once the stable dispersion of nanotube solution is prepared, an entangled mat or paper of nanotubes is formed by either casting nanotube solution onto an electrode surface or filtering under vacuum or pressure through a microporous membrane. L.Hussein et al [82]fabricated multiwall carbon nanotubes (MWNCTs) in the form of buckypaper and used it as electrode substrate for laccase-catalyzed cathode. They observed efficient direct interaction between laccase and buckypaper, with a high open circuit potential of 0.882 V vs. normal hydrogen electrodes (NHE), and high oxygen reduction performance with current densities 422±71 uA/cm^2 at a cathode potential of 0.744 V. San Hua Lim et al [87]prepared a glucose biosensor by electrodepositing palladium nanoparticles and glucose oxidase enzymes onto a nafion-solubilized carbon nanotube film modified glassy carbon electrodes. These electrodes allow for fast and sensitive glucose quantification, with a detection limit of 0.15 mM and exhibited good enzymatic stability. Maogen Zhang et al [88]prepared a glucose sensor by immobilizing glucose dehydrogenase in a carbon nanotube-chitosan

(CHIT) thin film using glutaric dialdehyde, achieving a low detection limit of 3 μM glucose.

Another popular nanotube structure for immobilizing enzymes is a vertically aligned nanotube forest. Short nanotubes were aligned normal to the electrode surface by either direct growth of CNTs onto an electrode or by self-assembly. The vertically aligned nanotube array provides the matrix for immobilizing biological molecules such as enzymes and DNA to construct a nano-electrode by either adsorption or covalent bonding. J.Justin Gooding et al described the preparation of a single wall carbon nanotube forest, where microperoxidase MP-11 redox enzyme was attached onto the free end of a tube by incubation[21]. The self-assembled monolayer structure of nanotube was formed on gold electrode surface via spontaneous reaction between the thiol group on the open ends of nanotube and cysteamine on gold surface. Their results indicated that the aligned SWNTs can act as molecular wires to allow electrical communication between the underlying electrode and the redox proteins covalently attached to the ends of the nanotube. However, one concern in constructing this self-assembled nanotube array is that the presence of an insulating cysteamine layer where the highly conductive nanotube array is positioned in series may impede electron transfer. Therefore, another strategy was proposed: to directly grow nanotubes on a metal substrate. Sofia Sotiropoulou et al prepared an aligned multi-wall carbon nanotube forest on a platinum substrate by a chemical vapor deposition (CVD) method, followed with acid or air oxidation to open and functionalize the nanotubes for the efficient immobilization of glucose oxidase [20]. Their results suggested that chemical etching by acid is more efficient in opening carbon nanotubes and allowing the entrance of enzyme into the inner channel. The high population density of carboxylic acid groups can be created via the chemical etching from an

overall electrophilic tip surface that minimizes hydrophobic adsorption of the protein. The sensor electrodes prepared by chemical etching showed a sensitivity of 93.9 μA/mm with a detection limit of 0.19 mM. G.D.Withey et al prepared a vertically aligned MWNTs array from a hexagonally patterned array of nanowires in an anodized aluminum oxide template, then covalently linked glucose oxidase enzyme onto the tips or side wall of the nanotube array (via an amine group to the carboxylic acid groups at the nanotube end created by acid chemical oxidation) [89]. The prepared sensor electrodes exhibited an enhanced electron transfer rate of 1500 s^{-1}. Nanomaterials such as gold, Pt, and copper oxide nanoparticles were integrated into the nanotube array to further increase the sensitivity and selectivity of the enzymatic electrodes. Yi-Ge Zhou et al prepared non enzymatic glucose electrodes by incorporating gold nanoparticles into the carbon nanotube array, which showed good catalytic activity toward glucose with a detection limit of 10 μM and no interference toward the presence of ascorbic acid in solution[90].

Preparing enzyme- SWNTs composite electrodes is another attractive way to enhance the electron communication between enzyme and electrode surface. Similar to conventional carbon paste composite electrodes, SWNTs-enzyme composite or paste electrodes were prepared by mixing SWNTs and enzyme with a binder. Various binder materials have been applied to construct enzyme- SWNTs paste composite electrodes, such as mineral oil, polypyrrole, Teflon, and chitosan. The composite electrodes were prepared by either firm packing into the electrode cavity or by solution casting on top of the electrode. Composite electrodes combine the ability of carbon nanotubes to promote an electron-transfer reaction with the attractive advantages of composite materials, and have been applied to construct a wide range of enzyme based electrodes. Mara D.Rubianes et al reported the preparation of a series

of enzymatic carbon paste electrodes, including lactate, phenols, catechols, and alcohol sensor electrodes by dispersion of a redox polymer in multiwall carbon nanotube and mineral oil composite matrix [91]. Their electrodes showed strong electro-catalytic activity towards substrates, as well as high sensitivity.

PROJECT BACKGROUND

Preparing SWNTs-enzyme-redox polymer composite electrodes emerged as a promising strategy for the development of enzymatic electrodes with high current density output. Previous studies by Pratixa P. Joshi et al[28]demonstrated the construction of amperometric biosensors based on incorporation of single wall carbon nanotubes modified with enzyme into redox polymer hydrogel film. The nanotube incorporated hydrogel electrodes were prepared by first incubating an enzyme in a SWNTs solution for 18 hours, prior to mixing with a poly[(vinylpyridine)Os(biyrdyl)$_2$Cl$^{2+/3+}$] polymer and poly(ethylene glycol)diglycidyl ether (PEGDGE) crosslinker, as shown in Figure 1.7. The results showed that the incorporation of SWNTs, modified with glucose oxidase by incubation method, resulted in a 2-10 fold increase in the oxidation and reduction peak currents, and a 3-fold increase in glucose electro-oxidation current, reaching 1mA/cm^2.

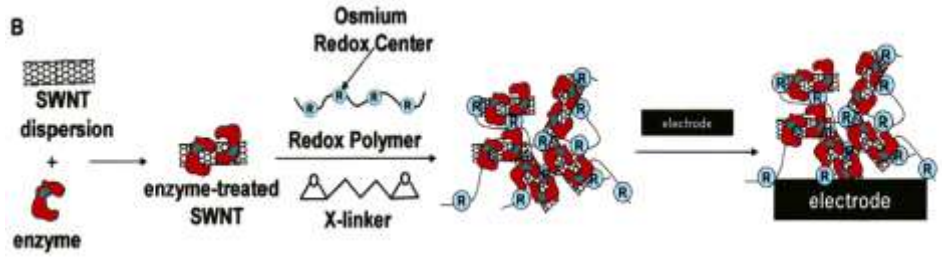


Figure 1.7 Schematic of construction of SWNTs incorporated redox hydrogel sensor, in which SWNTs were incubated with an enzyme solution, before incorporated into the redox hydrogel (from ref 28).

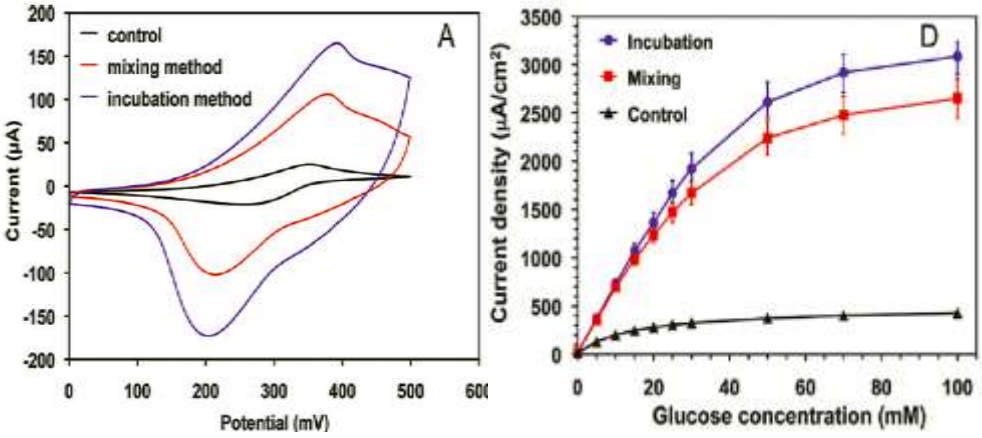


Figure 1.8 Effect of SWNTs incorporation method on electrochemical and enzymatic response of electrodes. (A) Representative CVs of glassy carbon electrodes (GCE) coated with redox polymer (Fc-C_6-LPEI) and enzyme (GO_X) alone (control), a GCE coated with a composite of Fc-C_6-LPEI-GOX-SWNT made by the mixing method (22 wt% SWNT), and a GCE coated with a composite of Fc-C_6-LPEI-GOX-SWNT made by the incubation method (22 wt % SWNT) (scan rate = 50 mV/s, T = 25 ^oC). (D) Glucose calibration curves for the three types of sensors described in (A) (T = 25 ^oC, E = 0.5 V vs SCE) (from ref 28).

Later, Tu O.Tran et al[27] developed a simple mixing method to incorporate SWNTs into redox polymer hydrogel film by directly mixing SWNTs into polymer solution followed by the addition of the enzyme and cross-linker. A comparison in the electrochemical and enzymatic performance of electrodes prepared by mixing method and incubation method was made. As shown in Figure 1.8, the incorporation of SWNTs by both methods resulted in significant increase in the electrochemical and enzymatic performance of redox hydrogel film. Electrodes prepared by both methods exhibited similar enzymatic results. However, the mixing procedure took much less time than the incubation method, reducing the preparation time from 18 hours in incubation method to 1 hour. The incorporation of SWNTs into cross-linked films of glucose oxidase (GO_X) and a ferrocene redox polymer (Fc-C_6-LPEI) hydrogel films by mixing method resulted in a 4-5 fold increase in the oxidation and reduction peak currents during cyclic voltammetry. The glucose electro-oxidation current increased 5 -fold with a maximum current density of 3000 $\mu A/cm^2$. Moreover, the enzymatic

stability of glucose electrodes with the incorporation of SWNTs increased. A proposed electron transfer mechanism is illustrated in Figure 1.9. The presence of SWNTs in the thick redox polymer and enzyme hydrogel film accelerates electron transfer between the hydrogel film and electrode surface, by either increasing self-exchange between the active sites of redox polymer, or by making more ferrocene redox centers electrochemically accessible through the interconnected nanotube network.

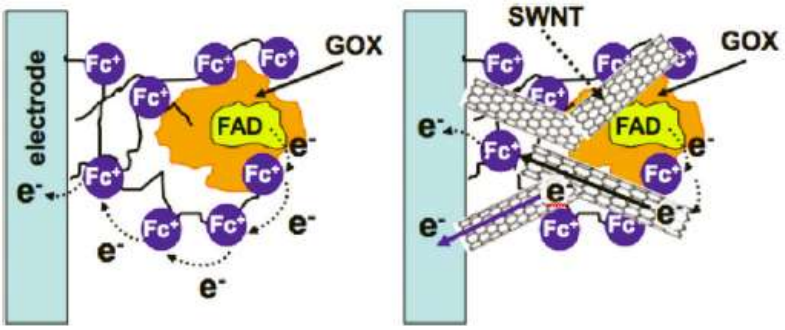


Figure 1.9 Electron transfer mechanism for enzymatic electrodes without (left) and with SWNTs (right). For electrodes without nanotubes, electrons are transferred from the enzyme's FAD enter through the film by self-exchange between neighboring reduced and oxidized redox centers. In an electrode with nanotube, electrons can be transferred not only by self-exchange between the active sites of polymer, but also directly to the electrode surface through an interconnected SWNTs network (blue line) (from ref 27).

OVERVIEW

The purpose of this work was to develop nanostructured enzymatic biofuel cells with the incorporation of nanotubes. The remainder of this dissertation documents the studies completed to investigate the effect of incorporated nanotube networks, nanotube incorporation methods, nanotube types, and the redox hydrogel solution loading on the electrochemical and enzymatic performance of enzymatic electrodes. In addition, the influence of incorporated nanotubes on the performance of enzymatic biofuel cells, including their power density output, current density output, and stability, is also presented. Each chapter begins with an introduction that

provides the motivation and purpose of the corresponding study along with background information corresponding to relevant literature.

Chapter 2 focuses on investigating whether providing a high surface single wall carbon nanotube would improve the electrochemical and enzymatic performance of redox polymer mediated glucose oxidase electrodes. Different surfactants were chosen to prepare a well dispersed nanotube solution, which was used to modify the surface of glassy carbon electrode by solution casing method. The effect of surfactant type, redox polymer type, and nanotube loading on the performance of electrodes was evaluated. The results presented in Chapter 2 demonstrate that surfactant applied to disperse carbon nanotubes and nanotube loading were important factors affecting the performance of nanotube incorporated enzymatic electrodes.

Chapter 3 discusses whether the Fc-C_6-LPEI redox polymer can efficiently wire the redox centers of fructose dehydrogenase (FDH). Using a widely distributed monosaccharide (fructose) as substrate, FDH electrodes allows for the construction of fructose/ O_2 biofuel cells, due to its good oxygen tolerance and similar optimal pH to that of laccase (pH 4-5). In addition, we tested the hypothesis that the aforementioned high surface area SWNT network would increase the electrochemical and enzymatic performance of FDH and laccase based electrodes, as well as the feasibility of using Fc-C_6-LPEI/FDH electrodes as bioanodes in enzymatic biofuel cells.

Chapter 4 evaluates the effect of single wall carbon nanotube types, nanotube loading, and redox polymer/enzyme hydrogel solution loading on the electrochemical and enzymatic performance of electrodes. Since the aforementioned nanostructured enzymatic electrodes were constructed based on (6,5) SWNTs network, we test the hypothesis that the modification of glassy carbon electrodes with a different SWNTs type (7,6), which has a higher electrical conductivity, would further improve the

electrochemical and enzymatic performance of electrode. We also demonstrated that carbon nanotube loading and redox polymer/enzyme hydrogel solution loading are important factors affecting the performance output of electrodes and biofuel cells.

Chapter 5 covers the effect of SWNTs incorporation methods on the electrochemical and enzymatic performance of electrodes and on the performance of biofuel cell output. Meanwhile, we investigated whether the incorporation of single wall carbon nanotubes can be applicable to construct other enzyme based electrodes and biofuel cells with improved performance. This chapter answers our questions about the effect of incorporating SWNTs on the performance of nanostructured enzymatic biofuel cells, including power density, current density, and stability.

Chapter 6 discusses the feasibility of constructing redox polymer/enzyme hydrogel electrodes using a high surface MWCNT forest prepared by chemical vapor deposition. The effect of burning to remove oil residue and surfactant treatment to change the surface property from hydrophobic to hydrophilic on the electrochemical and enzymatic performance of electrodes are investigated in this chapter.

Chapter 7 includes a summary of the major conclusions of this work. In addition, suggestions for future work are presented.

Chapter 2:

Effect of Surfactant Type, Redox Polymer Type and Nanotube Loading on Single-Walled Carbon Nanotube Modified Electrodes

Major portion of this chapter was reproduced in part with permission from:

Jie Chen , Tu O. Tran , Michael T. Ray, Daniel B. Brunski, Joel C. Keay, David Hickey, Matthew B. Johnson , Daniel T. Glatzhofer , and David W. Schmidtke. Effect of Surfactant Type and Redox Polymer Type on Single-Walled Carbon Nanotube Modified Electrodes. *Langmuir*, **2013**, 29, 10586-10595.

Published work copyright 2013 American Chemical Society.

INTRODUCTION

The development of carbon nanotube based structures for biomedical applications has attracted significant interest in recent years due their unique electrical, mechanical, and optical properties. Some of the more popular nanotube based structures developed include carbon nanotube arrays[92, 93], fibers[94, 95], films[96, 97], paper[44, 98], and yarns[99, 100]. The properties of these structures is dependent on the type of carbon nanotubes used (e.g. single-walled vs. multi-walled[101, 102], metallic vs. semiconducting[103, 104, 105], chirality[106]) as well as the degree of nanotube bundling and agglomeration[107], alignment[108, 109, 110], and nanotube length[111, 112].

A major challenge in developing nanotube-based biosensors is to integrate the nanotubes into the design in such a way that maximally exploits their exceptional properties. Normally as-produced carbon nanotubes are agglomerated into bundles due to strong van der Waals interactions between the tube walls. In addition pristine carbon nanotubes are relatively insoluble in the normal aqueous solutions that are compatible with most biological recognition molecules (e.g. enzymes, antibodies, DNA) used in biosensor construction. To take full advantage of the unique properties of SWNTs typically requires that the nanotubes be isolated rather than in bundles. Thus various methods of dispersing nanotubes via covalent and noncovalent

modification have been employed[113, 114, 115, 116, 117]. In the category of noncovalent modification, the use of surfactants[114, 118] such as sodium cholate, sodium dodecyl sulfate (SDS), and sodium dodecylbenzene sulfonate (NaDDBS) are commonly employed.

Once stable dispersions of carbon nanotubes are produced, two common approaches to incorporate them into biosensing platforms is the formation of carbon nanotube paper (also known as bucky paper) [119],[120] or simple solution casting of the carbon nanotubes onto an electrode surface[121,122, 123]. The main difference between these methods is that in bucky paper formation the solution is filtered under vacuum or pressure through a microporous membrane. In either method, an entangled mat of nanotubes is formed, providing a conductive, high surface area support for biomolecule immobilization.

Previously, we have reported that the incorporation of SWNTs into redox polymer/enzyme hydrogel film dramatically increased both the electrochemical and enzymatic response of sensors. The incorporation of SWNTs into cross-linked films of glucose oxidase (GOX) and a ferrocene redox polymer based on linear polyethylenimine (Fc-C_6-LPEI) film resulted in a 4-5 fold increase in the oxidation and reduction peak currents during cyclic voltammetry, while the glucose electro-oxidation current was increased 5 folds[124]. Similar effects were also observed when SWNTs were integrated into films of GOX and an osmium based redox polymer, poly[(vinylpyridine)Os(bipyridyl)$_2$Cl$^{2+/3+}$] (PVP-Os), which showed 3-fold increase in the glucose response[125]. In this chapter, we investigate whether providing a high surface area network of signal wall nanotubes would increase the electrochemical and enzymatic performance of sensor. We demonstrate that the choice of surfactants used to disperse SWNTs in aqueous solution is a significant factor that affects the

electrochemical and enzymatic performance of crosslinked redox polymer-enzyme films deposited onto SWNTs films. We also investigate the influence of redox polymer type and nanotube loading on the sensor performance with the different SWNTs networks. To the best of our knowledge, this is the first paper discussing the influence of different surfactants dispersed SWNTs films on the electrochemical and enzymatic response of redox polymer/GOX based sensor.

EXPERIMENTAL SECTION

Chemicals and solutions

Glucose oxidase (GOX) from *Aspergillus niger* (EC 1.1.3.4, type X-S, 179 units/mg solid,75% protein), sodium cholate and Tween 20 were purchased from Sigma Aldrich. Triton X-100 was purchased from EM Science. NaDDBS (sodium dodecylbenzenesulfonate) was purchased from TCI America. Poly(ethylene glycol) diglycidyl ether 400 (PEGDGE) and ethylene glycol diglycidyl ether (EGDGE) were purchased from Polysciences, Warrington, PA. Purified CoMoCAT single-wall carbon nanotube (batch WW2) was provided by South West Nanotechnologies. All nanotubes, chemicals and solvents were used as received without further purification. Phosphate-buffered saline solution (PBS) pH 7.4, was prepared in nanopure deionized water as previously described[125]. Stock solutions of glucose (2M) were prepared in water and refrigerated at 4°C when not in use. The redox polymers PVP-Os[126], Fc-C_6-LPEI[127], and Fc-C_3-LPEI[127] were prepared as previously described.

SWNTs were dispersed by adding 2 mg SWNTs into 5 ml aqueous solution with different surfactants: Triton X-100 (TX), Tween 20 (TW), sodium cholate (SC) and sodium dodecylbenzenesulfonate (NaDDBS) in 7 mL vials (Figure 2.1). The corresponding concentration of TX, TW, SC and NaDDBS surfactants in the aqueous solutions were 10, 5, 20 and 5 g/L, respectively. SWNTs aqueous solutions were

ultrasonicated for 1 hour with a horn sonic dismembrator (Model 500, Fisher Scientific) operating at 22% output.

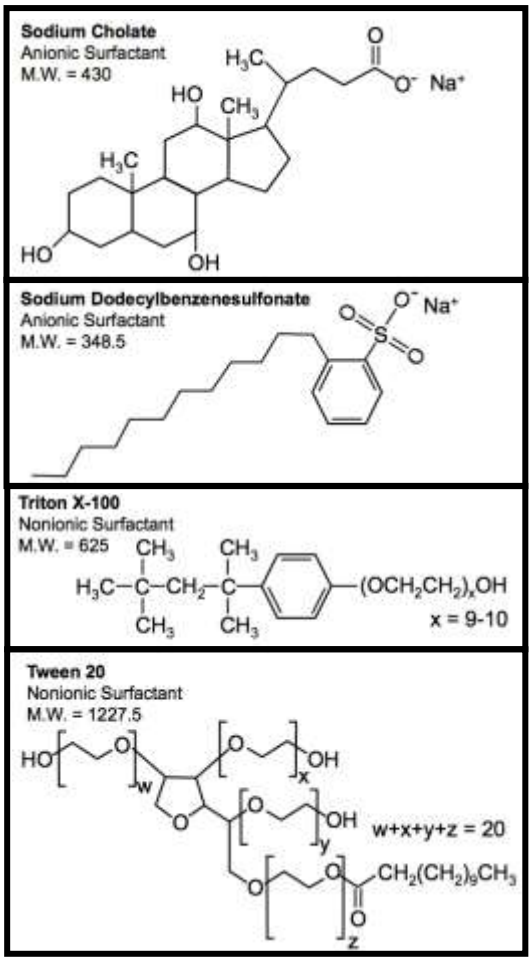


Figure 2.1 Chemical structure of the surfactants used to disperse single-walled carbon nanotubes in this study.

UV-vis Spectrophotometry

To assess the ability of the different surfactants to disperse the SWNTs, absorption spectra of the different SWNTs solutions were taken with a UV-Vis spectrophotometer (CARY-50, Varian) and a specialized adjustable quartz cuvette set with a 0.38-mm light path. All suspension solutions were at a concentration of 0.4 mg/ml SWNTs, and resonance ratios and normalized widths were calculated by the method of Tan[128].

Enzyme Sensor Construction

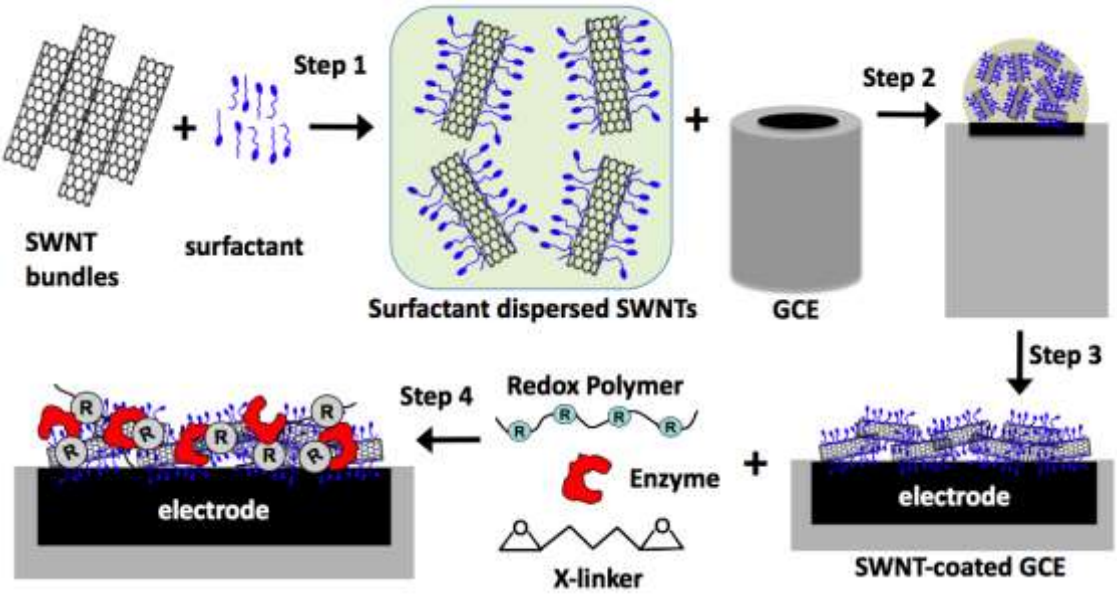


Figure 2.2 Schematic of the construction of redox polymer/enzyme biosensors incorporated with SWNTs film

Glassy carbon electrodes with a 3 mm diameter were polished successively on three grades of alumina (5, 1, and 0.3 μm), and washed thoroughly with nanopure water after each polishing step. The PVP-Os solution (10 mg/mL) was prepared by dissolving PVP-Os polymer in water, while solutions of Fc-C_3-LPEI and Fc-C_6-LPEI were prepared by dissolving them in water and adding 0.1 M HCl solution until the final concentration of the polymer solution was 10 mg/mL and pH was 5[127].

Glucose electrodes were prepared by the two-step procedure shown in Figure 2.2. First, 10 μl of a SWNTs dispersion in water, TX, TW, SC and NS solutions (0.4 mg/mL) was cast on top of a polished glassy carbon electrode and allowed to dry overnight at room temperature to form a SWNTs film on top of GCE. The nanotube loading on GCEs was 4 μg. Second, redox hydrogels were made from solutions of polymer [PVP-Os, Fc-C_3-LPEI, Fc-C_6-LPEI] (10 mg/mL in water), GOX, and a fresh crosslinker solution. Hydrogels made with PVP-Os were made by combining solutions of PVP-Os (10 mg/mL in water), GOX (13.9 mg/mL in H_2O), and freshly

dissolved PEGDGE (2.5 mg/mL in water) mixed in a 59:36:5 vol % ratio. Similarly, hydrogels made with Fc-C_3-LPEI, and Fc-C_6-LPEI consisting of 14 μL of polymer solution (10 mg/mL), 6 μL of GOX solution (10 mg/mL), and 0.75 μL of EGDGE solution (10% v/v) were mixed together. Next, a 3.3 μl aliquot of the respective redox polymer/enzyme/crosslinker mixture was then deposited on top of a SWNTs coated glassy carbon electrodes and allowed to dry for at least 12 h.

Electrochemical Measurements

Electrochemical characterization (i.e. cyclic voltammetry and constant potential experiments) was performed in a three-electrode cell configuration (counter electrode = platinum wire, reference electrode = saturated calomel electrode, SCE) with a CH Instruments model 832 bipotentiostat. The background electrolyte was phosphate buffered saline (PBS), pH 7.4, and the temperature was maintained at 25±1°C with a water-jacketed electrochemical cell. The response to glucose was measured by adding aliquots of a stock 2 M glucose solution to a well-stirred cell with the working electrode poised at 500 mV vs. SCE.

Characterization of SWNTs Films

To characterize the structure of the SWNTs films formed with the various surfactant suspensions, 2 mm diameter glassy carbon rods were attached to a custom-built tripod polisher with mounting wax (MWS 052, South Bay Tech.) and polished as described above. Aliquots (2 μl) of the SWNTs suspensions were cast on top of a polished glassy carbon and allowed to dry overnight at room temperature to form SWNTs films. Differential interference contract (DIC) images of the SWNTs films were acquired with a Nikon Optiphot-66 microscope with a 10x objective and a Nikon DS-Fi1 digital camera (1280 x 960 pixels). Scanning electron microscope images were taken with a Zeiss Neon 40 EsB cross-beam microscope (FE-SEM with

Gemini lens design and focused ion beam (FIB)). The images were taken at low accelerating voltage to reduce beam charging, with an in-lens secondary electron detector.

Calculation and Statistics

Current densities were calculated using the geometric surface area of a 3-mm-diameter electrode. Values are presented as mean ± standard error of the mean (SEM) unless otherwise specified.

RESULTS AND DICCUSION

SWNTs Dispersion Properties

To initially evaluate the stability of SWNTs dispersions prepared in pure water or in different aqueous surfactant solutions (SC, TX, TW and NaDDBS) qualitatively, optical images of the SWNTs dispersions were acquired on day 0 and day 7 (Figure 2.3). Suspensions of SWNTs in aqueous surfactant solutions (SC, TX, TW and NaDDBS) showed a homogenous black colored solution with no signs of aggregation after 7 days. In contrast, the SWNTs suspended in water showed aggregation on day 0 and after 7 days most of the SWNTs settled to the bottom of vial, indicating that the SWNTs/water suspension was unstable.

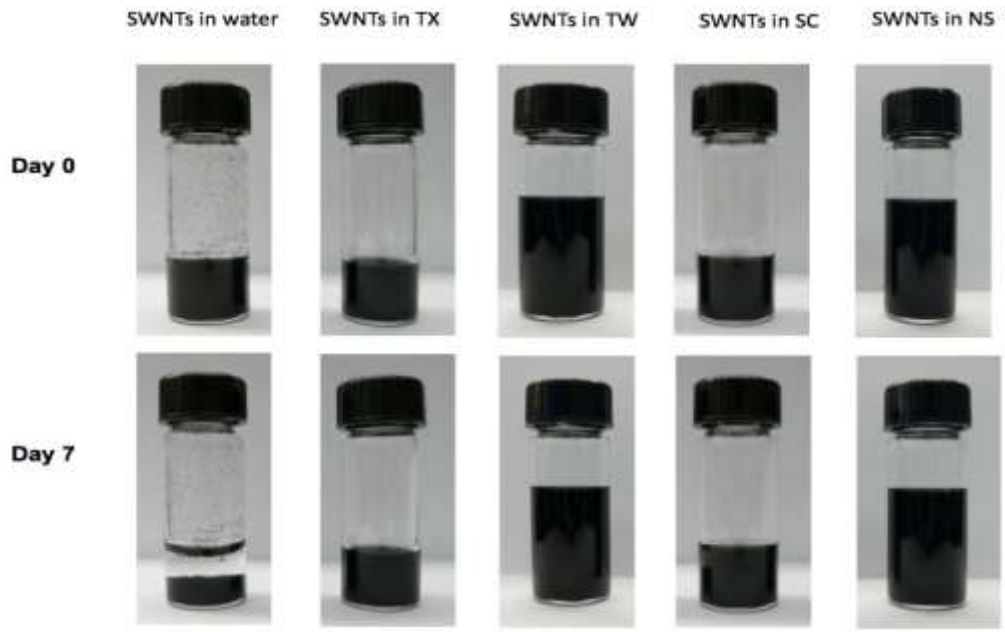


Figure 2.3 Optical images of SWNTs in different aqueous solutions on day 0 and 7.

To assess the quality of the SWNTs suspensions with the different surfactants, we performed UV-Vis spectroscopy. It is known that solutions of well-dispersed single-walled carbon nanotubes display distinct adsorption peaks, and as nanotubes are exfoliated into individual tubes they exhibit better resolved spectral features. As shown in Figure 2.4, all of the SWNTs suspensions containing surfactants exhibited spectra that contained sharp peaks in the visible and infrared regions that are a signature of well-dispersed SWNTs[128, 129]. The strong absorption bands at 980 nm and 570 nm are characteristic of CoMoCAT SWNT samples and are ascribed to the S11 and S22 transitions of (6,5) nanotubes[129]. In contrast, the suspension of SWNTs in water was essentially featureless with no well-defined peaks, which is indicative of SWNTs bundling. To quantify the quality of the suspension we measured the resonance ratio as described by Tan et al[128]. The resonance ratio is defined as the quotient of the resonant band area and its nonresonant background and is related to the fraction of individual nanotubes in the suspension. Table 2.1 shows the resonance ratios measured at the S22 transition (i.e. 570 nm) for the various SWNTs suspensions

ranged from 0.3 for sodium cholate to 0.14 for Tween 20. These values compare quite well with resonance ratios values measured previously[128, 130], and suggest a high fraction of individual SWNTs.

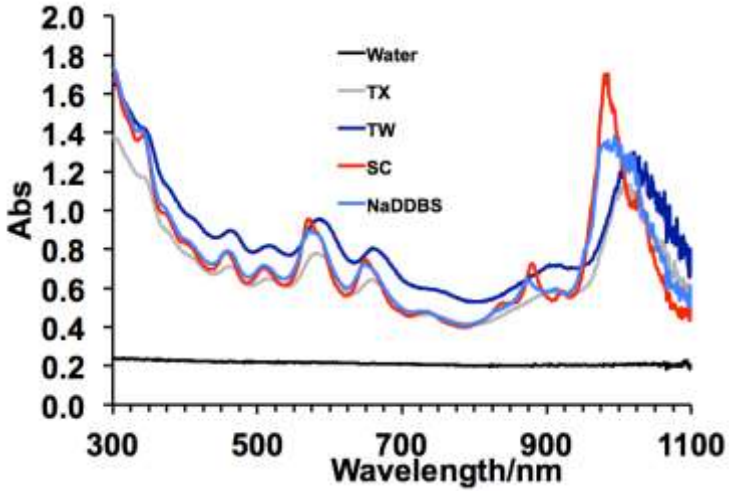


Figure 2.4 UV-VIS spectra of SWNTs solutions dispersed by different surfactants (TX, TW, SC and NaDDBS). The concentration of SWNTs solutions were 0.4 mg/ml.

Table 2.1 Resonance Ratio for the Various Surfactant Suspensions

Solution	Resonance Ratio
SWNTs in H_2O	0
SWNTs in TX	0.16
SWNTs in TW	0.14
SWNTs in SC	0.30
SWNTs in NaDBBS	0.21

Electrochemical Response is Surfactant and Redox Polymer Dependent

Cyclic voltammetry (CV) was performed to investigate how modifying the surface of a glassy carbon electrode with SWNTs via different SWNT-surfactant dispersions would affect the electrochemical response of crosslinked redox polymer/enzyme hydrogels. Figure 2.5A shows the CVs of bare GCE and SWNT-modified GCEs coated with a PVP-Os/GOx film in PBS. For GCE modified with a PVP-Os/GOX hydrogel film in the absence of SWNTs, a pair of well-defined redox

peaks corresponding to the oxidation and reduction of the redox polymer's Osmium complexes was observed at 353 and 274 mV versus SCE, respectively (ΔE=79 mV).

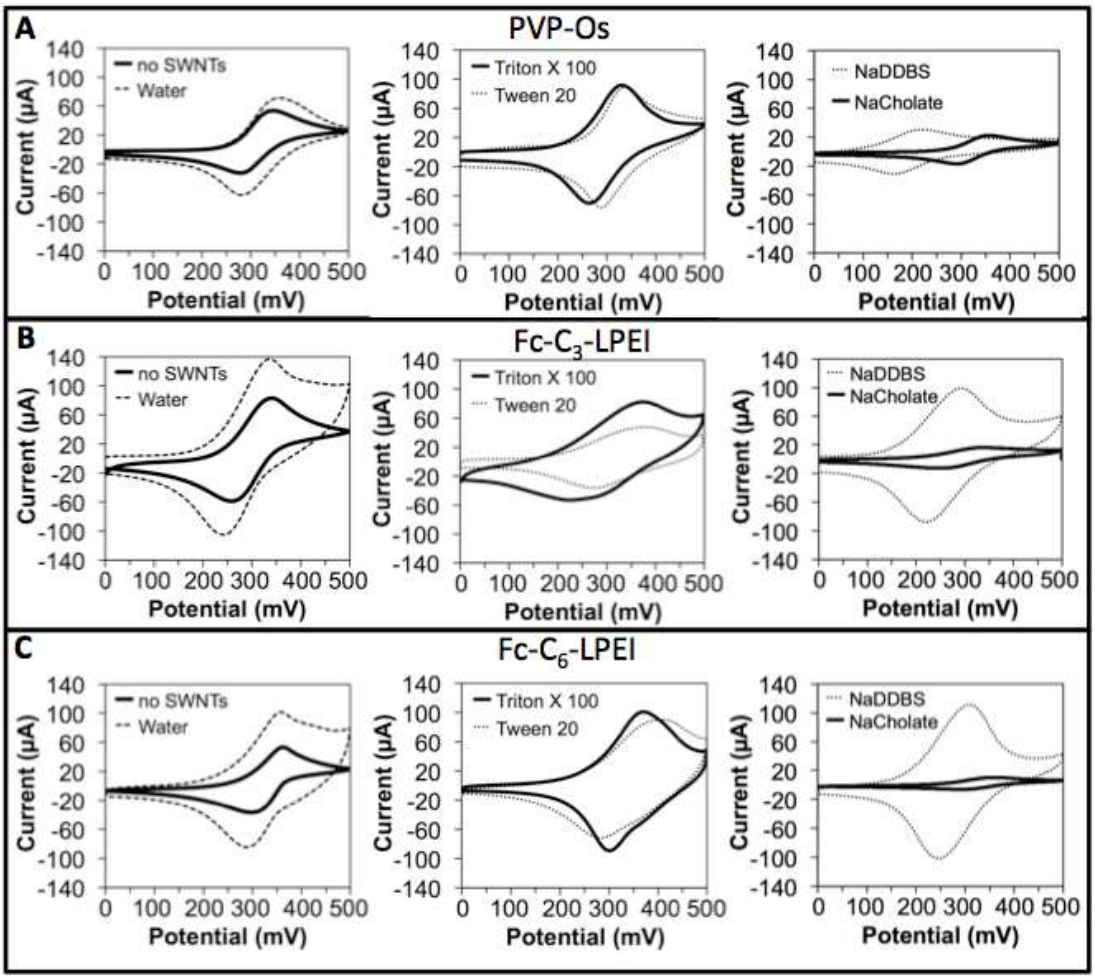


Figure 2.5 Effect of redox polymer and surfactant type on the electrochemical behavior of SWNT composite films. Cyclic voltammograms of GCEs coated with SWNT films and hydrogels containing Glucose oxidase and three different redox polymers: (A) PVP-Os; (B) Fc-C_3-LPEI; (c) Fc-C_6-LPEI. SWNT films were formed by drop casting SWNT dispersions made from solutions of water, nonionic surfactants (i.e. Triton X-100, Tween 20) or anionic surfactants (i.e. NaDDBS, sodium cholate). Scan rate=50 mV/s in PBS at 25°C

As shown in Figure 2.5A, the effect of modifying GCEs with SWNTs on the electrochemical response was highly dependent on the dispersion surfactant. When GCEs were modified with dispersions of SWNTs in water, there was a significant increase in both the oxidation and reduction peak currents with a slight change in the oxidation redox potential. Likewise modification of GCEs with SWNT dispersions in Triton X-100 or Tween 20 resulted in an increase in the background current and a ~2-

fold increase in the oxidation and reduction peak currents. In contrast, modification of the GCEs with SWNTs dispersed in NaDDBS resulted in a ~50% decrease in the oxidation and reduction currents and a surprising shift in the oxidation and reduction peak potentials by about 100 mV. In a similar manner, modification of GCEs with dispersions of SWNT in sodium cholate also decreased the peak currents (~70%), however the oxidation and reduction peak potentials did not significantly shift. The exact cause of why two of the surfactant-SWNT dispersions (Triton X-100 and Tween-20) increased the electrochemical response why the other two (sodium cholate and NaDDBS) caused a reduction in the response is not known. One potential explanation may be related to the fact that both Triton X-100 and Tween-20 are nonionic surfactants while both sodium cholate and NaDDBS are anionic surfactants. Thus the negative charge of the anionic surfactants may disrupt the normal electrostatic complexation that takes place between PVP-Os and GOX[131].

To investigate whether the type of redox polymer affects the electrochemical performance of GCE modified with SWNT-surfactant dispersions, we performed similar experiments to those with PVP-Os, but with two ferrocene based redox polymers (Fc-C_3-LPEI and Fc-C_6-LPEI) (Figure 2.5B and 2.5C). For GCE electrodes modified with SWNTs dispersions in water, Triton X-100 or Tween-20 and coated with Fc-C_6-LPEI/GOX hydrogels, we observed 2.5-, 2.9- and 3.1-fold increase of peak current, compared with GCEs without SWNTs film (Fig. 2.5C). In addition the background currents were increased as well. Although the magnitude of the increases with Triton X-100 and Tween-20 and Fc-C_6-LPEI based films was higher than with the PVP-Os polymer there were in the same direction.

Similar to the results with PVP-Os, GCEs coated with sodium cholate-SWNT dispersions and Fc-C_6-LPEI/GOX films resulted in a dramatic decrease in the

oxidation and reduction peak currents (Fig 2.5C). However, we surprisingly observed that GCEs coated with NaDDBS-SWNT dispersions and the Fc-C_6-LPEI/GOX films led to a significant increase in the oxidation and reduction peak currents which were on the same order of magnitude as both Triton X-100 and Tween-20. This was in direct contrast to the results with PVP-Os and suggests that the proposed decreases in the PVP-Os case were not solely due to the anionic nature of the NaDDBS.

Table 2.2 Effect of SWNT Films on Peak-to-Peak Separation Potential ΔE_p (mV) [a]

Solution	**ΔEp (mV)**		
	PVP-OS/GOx	Fc-C_3-LPEI/GOx	Fc-C_6-LPEI/GOx
no SWNTs	66±2	82±1	70±1
SWNTs in H_2O	77±4	94±6	82±2
SWNTs in Triton X-100	68±5	147±3	121±3
SWNTs in Tween 20	50±3	103±6	145±3
SWNTs in sodium cholate	62±4	55±5	95±3
SWNTs in NaDDBS	60±3	70±1	77±5
a Scan rate = 50 mV/s, PBS (pH 7.4), T = 25 °C.			

Figure 2.5B shows the results with GCEs coated with SWNTs and Fc-C_3-LPEI/GOX films. In contrast to the results with PVP-Os or Fc-C_6-LPEI, the highest response in terms of peak currents was observed with SWNTs dispersed in water. Surprisingly the response with GCEs coated with Triton X-100 showed minimal increase and the response with Tween-20 actually decreased. Similar to the results with PVP-Os and Fc-C_6-LPEI, GCEs coated with sodium cholate led to dramatic decreases in the sensor response. Finally the response of GCEs coated with NaDDBS and Fc-C_3-LPEI/GOX films (Fig. 2.5B) showed an increase in the response as well as a 100 mV shift in the redox potential similar to that of Fc-C_6-LPEI. In contrast to the results with PVP-Os, there were considerable shifts in the peak-to-peak separation

potentials when either the Fc-C_3-LPEI or theFc-C_6-LPEI films were coated onto the surfactant deposited SWNT films (Table 2.2). In particular Triton X-100 and Tween-20 films increased (ΔE_p) to greater than 100 mV, which is characteristic of sluggish electron transfer kinetics.

Taking all the electrochemical results into consideration, the only consistent observations were that (i) dispersion of SWNTs in water led to a significant increase in the electrochemical response; and (ii) dispersions of SWNTs in sodium cholate led to dramatic decreases in the electrochemical response. Like NaDDBS, sodium cholate is an anionic surfactant and given the fact the NaDDBS increased the electrochemical response with both Fc-C_6-LPEI and Fc-C_3-LPEI, the decreased response with sodium cholate is probably not due to the negative charge. The observation that sodium cholate led to decreases in the electrochemical response with all three of the redox polymers appears to support our suggestion above that some of the observed differences in the electrochemical response are due to differences in the surface coverage of surfactant on the SWNTs. This issue will be discussed in further detail below.

Enzymatic Response is Surfactant Dependent

Constant potential (0.5 V vs. SCE) experiments were performed to investigate how modifying the surface of a glassy carbon electrode with SWNTs via different SWNT-surfactant dispersions would affect the enzymatic response of crosslinked redox polymer/enzyme hydrogels to glucose. Figure 2.6 shows the response to glucose of bare GCE and SWNT-modified GCEs coated with a PVP-Os/GOX, Fc-C_6-LPEI/GOX, and Fc-C_3-LPEI/GOX films in PBS.

As shown in Figure 2.6A, all GCEs coated with films of PVP-OS/GOX with and without SWNTs film showed Michaelis-Menten type behavior. Compared with

the glucose response of electrodes without SWNTs (1100 μA/cm^2), GCEs coated with Triton X-100/SWNT, Tween-20/SWNT, or water/SWNT dispersions resulted in a 1.6-, 1.25-, or 1.1-fold increase in the limiting current density, reaching 1747, 1388, and 1200 μA/cm^2, respectively. In contrast, GCEs coated with sodium cholate/SWNT or NaDDBS/SWNT dispersions resulted in dramatic decreases of the glucose oxidation currents 200 μA/cm^2 and 10 μA/cm^2, respectively. It is interesting to note that this trend in glucose response of Triton X-100 and Tween-20 dispersed SWNTs giving enhanced responses while sodium cholate and NaDDBS dispersed SWNTs appear to be in agreement with the electrochemical results of Figure 2.5.

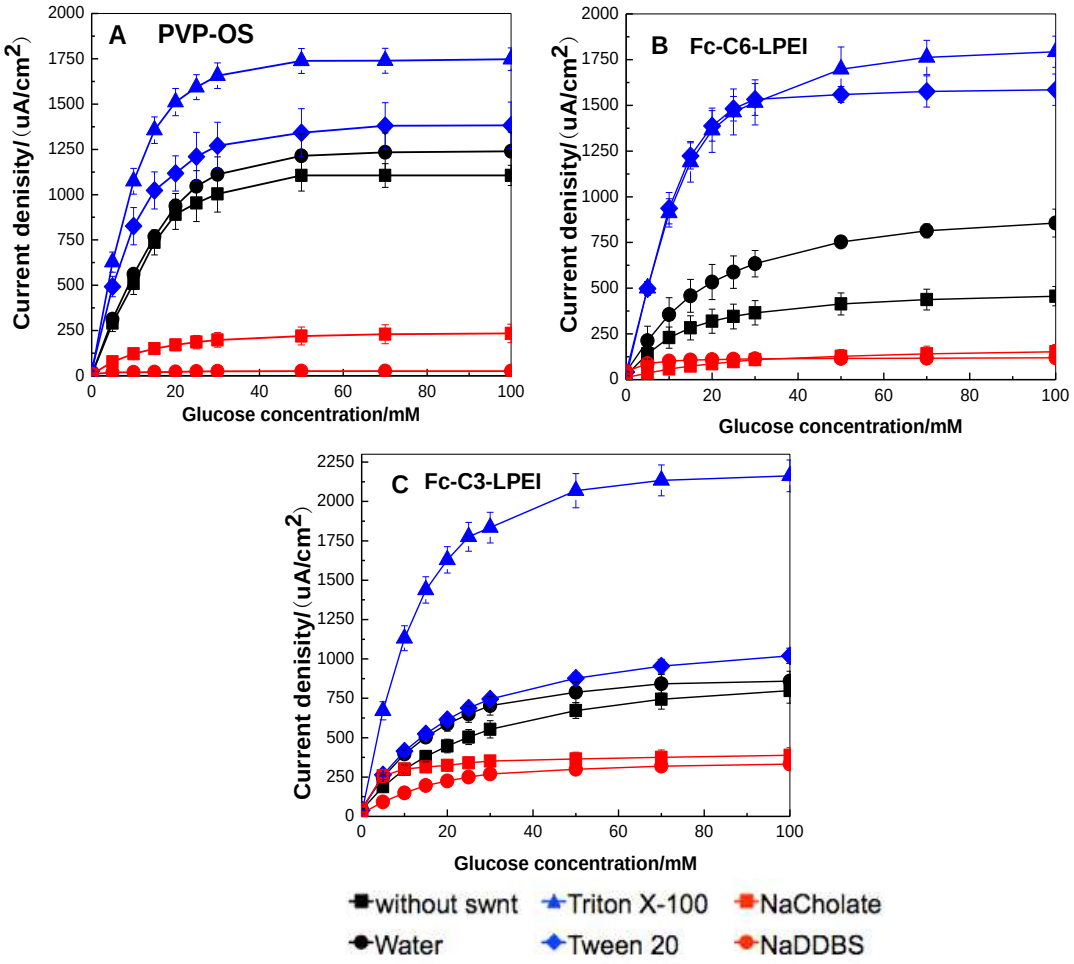


Figure 2.6 Glucose calibration curves for three different polymers (A) PVP-Os, (B) Fc-C_6-LPEI, (C) Fc-C_3-LPEI based electrodes incorporated with different SWNTs film. T=25°C, E=0.5 V vs. SCE. The data points are the average of 4-6 electrodes.(mean± SEM)

The response of GCEs coated with hydrogels of Fc-C_6-LPEI/GOx with and without SWNTs films are shown in Figure 2.6B. Similar to the results of Figure 2.6A with the PVP-Os redox polymer, GCEs coated with Triton X-100/SWNT and Tween-20/SWNT dispersions gave the highest responses. It should be noted however that the increase with Fc-C6-LPEI/GOX films was significantly greater (3.9- and 3.5-fold respectively). Likewise GCEs coated with Sodium cholate/SWNT or NaDDBS/SWNT dispersions resulted in dramatic decreases of the glucose oxidation current. Although the enzymatic responses of Triton X-100, Tween-20, and sodium cholate dispersed SWNTs were in agreement with the electrochemical results of Figure 2.5, the results with NaDDBS dispersed SWNTs were opposite (Figure 2.5).

Finally, the response of GCEs coated with hydrogels of Fc-C_3-LPEI/GOX with the different SWNTs films are shown in Figure 2.6C. Once again GCEs coated with Triton X-100/SWNT dispersions gave the highest response with a current response of 2200 $\mu A/cm^2$. GCEs coated with Tween-20/SWNT also gave an increased response, however the magnitude of this response was much smaller. GCEs coated with sodium cholate/SWNT or NaDDBS/SWNT dispersions resulted in decreases of the glucose oxidation current by 50 and 55% respectively.

Taking into account the results with the three different redox polymers, it appears that the use of SWNT dispersions with non-ionic surfactants (e.g. Triton X-100 and Tween-20) enhanced the enzymatic response, while SWNT dispersions with anionic surfactants (e.g. sodium cholate and NaDDBS) reduced the enzymatic response. At this time the causes of the enhancement and reduction are unknown. However given the fact that the formation of an electrostatic complex between redox polymer and enzyme is required for enhanced electrical communication[131], one possible mechanism for the reduced response observed with sodium cholate and

NaDDBS is that the negative charge on the anionic surfactants may interfere with the normal redox polymer/enzyme complexation. Likewise, studies[132] have suggested that ionic surfactants may denature proteins through hydrophobic, ionic, or hydrogen bonding interactions. Further experiments are underway to verify this hypothesis.

SEM imaging of SWNT films

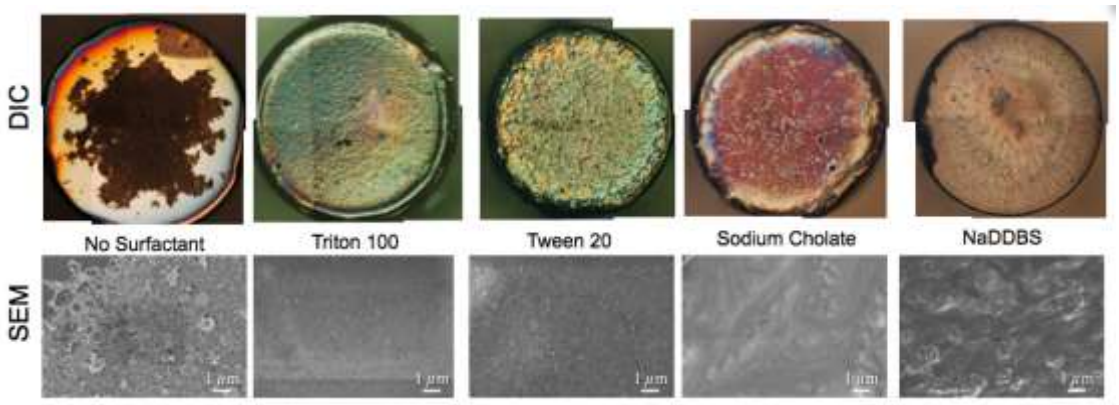


Figure 2.7 Differential interference contrast (DIC) and SEM images of electrodes coated with SWNT solutions with: no surfactant, non-ionic Triton 100 and Tween 20 surfactants, and ionic sodium cholate and NaDDBS surfactants. The DIC images show the whole 2 mm diameter glassy-carbon electrode and are montages of several images taken using a 10x objective. SEM images were taken with in an in-lens scanning electron detector. Some images show charging bands (Triton 100, especially) due to charging under the electron beam.

To investigate whether the changes in the electrochemical and enzymatic responses observed were related to the structure to the SWNT films deposited on the GCEs, we performed both differential interference contrast (DIC) and scanning electron microscopy (SEM). The DIC images (Figure 2.7) show the medium to coarse-scale (>10μ) nature of the SWNT solution coated glassy-carbon electrodes. The solution with no surfactant shows poor wetting and the NaDDBS solution shows some phase separation (similar to viscous fingering[133], while the Triton, Tween and sodium cholate films appear similarly homogeneous on this scale. The SEM images show the fine-scale nature (<10μm) of the coatings. The no surfactant coating shows poor uniformity, similarly both the NaDDBS and sodium

cholate surfactant solutions show inhomogeneity on this fine scale, whereas both the Triton 100 and the Tween 20 show good homogeneity below 1 μm.

The observations that (i) the electrodes fabricated with SWNTs dispersed in pure water, that poorly wetted the electrode surface displayed increased electrochemical and enzymatic responses, and (ii) electrodes fabricated with SWNTs dispersed in sodium cholate solutions that uniformly wetted the electrode surface displayed decreased electrochemical and enzymatic responses; suggest that the uniformity of the SWNT film was not the primary cause for changes in the enzymatic and electrochemical performance observed with the various surfactants.

Effect of SWNT films on Diffusional Mediators

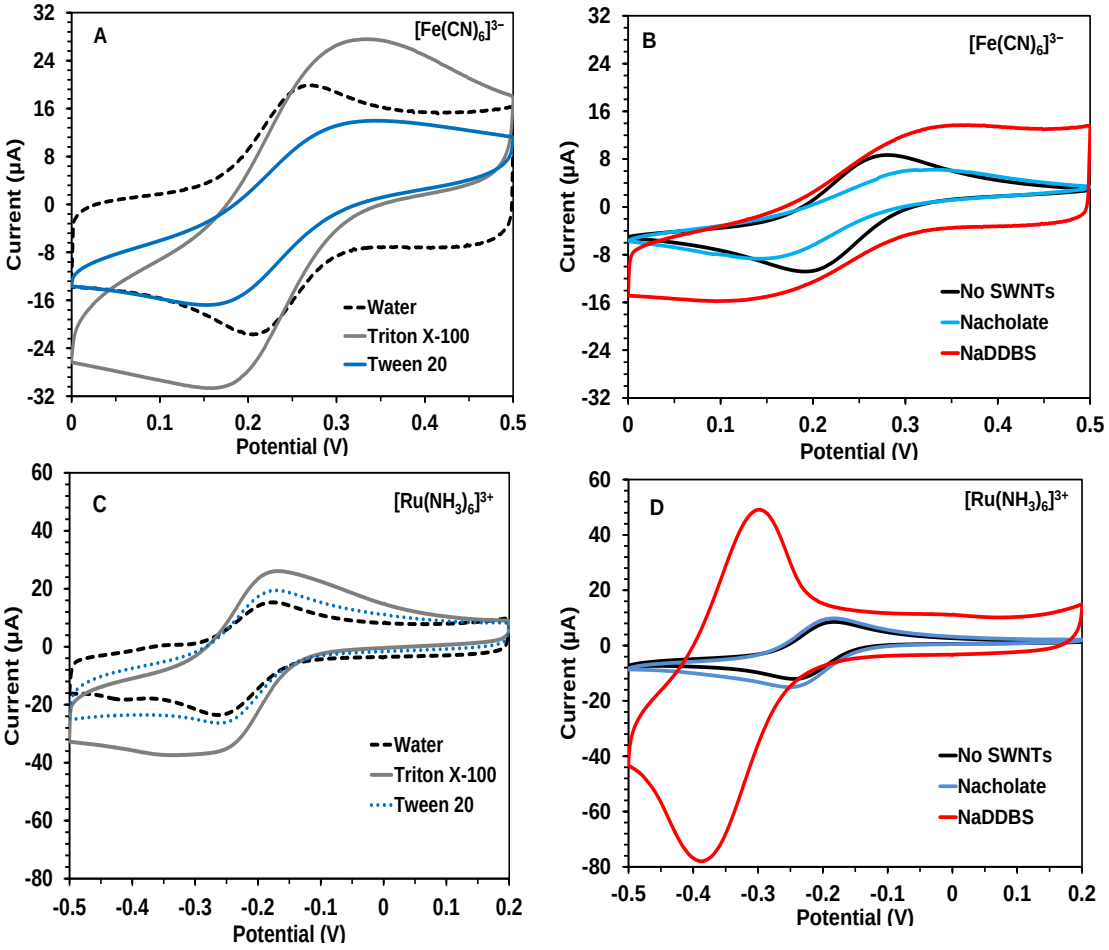


Figure 2.8 Electrochemical response of diffusional mediators on different SWNT films. Cyclic voltammograms of GCEs coated with different SWNT films in the presence of 1 mM $K_3[Fe(CN)_6]$ (A, B), or 1 mM $Ru(NH_3)_6Cl_3$ (C, D). Scan rate = 50 mV/s, T = 25 °C.

As discussed above, we hypothesize that some of the electrochemical results obtained with the redox polymer/enzyme hydrogels were related to the surfactant surface coverage of the SWNTs as well as to differences in the chemical structure of the surfactants. To further investigate this matter, we coated GCEs with the various dispersions of SWNTs as described previously (Figure 2.1, steps 1−3) but without applying the redox polymer/ enzyme mixture. Instead we placed these SWNT coated GCEs into aqueous solutions containing either a cationic diffusional mediator, ruthenium hexamine, $[Ru(NH_3)_6]^{3+}$, or an anionic diffusional mediator, ferrocyanide ($[Fe(CN)_6]^{3-}$). In theory, the presence of the anionic surfactants (sodium cholate, NaDBBS) should show a reduced response with ferrocyanide due to charge repulsion, and an enhanced response with ruthenium hexamine due to charge attraction.

When GCEs coated with SWNT films made from water,Triton X-100, or Tween 20 were tested in solutions of ferrocyanide (Figure 2.8A) or ruthenium hexamine (Figure 2.8C),there was a significant increase in the oxidation and reduction currents as compared to GCEs with no SWNT coatings (Figures 2.8B, 2.8D). These results are similar to the electrochemical results with the three different redox polymers and provide additional evidence that the SWNT films made from these dispersions provide additional electrochemical surface area.

Testing of NaDDBS films in ferrocyanide also showed an increase in the current response (Figure 2.8B), which was similar in magnitude to that of the Tween 20 films (Figure 2.8A). When NaDDBS films were tested in ruthenium hexamine solutions (Figure 2.8D), the response was ~2-fold higher than any other film, and both the oxidation and reduction peak potentials were significantly shifted. The fact that the NaDDBS response increased in the presence of the anionic mediator suggests that some of the SWNT surface was not covered by anionic surfactant and accessible

to an anionic diffusional mediator. The observation that the response was dramatically enhanced in the presence of the cationic mediator is consistent with a charge attraction process between the mediator and surfactant. In addition the shift to lower oxidation and reduction redox potentials is similar to our results with the Fc-C_3-LPEI and Fc- C_6-LPEI coatings.

As predicted, testing of the sodium cholate films in solutions of the anionic mediator ferrocyanide showed a decreased response (Figure 2.8B). However there was no increase in the response when tested in the cationic mediator ruthenium hexamine (Figure 2.8D). Both of these observations are consistent with the picture that the sodium cholate is essentially blocking the surface of the SWNTs and thus allowing for little to no increase in the electrochemical surface area. As suggested in the literature, the high affinity for sodium cholate to the SWNTs is most likely due to the presence of the hydrophobic naphthenic groups.

Effect of nanotube loading on the performance of electrodes

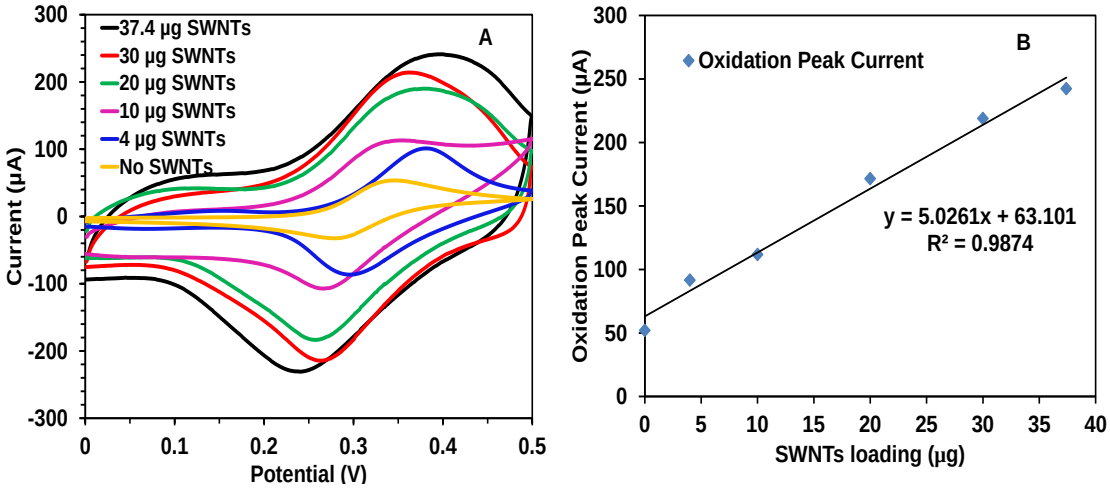


Figure 2.9 (A) Effect of the SWNTs film loading on electrochemical performance of PVP-OS/GOx based biosensors: scan rate: 50 mv/s in PBS (pH 7.4) at 25 ℃. (B) Dependence of the oxidation and reduction peak current on the SWNT film modified electrodes with different loading

To explore the effect of SWNTs film loading on the electrochemical performance of redox polymer hydrogel, different concentrations of SWNTs films

(0.4-3.74 mg/ml) were cast onto bare glassy carbon electrodes followed by coating with a PVP-OS/GO_X hydrogel film. The amount of SWNTs solution applied was kept constant (10 µL). Figure 2.9 (A) shows cyclic voltammograms of PVP-OS/GO_X electrodes with different SWNTs film loadings. Compared with control GCEs, electrodes modified with nanotube films exhibited higher oxidation and reduction peak current. The oxidation and reduction peak current increased as the SWNT film loading increased. Meanwhile, it can be observed that the modification of GCEs with SWNT films broadened the oxidation and reduction peak separation, indicating sluggish electron transfer kinetics. The broadening of redox peak separation was consistent with our previous reports and others. The relationship between SWNTs film loading and oxidation peak currents is shown in Figure 2.9 (B). From this figure, the oxidation peak currents of electrodes showed a linear relationship with the SWNTs film loading, indicating more and more active sites of redox polymer became electrochemical accessible with the increase of SWNT loading. The increase of electrochemical performance may due to the three dimensional structure of the SWNT network providing an alternative electron transfer pathway for electrons to be transported from distant redox polymer active sites to electrode surface or between the neighboring of redox polymer centers.

Figure 2.10 shows the effect of SWNTs film loading on the enzymatic response to glucose. Compared with electrodes without SWNTs, the glucose response of electrodes increased initially with the increase of SWNT film loading, then plateaued. Electrodes with a SWNTs film of 10 µg exhibited the highest glucose response of 2664 µA/cm^2, 2.4 folds higher than electrodes without SWNTs films. Further increasing the SWNTs film loading from 10 µg to 37.4 µg resulted in a slight decrease of glucose response. The enzymatic response was not quite in full agreement

with the electrochemical results in Figure 2.9 where the oxidation peak current kept increasing with high SWNTs loading. These results indicated that the enzymatic response or current is not limited by the electron transport through the redox polymer matrix to the electrode surface, but rather electron transfer from the FAD active sites of enzyme to the SWNTs film or redox polymer. Besides, it is interesting to observe that the incorporation of SWNTs film into PVP-OS/GOx electrodes decreased the apparent K_m value. The apparent K_m for PVP-OS/GOX electrodes without SWNTs film was around 10.97, while the K_m for electrodes incorporated with different SWNTs film loading (4, 10, 20, 30, 37.4 µg) were 7.97, 8.05, 7.7, 7.3 and 7.08, respectively. The decrease of K_m value with the modification of nanotube suggested that the incorporation of SWNTs film could lead to an obvious increase in the affinity between glucose oxidase and substrate, which may due to the 3D network of nanotube network led to a decreased mass transfer resistance.

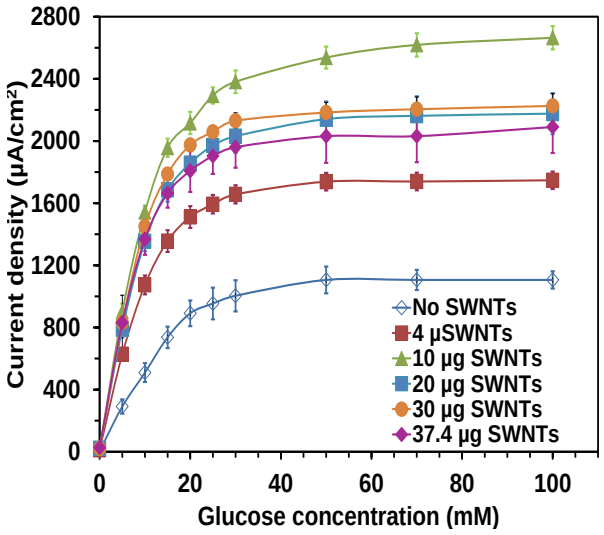


Figure.2.10 Glucose response for PVP-OS /GO_X based electrodes incorporated with different SWNTs film loading. T=25℃, E=0.5 V vs SCE

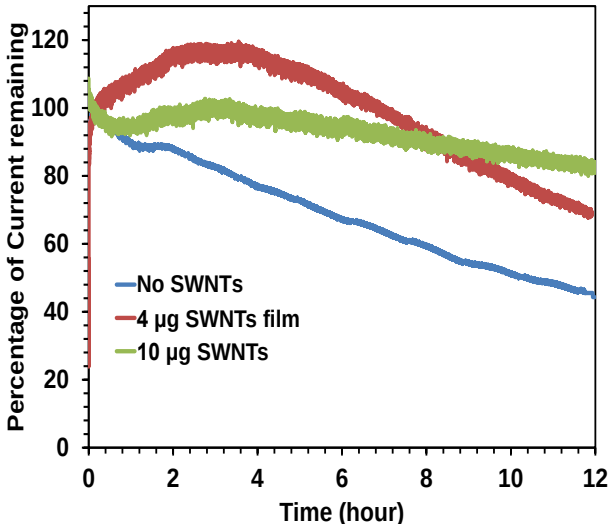


Figure 2.11 Effect of SWNTs films on the enzymatic stability of PVP-OS/GO_X biosensors. Cross-linked films of GOX and PVP-OS films containing no SWNTs, 4 µg SWNTs films and 10 µg SWNTs films were operated continuously in PBS at pH 7.4 and 10 mM glucose. E= 0.5V, T=25 ℃

Stability tests were performed to determine whether the incorporation of different SWNT films into the PVP-OS/GOX based electrodes would affect the enzymatic stability of the electrodes. Figure 2.11 shows continuous operation stability tests for PVP-OS/GO_X based electrodes without SWNT and with SWNTs films loading of 4 µg and 10 µg. After 12 hours of operation, PVP-OS/GO_X electrode without SWNTs retained 45.2% of its original current. For electrodes with the modification of 4 µg and 10 µg SWNTs film, the percentage of current remaining was 69.5% and 83.2%, respectively. From the results shown above, the incorporation of SWNT film into redox polymer hydrogel film improved the enzymatic stability of the films obviously.

CONCLUSIONS

In this study we investigated the electrochemical and enzymatic performance of glassy carbon electrodes (GCEs) modified with SWNT films and redox polymer/enzyme hydrogels. All of the surfactants examined were able to disperse the SWNTs and form stable suspensions in solution, but different SWNT film

morphologies were observed on the electrode surface upon drying. We demonstrated that the enzymatic response of the biosensors was dependent on (i) the type of surfactant used to form the aqueous SWNT dispersion and subsequent SWNT film; and (ii) the type of redox polymer. Biosensors constructed with SWNT suspensions of the non-ionic surfactant Triton X-100 produced the highest enzymatic responses to glucose (~1.7–2.1 mA/cm^2), while biosensors fabricated with either of the anionic surfactants (sodium cholate or NaDDBS) significantly reduced the enzymatic response (> 0.4 mA/cm^2). The fact that these trends in the enzymatic response with the same surfactant type were consistent with three different redox polymers provides evidence for the importance of surfactant type in the fabrication of SWNT-modified GCE biosensors. Similarly, we also observed that the electrochemical response of the biosensors was highly dependent on surfactant type and redox polymer type. We generally observed increases in the electrochemical response with both nonionic surfactants (Triton X-100 or Tween 20). However, the results with anionic surfactants (sodium cholate and NaDDBS) were conflicting. For example NaDDBS significantly reduced the electrochemical response with films made with the PVP-Os redox polymer, but increased the response with both the Fc-C_6-LPEI or Fc-C_3-LPEI redox polymers. In contrast, sodium cholate reduced the electrochemical response with all three redox polymers. We hypothesize that these differences in the electrochemical response maybe related to the differences in the chemical structure between NaDDBS and sodium cholate (e.g. carboxylate vs. sulfonate groups) that may affect their affinity/interaction with to SWNTs and/or the redox polymer.

Furthermore, the effect of nanotube loading on the electrochemical and enzymatic performance of redox polymer hydrogel film was evaluated. Our results showed that compared with electrodes without nanotube film, the incorporation of

different loading of SWNTs films into PVP-OS/GO_X based electrodes resulted in an obvious increase in the electrochemical and enzymatic response. In term of glucose response, the optimum SWNTs film loading on electrodes was **10 µg**. Electrodes with the modification of 10 µg SWNTs film could exhibited a limiting current density of 2664 µA/cm^2, which is 2.4 folds higher than electrodes without nanotube .Further increasing of nanotube film loading decreased the current density output slightly. Meanwhile, the enzymatic stability of electrodes got improved with the incorporation of nanotube film.

Acknowledgements:

I would like to thank Dr. Glatzhofer and Dr. Johnson for all of their suggestions and valuable conversations concerning this work. I would also like to thank David Hickey for synthesizing redox polymers, Michael Ray for taking DIC and SEM images, and Joel Keay for the useful discussion in the SEM images.

Chapter 3:

Development of Fructose Dehydrogenase-Ferrocene Redox Polymer Films for Biofuel Cell Anodes

Major portion of this chapter was reproduced in part with permission from:

Jie Chen, Daniel Bamper, Daniel T. Glatzhofer, and David W. Schmidtke. Development of Fructose Dehydrogenase-Ferrocene Redox Polymer Films for Biofuel Cell Anodes. *J. Electrochem.Soc.* **2014**, submitted for publication.

Unpublished work copyright 2014 Electrochemical Society.

INTRODUCTION

The use of redox polymers to electrically "wire" redox enzymes to electrode supports has been an area of active research since Degani and Heller introduced the concept 25 years ago[134]. Due to the high current output produced by these redox polymer-enzyme hydrogels, a wide variety of bioelectronic devices have been developed, such as biosensors for the monitoring of beverages[135, 136], food[137, 138], *in vivo* metabolites[139, 140, 141, 142], and neurotransmitters[143, 144]. In addition, the strategy of wiring enzymes has been utilized in developing electrochemical immunoassays[145, 146, 147], DNA detection[148], and enzymatic biofuel cells[149, 150, 151, 152]. Another advantage of redox polymers is that they have demonstrated an ability to electrically communicate with a wide range of redox enzymes, such as amine oxidase[137], bilirubin oxidase[153], glucose oxidase [154], glucose dehydrogenase[155], lactate oxidase[142], glycerol oxidase[142], laccase[156, 157], pyruvate oxidase[141], horseradish peroxidase[158], and sulfite oxidase[136].

Given the widespread use of redox polymers, it is surprising that there are only a handful of reports about combining enzyme fructose dehydrogenase (FDH) with redox polymers (Table 3.1). Narvaez et al. first demonstrated the construction of a fructose biosensor by layer-by-layer (LBL) electrostatic self-assembly of a cationic osmium redox polymer, poly[(vinylpyridine)Os(bpy)$_2$Cl] (PVP-Os), and FDH on gold

electrodes[159]. Similarly, Dominguez et al., also employed LBL technique to prepare fructose biosensors based on PVP-Os redox polymer and FDH[160]. More recently, Antiochia et al., reported the preparation of an osmium redox polymer (poly(1-vinylimidiazole)$_{12}$-[osmium(4,4'-dimethyl-2,2'-dipyridyl)$_2$Cl$_2$]$^{2+/+}$(PVI-Os) mediated fructose dehydrogenase biosensor by direct wiring of FDH into the PVI-Os hydrogel for the detection of fructose in fruit juices and soft drinks[135]. Finally, Hickey et al. immobilized FDH into 3-(tetramethylferrocenyl)propyl-modified linear poly(ethylenimine) (FcMe$_4$-C$_3$-LPEI) polymer, to develop bioanodes for fructose as part of an enzyme cascade that catalyze the hydrolysis of sucrose to fructose and glucose, and subsequent oxidation of fructose and glucose[161].

Previously, we have reported that redox polymers based on coupling ferrocene to a linear poly(ethylenimine) (LPEI) backbone can efficiently wire the redox centers of glucose oxidase[162, 163] or horseradish peroxidase to electrode[162] surfaces, producing high current densities of $\geq$ ~1 mA/cm^2. We have also demonstrated that either (i) direct incorporation of SWNTs into redox polymer-enzyme hydrogels[124, 125], or (ii) deposition of redox polymer-enzyme hydrogel onto electrode modified with SWNT film[164], also increases the signal output. In this study, we investigate whether the Fc-C$_6$-LPEI redox polymer can efficiently wire the redox centers of fructose dehydrogenase. To optimize the signal output to fructose, we characterized the effect of the pH of enzyme solution and redox polymer solution used for film formation on the electrochemical and enzymatic response. We also tested the hypothesis that providing a high surface area SWNTs network would increase the electrochemical and enzymatic performance of Fc-C$_6$-LPEI/FDH electrodes. Finally, we investigated the feasibility of using Fc-C$_6$-LPEI/FDH electrodes as bioanodes in enzymatic biofuel cells.

EXPERIMENTAL SECTION

Chemicals and solutions

D-Fructose dehydrogenase from *Gluconobacter sp.* (EC 1.1.99.11, grade III, 179 units/mg solid) was purchased from Toyobo Co. Triton X-100 was purchased from EM Science. Ethylene glycol diglycidyl ether (EGDGE) and Poly(ethylene glycol) diglycidyl ether 400 (PEGDGE) were purchased from Polysciences. Mcilvaine buffer (pH 5) was prepared by dissolving 14.6 g Na_2HPO_4 and 9.3 g citric acid in 1 L of nanopure deionized water. Stock solutions of 2 M D-fructose were prepared in water and subsequently kept refrigerated at 4°C. Purified CoMoCAT single-wall carbon nanotubes (SWNTs) were generously provided by South West Nanotechnologies. All chemicals, solvents and nanotubes were used as received without further purification. Both of the PVP-OS and Fc-C_6-LPEI redox polymers were provided by Dr.Glathofer's lab and synthesized by Daniel Bamper in Glathofer lab [125 ,163].

Dispersions of SWNTs were prepared as previously described[164] by adding 2 or 5 mg of SWNT powder to 5 ml of a Triton X-100 aqueous solution resulting in a final SWNT concentration of 0.4 and 1.0 mg/ml, respectively. The concentration of Triton X-100 in the aqueous solution was 5 g/L. Following initial mixing the solution was ultrasonicated for 1 hour with a horn sonic dismembrator (Model 500, Fisher Scientific) running at 22% output to disperse the SWNTs.

Fructose Dehydrogenase Electrodes

3 mm diameter glassy carbon electrodes (GCE) were successively polished on three grades of alumina (5, 1, 0.3 μm). After each polishing step the electrodes were thoroughly washed with nanopure water. A solution of redox polymer Fc-C_6-LPEI was prepared by dissolving the solid polymer in water and adding small aliquots of a

0.1 M HCl solution until the final concentration of the polymer solution was 10 mg/mL and the pH was 5. A FDH solution (10 mg/ml) was prepared by dissolving 5 mg of FDH in 0.5 ml of water. Crosslinked films of Fc-C_6-LPEI and FDH were prepared by first mixing 14 µL of the 10 mg/ml Fc-C_6-LPEI solution, 6 µL of a 10 mg/ml FDH solution, and 0.75 µL of and aqueous EGDGE (10% v/v) solution, and then depositing a 3 µL aliquot of the mixture onto the surface of a glassy carbon electrode. The mixture was allowed to dry and crosslink overnight under room temperature. In some experiments, a film of entangled SWNTs was formed on the surface of the GCE prior to coating redox polymer/enzyme hydrogel as previously described [164]. To form the SWNTs film, 10 µl of the Triton X-100/SWNTs dispersion was cast on top of a polished glassy carbon electrode and allowed to dry overnight at room temperature. Next a 3 µL aliquot of the Fc-C_6-LPEI/FDH/EGDGE mixture was deposited on top of the SWNTs film and allowed to dry and crosslink overnight.

Laccase Electrodes

A solution of the osmium redox polymer PVP-Os was prepared by dissolving 10 mg of solid polymer in 1 ml of water (10 mg/ml PVP-Os). A laccase solution (35 mg/ml) was prepared by dissolving 10.5 mg of laccase in 0.3 ml of water. Crosslinked films of PVP-Os and laccase were prepared by mixing 14 µL of 10 mg/ml PVP-Os, 6 µL of 35 mg/ml laccase, and 1 µL of PEGDGE (2.5 mg/ml) together, and subsequently casting a 3 µL aliquot onto a 3 mm glassy carbon electrode. The mixture was allowed to dry and crosslink overnight under room temperature. Similar to the FDH electrodes, in some experiments, a film of entangled SWNTs was formed on the surface of the GCE prior to coating with 3 µl of the PVP-Os/laccase/PEGDGE mixture.

Electrochemical Measurement

Constant potential experiments and cyclic voltammetry were performed with a CH Instruments model 832 bipotentiostat. Unless otherwise noted, experiments were conducted in a three-electrode cell configuration with a saturated calomel reference electrode (SCE) and a platinum wire counter electrode with Mcilvaine buffer (pH 5) as the background electrolyte. Constant temperature (25±1°C) was maintained during the experiments by using a water-jacketed electrochemical cell connected to a circulating water bath. Fructose calibration curves were obtained by adding aliquots of a stock 2 M D-fructose solution to a well-stirred cell with the working electrode poised at 500 mV vs SCE.

Enzymatic biofuel cells were assembled by placing one electrode (anode) coated with a Fc-C_6-LPEI/FDH/EGDGE film and a second electrode (cathode) coated with a PVP-Os/Laccase/PEGDGE film into a one-compartment electrochemical cell filled with McIlvaine buffer pH 5 and 60 mM fructose. Polarization and power curves were obtained by measuring the current as a function of potential during slow scan polarization (1 mV/s). At a minimum, each experiment was performed in triplicate using separately constructed electrodes, and the current and power densities were calculated using the geometric surface area of the electrode (0.07 cm^2).

RESULTS AND DISCUSSION

Effect of enzyme solution pH on Electrochemical and Enzymatic Response

The efficient transfer of electrons between redox polymers and redox enzymes is dependent upon an electrostatic complex being formed between them [165]. Thus the pH of both the enzyme solution and the redox polymer solution will have a significant effect on the enzyme's and polymer's charge in solution and the electrostatic complex that forms. With this in mind, we investigated the influence of the pH of the enzyme solution used in forming the hydrogel between Fc-C_6-LPEI and Fructose

dehydrogenase (FDH) on the electrochemical and enzymatic performance. As the pH of enzyme solution increased from 3.3 to 4, there was no obvious change in the shape of cyclic voltammograms (Figure 3.1A). Further increase of enzyme solution pH caused a small shift in the oxidation peak potential that resulted in a broader potential peak separation (ΔE_p) that ranged between 123 to 130 mV. Similarly, we also observed a small increase in the oxidation peak current as the solution pH increased from pH 3.3 to 6.0 (Fig. 3.1C). These results suggest that the pH of the enzyme solution had a minimal effect on the electrochemical behavior of the crosslinked redox polymer-enzyme hydrogels.

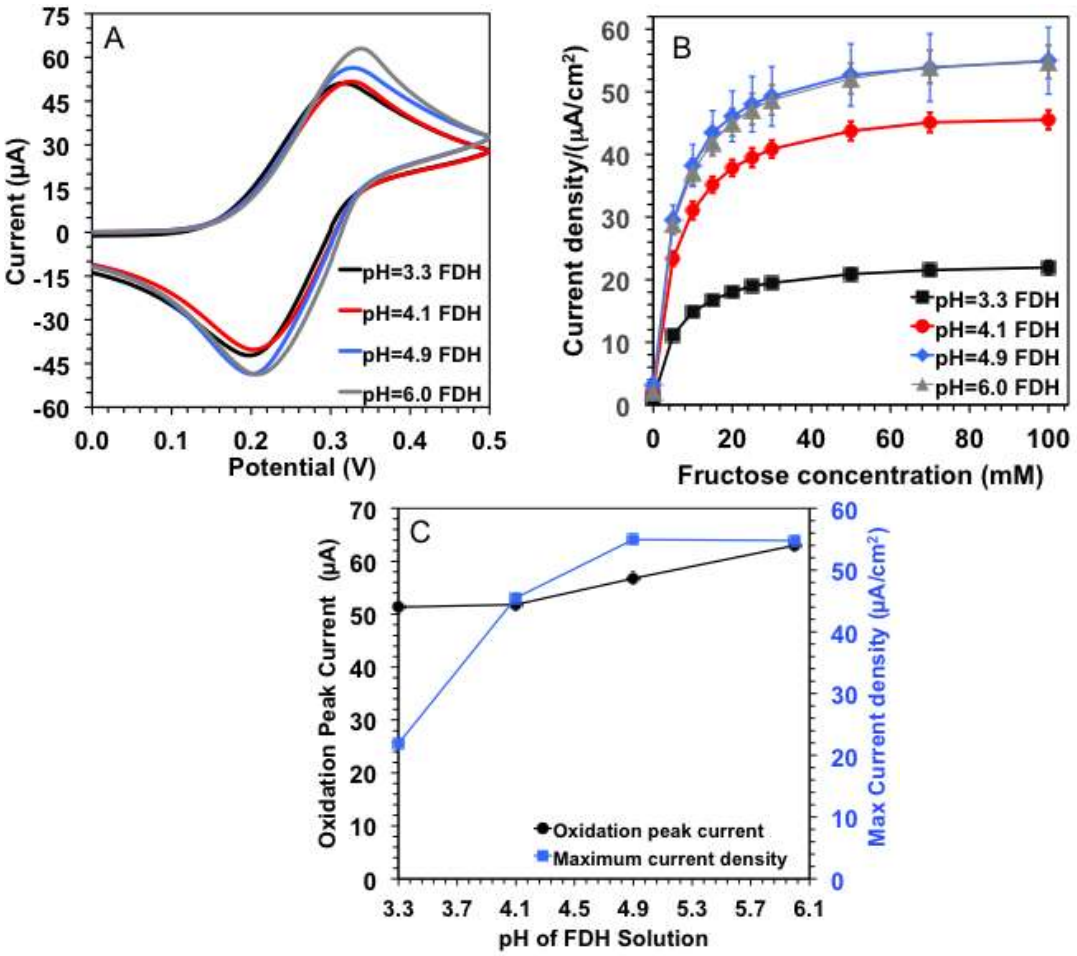


Figure 3.1 Effect of enzyme solution pH on sensor performance. (A) Representative cyclic voltammograms of Fc-C_6-LPEI/FDH electrodes prepared by using FDH enzyme solutions with different pH (scan rate 50 mV/s, in Mcilvaine buffer (pH=5), 25°C. The pH of Fc-C_6-LPEI solution was 5.0. (B) Steady-state fructose response of Fc-C_6-LPEI/FDH electrodes, E = 0.5 V vs SCE, in Mcilvaine buffer. (C) Dependence of oxidation peak current and maximum current density on the pH of enzyme solution.

To investigate how the pH of the enzyme solution affects the enzymatic response of crosslinked redox polymer/enzyme hydrogels to fructose, we performed constant potential experiments and measured the current output following fructose injections. Figure 3.1B shows that the GCE electrodes coated with crosslinked hydrogels of Fc-C_6-LPEI/FDH displayed Michaelis-Menten type behavior in response to fructose. In contrast to the minimal changes in the electrochemical response with enzyme solution pH, the enzymatic response showed a significant effect of pH. (Fig 3.1C). The optimal pH of enzyme solution for constructing fructose dehydrogenase hydrogels was in the range between 5 and 6. Decreasing the pH to 4 or lower resulted in a decrease of enzymatic response. This optimal pH of the enzyme solution used to construct redox polymer-enzyme films was higher than the optimal pH (4.0 or 4.5) reported for soluble FDH[166, 167]. The differences may be related to solution vs immobilized FDH or the nature of the electron acceptor (hexacyanoferrate (III) vs ferrocene). In order to optimize the signal output, enzyme solution with pH 6.0 was used for constructing Fc-C_6-LPEI/FDH films for subsequent experiments.

Effect of Fc-C_6-LPEI redox polymer solution with different pH

We also investigated the effect of redox polymer solution pH on the electrochemical and enzymatic performance of Fc-C_6-LPEI/FDH electrodes by constructing electrodes using redox polymer solutions with varying pH while keeping the enzyme solution pH constant (pH = 6). Figure 3.2 (A) shows the cyclic voltammograms of Fc-C_6-LPEI/FDH based electrodes constructed using Fc-C_6-LPEI solutions with pH from 3.1 to 7.0. As the pH of redox polymer solution decreased from 7.0 to 3.9, the oxidation peak potential decreased by around 30 mV, indicating that the pH of polymer solution affected the electron transport process between the redox polymer film and electrode surface. Previous studies[168, 169, 170] suggested that

configuration of the redox polymer is pH dependent, with the redox polymer adopting an extended rod conformation at low pH due to high linear charge density, whereas at high pH, the linear charge density is reduced and the polymer adopts a coiled conformation. The conformation shift, in turn, leads to changes in the electrochemical performance of electrodes. As the redox polymer solution pH further decreased from 3.9 to 3.1, the oxidation peak potential slightly increased, and the redox peaks of electrodes exhibited a diffusion tail, suggesting a mass transfer effect in the redox mechanism. The relationship between the oxidation peak current of the redox polymer-enzyme films and the redox polymer solution pH are shown in Figure 3.2C. Decreasing the redox polymer solution pH from 7.0 to 3.9 did not result in an obvious change in the oxidation peak current. Further decrease of the redox polymer solution pH to 3.1 increased the oxidation peak current.

Figure 3.2B shows the enzymatic response of electrodes to fructose for the electrodes coated with different redox polymer pH solutions. As shown in Figures 3.2B and 3.2C, the pH of the redox polymer solution had a significant effect on the enzymatic performance of the Fc-C_6-LPEI/FDH coated electrodes. As the pH of redox polymer solution decreased from 7.0 to 6.0, there was a ~ 5-fold increase in the maximum current density. Further decreasing the pH of polymer solution to 3.9 resulted in a large increase in the enzymatic response, with the limiting current density reaching 245 $\mu A/cm^2$ at the saturating fructose concentration. Additional decreases of the pH to 3.4 and 3.1 significantly reduced the enzymatic response. To summarize, we observed no enzymatic response to fructose for sensors constructed with a redox polymer solution pH of 7.0 or 3.1. These results agree with a previous report that FDH is denatured at pH <3.0 and >6.0[171]. Since the optimized pH of the redox polymer solution for constructing fructose dehydrogenase based electrodes was

around 3.9, all subsequent FDH/Fc-C_6-LPEI films were prepared with this redox polymer solution pH. It is important to note that the fructose current densities observed in this study are approximately 5-15 times higher than those reported for other fructose dehydrogenase electrodes that utilize redox polymers (Table 3.1) or other redox mediators, such as lipophilic ubiquinone-6 (45 µA/cm^2)[172], Meldola's blue (4.5 µA/cm^2)[173] and ferricyanide[174].

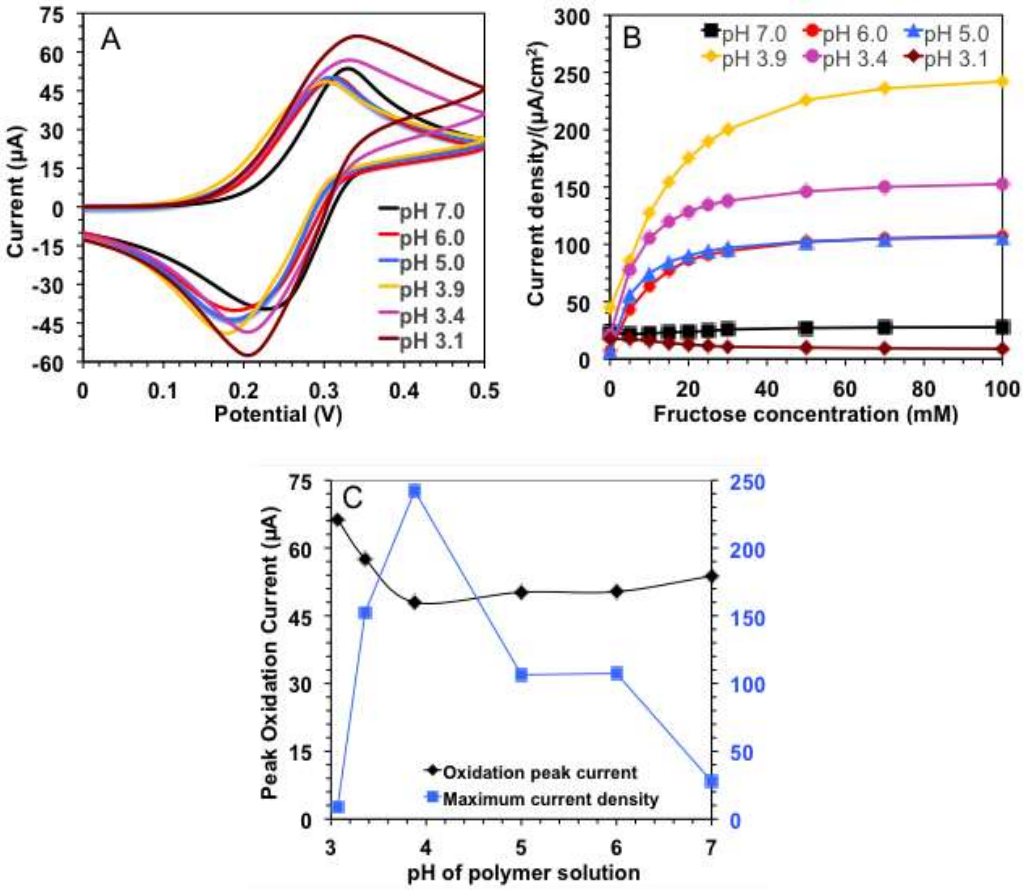


Figure 3.2 Effect of redox polymer solution pH on sensor performance. (A) Representative cyclic voltammograms of Fc-C_6-LPEI/FDH electrodes prepared by using different pH Fc-C_6-LPEI solutions (scan rate 50 mV/s, in Mcilvaine buffer (pH=5), 25°C. The pH of the FDH solution was 6.0. (B) Steady-state fructose response of Fc-C_6-LPEI/FDH electrodes, E = 0.5 V vs SCE, in Mcilvaine buffer. (C) Dependence of oxidation peak current and steady state current density on the pH of redox polymer solution

Table 3.1 Comparison of the Enzymatic Response of Various Fructose Sensors Based on Redox Polymer-Fructose Dehydrogenase Films

Redox Polymer	Film Type	Km (mM)	Sensitivity ($\mu A/cm^2 \cdot mM$)*	J_{Max} ($\mu A/cm^2$)	Ref
PVP-Os	LBL	1.0	19.3	19.7	[159]
PVI-Os	CNP	3.7	1.95	15.6	[135]
PVI-Os	SPGE	10.5	2.1	23.9	[175]
$FcMe_4$-C_3-LPEI	SCF	7.9	4.0	53.2	[161]
Fc-C_6-LPEI	SCF	9.1	17.1	245	This work
Fc-C_6-LPEI	SCF/SWNT	6.3	93.6	1040	This work

PVI-Os = poly[(1-vinylimidazole)Os(bpy)$_2$Cl]; LBL = Layer-By-Layer; CNP = Carbon Nanotube Paste; SC = Solution Cast Film; SPGE = Screen-printed graphene electrode. J_{Max} is the maximum current obtained experimentally at saturating fructose concentrations. K_m is the Michaelis-Menten constant and was determined graphically from a Lineweaver-Burke plot. *Sensitivity was determined from the experimental current response at 5 mM fructose concentration or values reported in the literature.

Effect of incorporating SWNTs film into FDH/Fc-C_6-LPEI electrodes

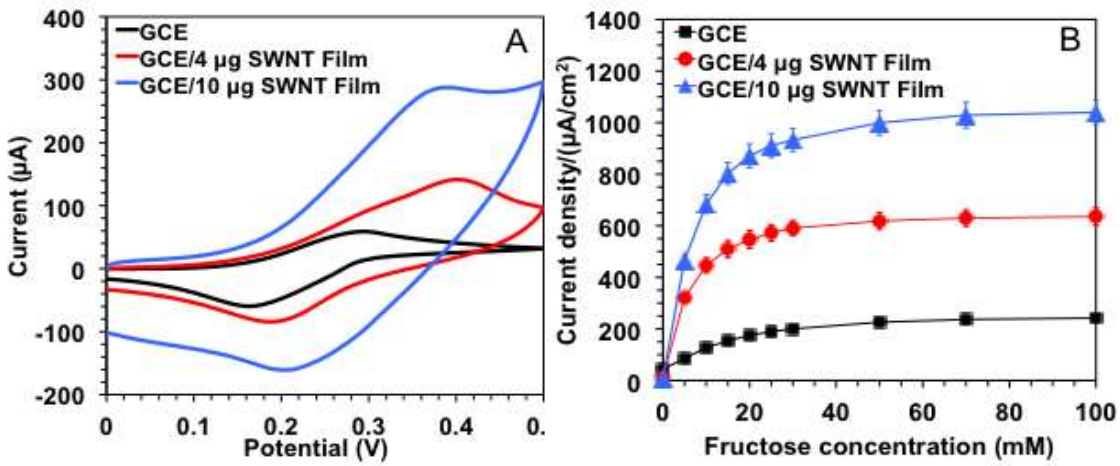


Figure 3.3 Effect of SWNT films on the electrochemical and enzymatic response of Fc-C_6-LPEI/FDH modified electrodes. (A) Cyclic voltammograms of Fc-C_6-LPEI/FDH electrodes with the incorporation of SWNTs films. Scan rate=50 mV/s in Mcilvaine buffer (pH=5) at 25°C. (B) Calibration curves of Fc-C_6-LPEI/FDH based electrodes with SWNT films, E=0.5 V vs SCE

We have recently demonstrated that modifying the surface of glassy carbon electrodes with a network of SWNTs prior to coating with a redox polymer/enzyme film containing glucose oxidase led to a significant increase in the enzymatic response to glucose, reaching a current density of ~1.7–2.1 mA/cm^2[164]. To determine whether this technique would increase the response to fructose, we performed similar experiments with two different SWNTs film loadings (4 µg and 10 µg). Figure 3.3A

shows the CVs of Fc-C_6-LPEI/FDH electrodes coated with 4 µg and 10 µg SWNTs film loadings and without SWTNs. For the electrodes without SWNTs films, a pair of well-defined redox peaks corresponding to the oxidation and reduction of the redox polymer's ferrocene complexes was observed at 290 and 166 mV versus SCE, respectively. In contrast, modifying the GCEs with SWNT films resulted in a significant change in the electrochemical response (Figure 3.3A). The modification of GCE with the 4 µg and 10 µg SWNT films resulted in a 1.6- and 4.8-fold increase in the oxidation peak current, respectively, and shifted the oxidation and reduction peak potential, resulting in a broader potential peak separation ($\Delta E_{4\ \mu g\ SWNTs\ film}$= 184mV, $\Delta E_{10\ \mu g\ SWNTs\ film}$= 186 mV) as compared to the peak separation for electrodes without SWNTs films ($\Delta E_{no\ SWNTs\ film}$= 124mV). The increase in the current response is most likely related to both an increase in the electrochemical surface area provided by the SWNTs and more of the redox polymer's ferrocene centers being electrochemically accessible[124, 164]. The large shift in the peak separation potentials is inconsistent with our previous reports[124, 164]. The cause of the change in the oxidation and reduction potentials is unknown and may be related to differences in the ability of SWNTs to donate or accept electrons at (i) the glassy carbon interface, (ii) junctions between interconnected SWNTs, or (iii) with ferrocene redox centers.

Similar to the electrochemical results, modification of the GCEs with the SWNT films had a significant effect on the enzymatic response to fructose. Figure 3B shows the calibration curves to fructose for electrodes with and without SWNTs. Electrodes without SWNTs film exhibited a maximum current density of 245 µA/cm^2 at saturating fructose concentrations, while electrodes coated with the 4 µg and 10 µg SWNTs films produced maximum current densities of 636 µA/cm^2 and 1040 µA/cm^2.

Similarly the sensitivity of the SWNT coated electrodes at low fructose concentrations (5 mM) were 3.6-fold or 5.8-fold higher then control electrodes.

Effect of incorporating SWNTs on the performance of PVP-OS/Laccase cathode electrodes

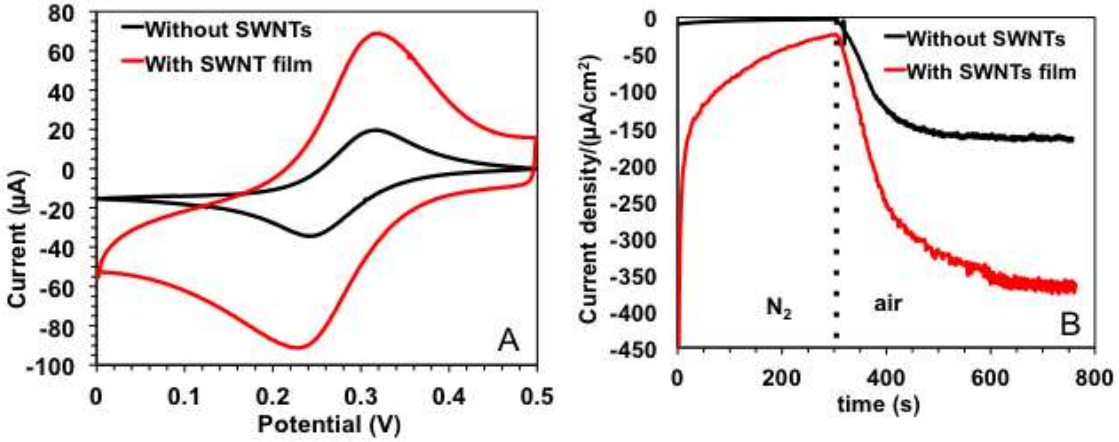


Figure 3.4 Effect of SWNT films on the electrochemical and enzymatic response of PVP-Os/Laccase modified electrodes. (A) Representative cyclic voltammograms of 3 mm GCEs coated with cross-linked hydrogels of PVP-Os/laccase and modified with and without SWNT a film. CVs were obtained in a Mcilvaine buffer (pH=5) at a scan rate = 50 mV/s, and T=25^{o}C, (B) Amperometric response of 3 mm GCEs coated with cross-linked hydrogels of PVP-Os/laccase and modified with and without SWNT a film in a N_2-saturated solution changed to an air-saturated solution at E=0.2 V, T=25^{o}C, and Mcilvaine buffer (pH 5).

Multi-copper oxidases such as laccase or bilirubin oxidase are widely used for the bioelectrocatalytic reduction of dioxygen in biofuel cell cathodes. To determine whether the modification of GCEs with high surface SWNT films would improve the electrochemical and enzymatic performance of PVP-OS/laccase cathode electrodes, we prepared PVP-OS/laccase cathode electrodes without and with 10 µg SWNTs films. Figure 3.4A shows the CVs of PVP-OS/laccase coated electrodes with and without a SWNT film. Similar to aforementioned results in Figure 3.3A, the incorporation of SWNTs film resulted in a 3.5-fold increase in the oxidation and reduction peak current.

The corresponding enzymatic response of the prepared PVP-OS/laccase

electrodes is shown in Figure 3.4B. Compared with electrodes without SWNTs film, the incorporation of 10 µg SWNTs film into electrodes resulted in a 2.3- fold increase in the response to oxygen, reaching a current density of 366 µA/cm^2. Taken together, these results provide evidence that the modification of GCEs with a high surface SWNT network is applicable to construct various enzyme and redox polymer based electrodes with enhanced electrochemical and enzymatic signal output.

Fructose/O_2 biofuel cells

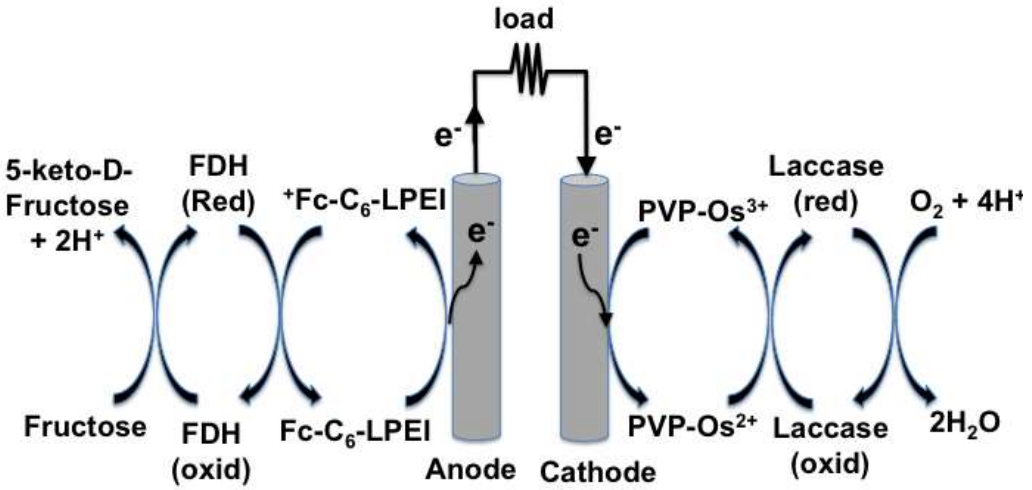


Figure 3.5 Fructose/O_2 biofuel cell schematic with Fc-C_6-LPEI mediated fructose anode electrodes and PVP-OS mediated laccase cathode electrodes. Flow of electrode from the oxidation of fructose to the reduction of oxygen, with the redox reaction.

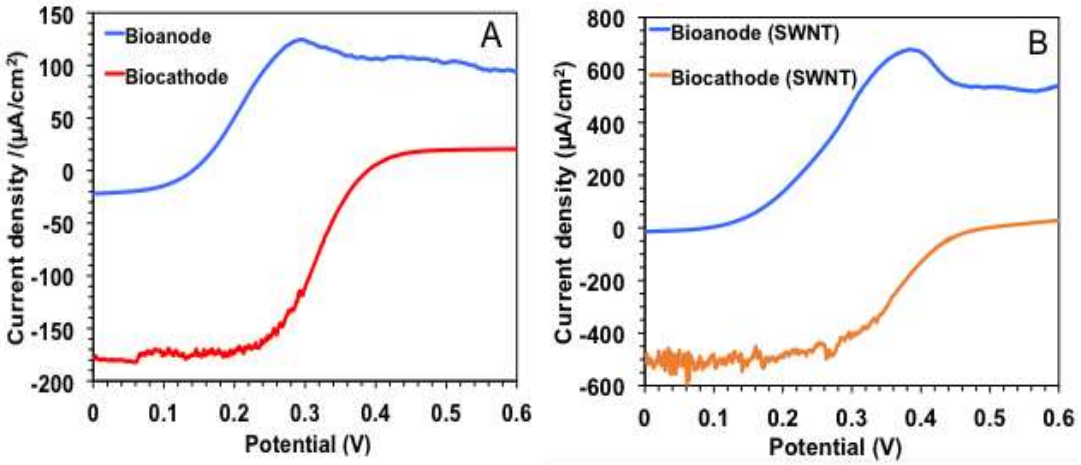


Figure 3.6 Effect of SWNT films on Bioanode and Biocathode Response**.** Representative polarization curves of Fc-C_6-LPEI/FDH bioanodes and PVP-Os/laccase biocathodes without (A) and with a SWNT film (B). Measurements were made in a stirred solution under air-saturating conditions, Mcilvaine buffer (pH 5), 60 mM fructose, scan rate 1 mV/s, 25^{o}C.

To determine the usefulness of the Fc-C_6-LPEI/FDH hydrogel as an anode material, we constructed one-compartment fructose/O_2 biofuel cells consisted of a Fc-C_6-LPEI/FDH anode and a PVP-OS/laccase cathode both with or without SWNT films. A schematic of fructose/O_2 biofuel cell is shown in Figure 3.5. The electrons from the oxidation of fructose are passed from fructose dehydrogenase to the oxidized ferrocenium active sites in the Fc-C_6-LPEI polymer until they reach the electrode surface. Then, through external circuit, the electrons transfer through the PVP-OS hydrogel film until they reach the active site of laccase, where the reduction of molecule oxygen to water occurs.

Figure 3.6 shows the polarization curves for anodes and cathodes without (Fig. 3.6A) and with SWNTs film (Fig. 3.6B). The biofuel cells were operated in a McIlvaine buffer (pH 5.0) containing 60 mM fructose under O_2-saturated conditions at room temperature. For the biofuel cell without SWNTs films, the catalytic electro-oxidation current of fructose appeared at 0.07 V and reached a maximum current density of 124 μA/cm^2 at 0.3 V. The catalytic electroreduction current of oxygen occurred at 0.45 V and reached a maximum value of 180 μA/cm^2 at 0.2 V. Comparing the midpoints of each anodic polarization curve to the midpoint of the cathodic curve, the cell voltage of biofuel cell was determined to be 0.12 V at maximum power. Figure 3.6B shows the polarization curve for anodes and cathodes with SWNTs films. Compared to the results of electrodes fabricated without SWNTs (Figure 3.6A), the incorporation of SWNTs increased both the maximum current density and the redox potential. The current density of Fc-C_6-LPEI/FDH anodes that contained SWNT films reached a maximum of 680 μA/cm^2 at 0.38V. This current density was ~4 times higher than that without SWNTs film. Likewise, the current density of PVP-OS/laccase electrode with SWNTs film reached a maximum of ~502 μA/cm^2 at 0.26V.

The exact cause for this shift in redox potential is unknown and currently under investigation.

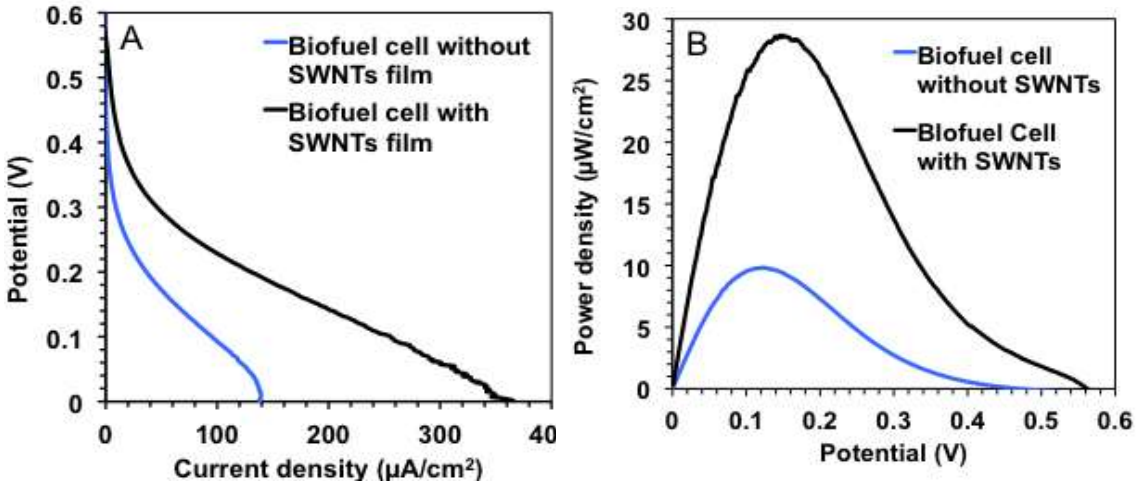


Figure 3.7 Effect of incorporating SWNTs on the biofuel cell performance. Representative polarization (A) and power density (B) curves of biofuel cells fabricated with bioanodes and biocathodes, modified with and without SWNT films. Measurements were made in stirred solutions under air-saturating conditions, Mcilvaine buffer (pH 5.5), and 60 mM fructose. The bioanode was a 3 mm GCE coated with the Fc-C_6-LPEI/FDH film while the biocathode was a 3 mm GCE coated with the PVP-Os/laccase film.

Figure 3.7A shows the polarization curve of biofuel cells using Fc-C_6-LPEI/FDH anodes and PVP-OS/Laccase cathodes with or without SWNTs, while Figure 3.7B shows the power density dependence of the voltage. For biofuel cell without SWNT film, the maximum current density was ~136 μA/cm^2, and the maximum power density was 9.8 μW/cm^2 at a cell voltage of 120 mV. The open-circuit voltage (OCV) was estimated to be 470mV. Incorporation of SWNTs into both the anode and cathode resulted in a 2.7-fold increase in the maximum current density, reaching 360 μA/cm^2, and a 2.9-fold increase in the maximum power density output, to 29 μW/cm^2 at the cell voltage of 152 mV. The biofuel cell with SWNTs film exhibited the OCV of 550 mV. From the results above, it can be concluded that the incorporation of SWNTs into biofuel cells improved the current density and power density output, as well as the cell voltage output and OCV.

CONCLUSIONS

In this study, we reported the construction and characterization of reagentless amperometric fructose electrodes by immobilizing fructose dehydrogenase (FDH) in ferrocene-modified linear poly(ethylenimine) (Fc-C_6-LPEI) hydrogels. We demonstrated that the electrochemical and enzymatic properties of FDH/redox polymer electrodes were highly dependent upon both the pH of enzyme solution and the pH of redox polymer solution. The optimal pH range of enzyme solution and redox polymer solution were in the range of 5 to 6 and around 3.9, respectively. This is an important finding because most reports on redox polymer enzyme films only investigate the effect of buffer pH on sensor performance after the redox polymer-enzyme film has been crosslinked. Very few papers have investigated the effect of polymer and enzyme solution pH. The pH will affect the charge on both the enzyme and redox polymer, which in turn, affects the electrostatic complex that initially formedbetween the enzyme and redox polymer, and consequently the crosslinked film formed and the sensor response. The Fc-C_6-LPEI/FDH electrodes exhibited a limiting current density of 245 $\mu A/cm^2$ at saturating fructose concentration, which is significantly higher than other reports of redox mediated fructose sensors. We also demonstrated that the modification of GCEs with SWNTs (6,5) films prior to coating of the Fc-C_6-LPEI/FDH films resulted in an increase in the electrochemical and enzymatic performance of electrodes, with the limiting current density of ~ 1 mA/cm^2. Although the use of SWNTs networks to increase the response of redox polymer-enzyme films has been reported previously with glucose oxidase, to our knowledge, this is the first report using fructose dehydrogenase as the enzyme. Similarly, we also applied this SWNTs network technique to improve the response of films consisting of an osmium-based redox polymer (PVP-Os) and the enzyme laccase and

demonstrateds an increased signal output. The SWNTs network results with laccase and fructose dehydrogenase are important because they demonstrate that the fabrication of SWNTs networks can be used as a general technique for improving the signal output of redox polymer-enzyme films. Finally, we demonstrated that these films have potential use in enzymatic biofuel cell applications that utilize fructose as the biofuel by producing a maximum power density of 9.8 μW/ cm^2 in biofuel cells without SWNTs. The incorporation of SWNTs into the bioanode and biocathode films resulted in an increase in the cell voltage and open circuit potential.and a ~3 fold increase in the maximum power density output, to 29 μW/ cm^2.

Acknowledgements:

I would like to thank Dr. Glatzhofer for his valuable insight and suggestions concerning this work. I would also like to thank Daniel Bamper for synthesizing Fc-C_6-LPEI redox polymers.

Chapter 4:

Single Wall Carbon Nanotube (7,6) film modified Ferrocene-modified Linear Poly(ethylenimine) Hydrogel film for Biofuel Cell

INTRODUCTION

The excellent electronic properties of single wall carbon nanotubes (SWNTs), along with their extraordinary chemical structure, have gained enormous interest in designing high performing electronic devices and sensors[176, 177]. Kong et al were the first to build a carbon nanotube molecular sensor using semiconducting SWNTs for the detection of NO_2 and NH_3 gas[178]. Since then, semiconducting SWNTs have been widely employed in constructing nanostructured enzymatic electrodes for biosensor and enzymatic biofuel cells [179, 180, 181].

In order to maximally take advantage of nanotube's exceptional bulk properties, different carbon nanotube based structures were developed, including nanotube array[182], fibers[183], films[96], paper [42]and yarns[184]. There are some factors affecting the properties of these structures, such as the type of carbon nanotubes used (e.g. single-walled vs. multi-walled[101, 102], metallic vs. semiconducting[103, 104, 105], chirality[106]), the degree of nanotube bundling[107], alignment[108, 109, 110], and nanotube length[111, 112]. Peng Zhao et al[185] studied the effect of chirality of single wall carbon nanotube on the electronic properties of a diarylethene-based molecular switch, suggesting that the chirality of SWNTs is an important factor determining the conductance of molecular switches. Recently, we reported [24]that modification of bare glassy carbon electrodes with high surface semi-conductive single wall carbon (SWNTs (6,5)) nanotube film from solutions dispersed by Triton X-100 increased the electrochemical and enzymatic performance of redox polymer/enzyme hydrogel film significantly, with glucose electrooxidation current densities of ~2.1 mA/cm^2.

Therefore, in this study, we investigated whether modifying the surface of a glassy carbon electrode with a type of SWNTs(7,6) that are electrically more conductive would further increase the electrochemical and enzymatic performance of crosslinked redox polymer-enzyme films deposited onto nanotube films modified glassy carbon electrodes. We also evaluated how the nanotube loading and redox polymer/enzyme hydrogel solution loading affects the electrochemical and enzymatic performance of electrodes. To test whether these conductive SWNT networks were applicable to redox polymer-enzyme films in general, we tested this strategy with two different enzymes (Glucose oxidase, and Laccase). Finally, we constructed enzymatic biofuel cells with the optimized SWNT/redox polymer enzyme composite structures.

EXPERIMENTAL SECTION

Chemicals and solutions

Glucose oxidase from *Aspergillus niger* (EC 1.1.3.4, type X-S, 147.9 units/mg of solid, 75% protein) was purchased from Sigma Aldrich. Triton X-100 was purchased from EM Science. Ethylene glycol diglycidyl ether (EGDGE) was purchased from Polysciences, Warrington, PA. All chemicals and solvents were used as received without further purification. $FcMe_2$-C_3-LPEI and Cl-Fc-LPEI redox polymer were kindly provided by Dr.Glatzhofer's lab and synthesized by David Hickey [186, 187]. 50 mM phosphate buffer solution (pH=7) was prepared by dissolving 6g of NaH_2PO_4 in 1 L of nanopure deionized water. 2M glucose solution was prepared in water 24 h before use and refrigerated at 4°C when not in use. Semi-conductive SWNTs (6,5) and SWNTs (7,6) were purchased from South West Nanotechnologies. The nanotube suspensions with different concentrations were sonicated in 5 g/L Triton X-100 aqueous solutions with a horn sonic dismembrator

(Model 500, Fisher Scientific) running at 22% output for 1 hour to de-bundle the tube aggregates.

Anodic enzyme electrodes

Glassy carbon electrodes (3 mm diameter stationary disk or 5 mm diameter rotating disk) were polished successively on three grades of alumina (5, 1, 0.3μm), and washed thoroughly with nanopure water after each polishing step.

$FcMe_2$-C_3-LPEI solution was prepared by dissolving in water and the addition of a 0.1 M HCl solution until the final concentration of the polymer solution was 10 mg/mL and pH was 5. Anodic glucose electrodes were prepared by a two-step procedure: first, 10 μl of a nanotube dispersion was cast on top of a polished glassy carbon electrode and allowed to dry overnight at room temperature to form a nanotube film on top of GCE. Second, redox hydrogels were made from mixing 14 μL of $FcMe_2$-C_3-LPEI polymer solution (10 mg/mL in water), 6 μL of GOX solution (10 mg/mL), and 0.75μL of EGDGE crosslinker solution. Next, different amounts of the respective redox polymer/enzyme/crosslinker mixture were deposited on top of a nanotube coated glassy carbon electrodes and allowed to dry for at least 12 h. Anodic electrodes with SWNTs film were prepared by a two-layer procedure shown in our previous publication[24]. First, 10 μl of different concentration SWNT dispersions in Triton X-100 solutions was cast on top of a polished glassy carbon electrode and allowed to dry overnight at room temperature to form a SWNTs film, followed by $FcMe_2$-C_3-LPEI /GOX hydrogel films as described previously.

Cathodic enzyme electrodes

12 mg/ml Cl-Fc-LPEI solution was prepared by dissolving Cl-Fc-LPEI polymer in water. Cathodic electrodes without SWNTs film were prepared by crosslinking Cl-Fc-LPEI with laccase to form enzymatic redox hydrogel film: mixing

14 µL of Cl-Fc-LPEI solution (12 mg/ml), 6 µL of Laccase solution (35 mg/ml) and 10 µL of PEGDGE (2.5 mg/ml) together, and casting aliquot of different volumes onto 3mm glassy carbon electrode surfaces. The catholic electrodes with SWNTs films were prepared by a two layer procedure. First, 10 µl of 3 mg/ml SWNTs dispersion in TX solutions was cast on top of a polished glassy carbon electrode and allowed to dry overnight at room temperature to form a SWNTs film on top of GCE, followed by Cl-Fc-LPEI /Laccase hydrogel films as described previously.

Electrochemical and Spectroscopic Measurement

Electrochemical characterization (i.e. cyclic voltammetry and constant potential experiments) was performed in a three-electrode cell configuration (counter electrode = platinum wire, reference electrode = saturated calomel electrode, SCE) with a CH Instruments model 832 bipotentiostat. The temperature was maintained at 25±1°C with a water-jacketed electrochemical cell. The background electrolyte was 50 mM phosphate buffer solution, pH 7. Glucose response was measured by adding aliquots of a stock 2 M glucose solution to a well-stirred cell with the working electrode poised at 400 mV vs SCE. The biofuel cells were assembled by placing one anodic enzyme electrode and one cathodic enzyme electrode into a one-compartment electrochemical cell filled with pH 5.5 citric buffer and 60 mM glucose.

Calculation and Statistics

Current densities were calculated using the geometric surface area of a 3-mm-diameter electrode. Values are presented as mean ± standard error of the mean (SEM) unless otherwise specified.

RESULTS AND DISCUSSION

Effect of different SWNTs on the performance of $FcMe_2$-C_3-LPEI /GOX electrodes

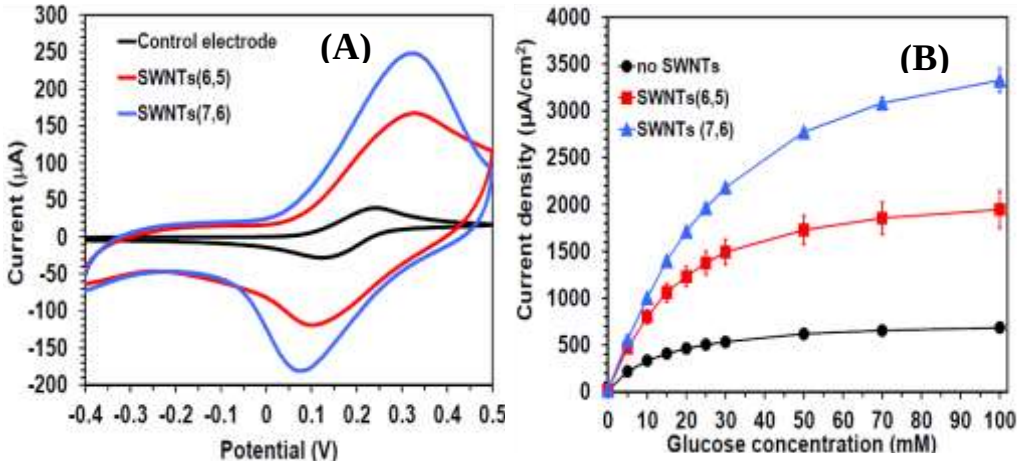


Figure 4.1 Effect of different SWNTs on the performance of $FcMe_2$-C_3-LPEI /GOX based electrodes. (A) Cyclic voltammetry and Calibration curves (B) of $FcMe_2$-C_3-LPEI /GOX electrodes without and with different SWNTs films; For CV curves, Scan rate = 50 mV/s, T=25°C, pH=7 sodium phosphate buffer. For calibration curves, E= 0.4V

Previously, we demonstrated that the incorporation of semi-conductive SWNTs (6,5) film dispersed by Triton X-100 into cross-linked redox polymer and enzyme electrode led to significant increase in the electrochemical and enzymatic response of these electrodes[24]. In order to investigate whether modifying the surface of a glassy carbon electrode with different SWNTs network would improve the electrochemical and enzymatic performance of cross-linked redox polymer-enzyme based electrode, cyclic voltammetry and constant potential experiments were performed with a more conductive SWNTs(7,6) film modified $FcMe_2$-C_3-LPEI /GOX electrode. Figure 4.1(A) shows the cyclic voltammograms of bare GCE and different nanotube films modified GCEs with a $FcMe_2$-C_3-LPEI /GOX film in sodium phosphate buffer solution. For bare GCEs modified with a $FcMe_2$-C_3-LPEI /GOX hydrogel film, a pair of well-defined redox peaks corresponding to the oxidation and reduction of the redox polymer's ferrocene complexes were observed at 240 and 123

mV versus SCE, respectively (ΔE=118 mV). The incorporation of either type of SWNTs film into $FcMe_2$-C_3-LPEI/GOX electrodes resulted in significant increase in the background current and redox peak current. The increase of background current was consistent with our previous reports[27, 28] and others[188, 189]. Compared with electrodes without nanotubes, the incorporation of SWNTs (7,6) film and SWNTs (6,5) films onto electrodes led to 6.2-fold and 4.15-fold increase in the oxidation peak current, respectively, suggesting that electrodes modified with SWNTs (7,6) film showed better electrochemical performance than those with semi-conductive SWNTs(6,5) film. Besides, the presence of SWNTs film shifted both the oxidation and reduction potential peaks, and resulted in a broader potential separation ($\Delta E_{SWNTs(6,5)}$=222 mV, $\Delta E_{SWNTs(7,6)}$=248 mV). The broader potential separation might result from the presence of SWNTs film taking part in the process of donating or accepting electron between the redox centers of redox polymer or from the redox center to electrode surface.

To determine the effect of different nanotube networks on the enzymatic response of $FcMe_2$-C_3-LPEI /GOX electrodes to glucose, we performed constant potential amperometry by poising the electrodes at 50 mV higher than oxidation peak potential and measuring the current output as aliquots of a stock 2 M glucose solution were added to a well-stirred sodium phosphate buffer solution Figure 4.1 (B) shows the corresponding glucose response of SWNTs (6,5) and SWNTs(7,6) film modified GCE coated with $FcMe_2$-C_3-LPEI /GOX film in sodium phosphate buffer. Electrodes with and without SWNTs films exhibited Michaelis-Menten type behavior. Compared with electrodes without nanotube, the incorporation of SWNTs(6,5) and SWNTs(7,6) films into $FcMe_2$-C_3-LPEI /GOX electrodes resulted in 2.84 and 4.87 fold increases in the maximum current density at the glucose saturating concentration, reaching 1946

and 3326 uA/cm^2, respectively. Taking the CV results and glucose response results into consideration, it can be observed that electrodes modified with SWNTs(7,6) film showed better electrochemical and enzymatic performance than those modified with SWNTs (6,5) film, suggesting that the chirality of nanotube is another important factor affecting the performance of redox polymer and enzyme electrodes. In order to maximum the current density output of electrode, SWNTs(7,6) nanotube was selected to modified GCE in the following experiments.

Effect of SWNTs (7,6) film loading on the performance of $FcMe_2$-C_3-LPEI /GOX electrodes

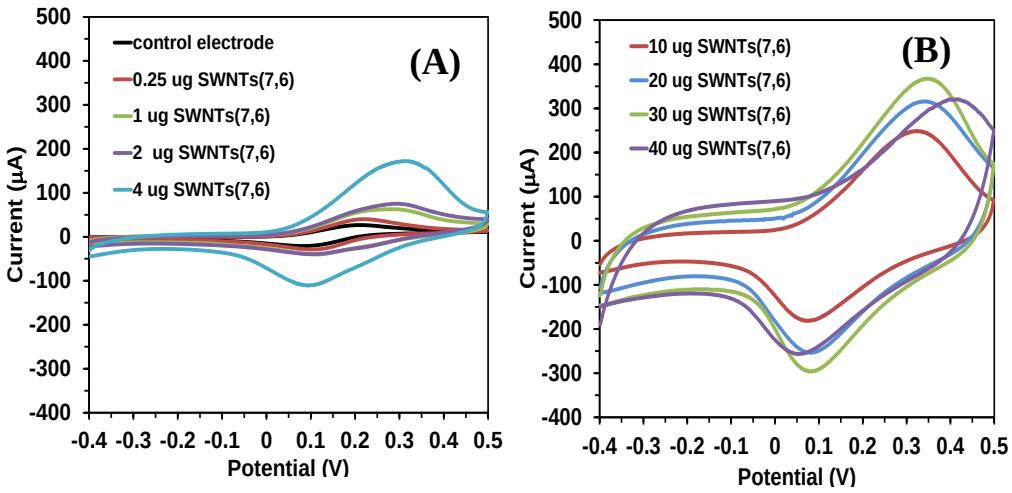


Figure 4.2 Effect of SWNTs(7,6) film loading on electrochemistry of $FcMe_2$-C_3-LPEI /GOX based electrodes; Scan rate= 50 mv/s in sodium phosphate at 25℃.

In order to optimize the performance of SWNTs(7,6) film modified electrodes, the effect of nanotube film loading on the electrochemical performance of redox polymer/GOX based electrodes was investigated by casting different concentrations of SWNTs solutions (0.025-4 mg/ml) onto bare glassy carbon electrodes followed by $FcMe_2$-C_3-LPEI /GOX hydrogel film while keeping the volume of SWNTs solution applied constant (10 µL). Figure 4.2 shows the cyclic voltammograms of $FcMe_2$-C_3-LPEI /GOX based electrodes with different SWNTs film loadings. As the nanotube film loading increased from 0.25 µg to 30 µg, the oxidation and reduction peak

current increased gradually, indicating more and more active sites of redox polymer became accessible with increasing loading of SWNTs. The initial increase in oxidation peak current with higher SWNTs film loading (10-30 µg) may be the result of redox centers distant from electrode surface became electrochemically accessible with the aid of the continuous 3D high surface carbon nanotube network formed. However, further increase of SWNTs loading to 40 µg resulted in a slight decrease of oxidation peak current, which may result from the mass transfer resistance with higher loading of SWNTs film. The fact that the diffusion tails at the limits of the potential scans, which is governed by mass transfer, increased with higher loading of SWNTs film supports this explanation.

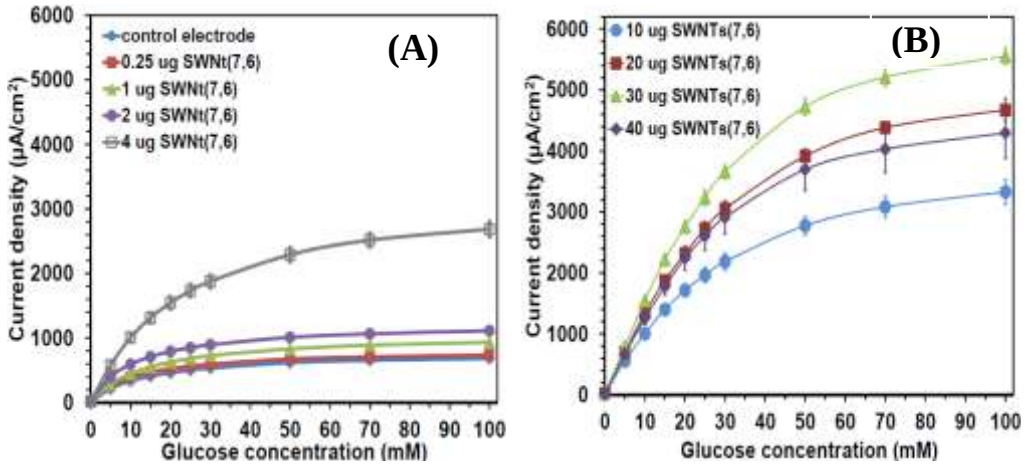


Figure 4.3 Glucose responses for $FcMe_2$-C_3-LPEI /GOX based electrodes modified with different SWNTs loading in sodium phosphate buffer. T=25℃, E=0.4 V.

The effect of SWNTs film loading on the enzymatic response of $FcMe_2$-C_3-LPEI /GOX electrodes is shown in Figure 4.3. Low SWNTs loading (0.25 µg) had little effect on the glucose response output. Increasing the film loading resulted in an obvious increase in the enzymatic response to glucose initially, and then plateaued with the SWNTs loading of 40 µg. Electrodes with the SWNTs film loading of 30 µg showed the highest current density output at the glucose saturating concentration reaching 5556 µA/cm^2, which is 8.12-fold higher than electrodes without SWNTs.

Effect of redox hydrogel loading on the performance of $FcMe_2$-C_3-LPEI /GOX electrodes

To characterize the effects of polymer and enzyme solution loading on the electrochemical properties of SWNTs(7,6) film modified electrode, cyclic voltammetry was performed. Figure 4.4(A) shows CV curves of SWNTs (7,6) film modified F_cMe_2-C_3-LPEI /GOX electrodes with different redox hydrogel loadings. As the polymer solution loading increased, the oxidation peak current increased linearly initially, and stayed relatively constant with the polymer solution loading higher than 21 µL. Similarly, as shown in figure 4.4 (B), the oxidation and reduction peak potential separation increased with higher loading of polymer solution.

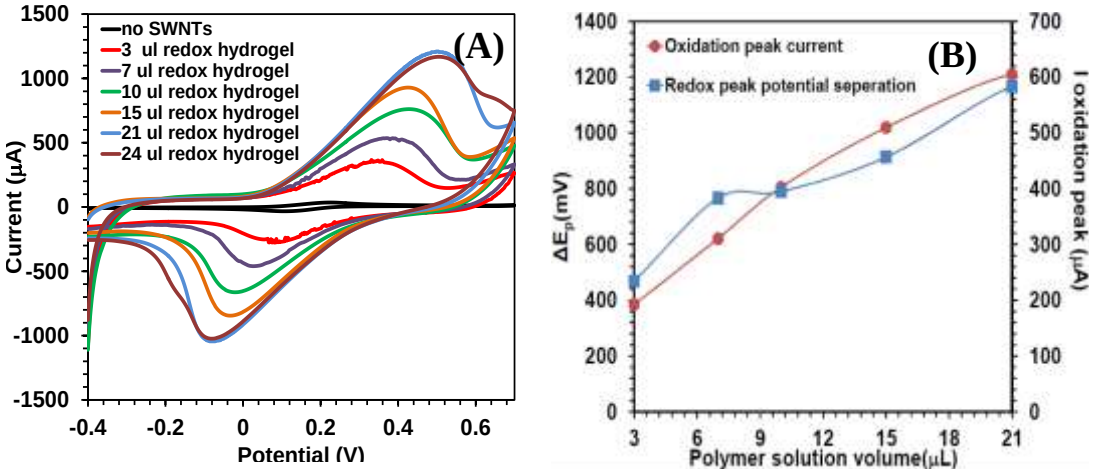


Figure.4.4 Effect of redox polymer and enzyme solution loading on the electrochemical performance of electrodes. (A) CV curves for SWNTs film modified F_cMe_2-C_3-LPEI /GOX electrodes with different redox hydrogel solution loading in sodium phosphate buffer. T=25℃; (B) the relationship between the polymer solution loading and the redox polymer potential separation or oxidation peak current.

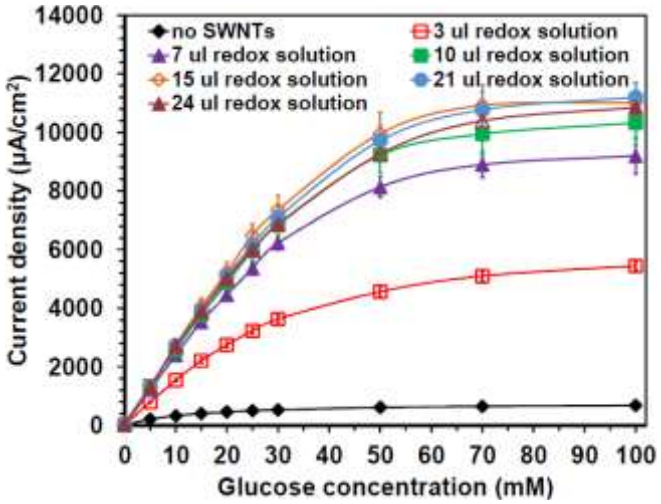


Figure.4.5 Glucose calibration curves for SWNTs(7,6) incorporated $FcMe_2$-C_3-LPEI /GOX based electrodes with different redox hydrogel loading. T=25℃, E=0.4 V vs SCE;

The effects of polymer solution loading on the enzymatic response of electrode to glucose are shown in figure 4.5. Similar to the CV results in figure 4.4, as the redox polymer solution loading increased, the glucose response of electrodes enhanced initially, and reached plateau with the polymer loading higher than 15 μL. Electrodes with 21 μL polymer loading exhibited the highest limiting current density output of 11.2 mA/cm^2 at glucose saturating concentration, which is 17.6 fold higher than electrodes without SWNTs. The current density achieved in this study was among the highest value of nanostructured glucose electrodes reported, such as using CdS nanoparticles[190], gold nanoparticles modified Pb nanowires[191], and single [16, 27]or multiwall carbon nanotube[192]. Meanwhile, there were 6.12 fold increase in sensitivity at low glucose concentration (5mM), reaching 260 $\mu A/(cm^2 \cdot mM)$. The apparent Michaelis-Menten constant (Km) for electrodes with 21 μL polymer solution was 22 mM, which is lower than that of the native enzyme in solution phase (33 mM)[193]. The smaller value of Km indicated that with the modification of SWNTs film on GCEs, glucose oxidase enzyme in our system has higher affinity for glucose than the native enzyme. However, comparing with electrodes without SWNTs, there was a 2.1 fold

increase in Km, which might due to the increased mass transfer resistance with higher polymer loading, inhibiting glucose diffusion to the enzyme active sites.

The detailed reason why the electrochemical and enzyme response increased initially with the increase of polymer solution loading, then became saturated is unknown, and under investigation. The possible explanation is that the modification of GCE with SWNTs(7,6) film created high surface 3D network for redox hydrogel-enzyme film. Initially, increasing polymer solution loading allows for more enzyme or polymer active center to be electrically contacted with electrode surface by SWNTs network within the electron transfer distance. When redox polymer and enzyme film loading reached a certain threshold, some of the redox polymer and enzyme active sites on the outer edge of the polymer hydrogel film are beyond the electron transfer distance from the electrode surface. Electrons from these active centers cannot diffuse to electrode surface within the timeframe of experiment, hence making no contribution to current generation. Therefore, further increasing the redox polymer and enzyme loading did not improve the electrochemical and enzymatic performance of electrodes.

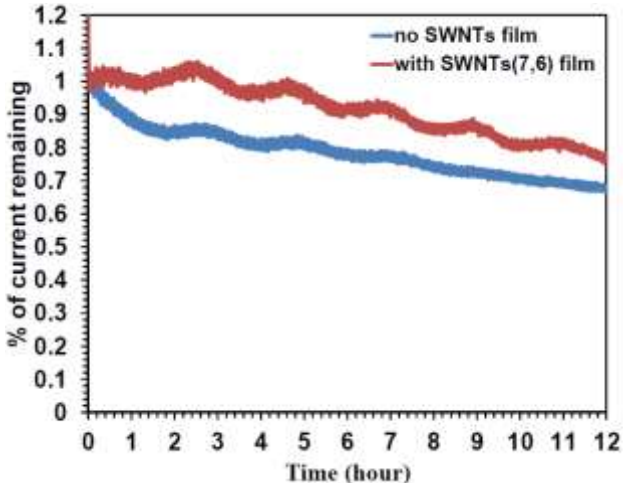


Figure 4.6 Effect of SWNTs(7,6) film on the enzymatic stability of $FcMe_2$-C_3-LPEI /GOX electrodes. Cross-linked films of GOX and $FcMe_2$-C_3-LPEI films without and with 30 µg SWNTs films were operated continuously in sodium phosphate at pH 7 and 10 mM glucose. E= 0.4V, T=25 ℃

Stability tests were performed to determine the effect of incorporating SWNTs(7,6) film and increasing polymer loading on the enzymatic stability of $FcMe_2$-C_3-LPEI /GOX electrodes. Figure 4.6 shows continuous operation stability tests for electrodes without SWNTs and electrodes with 30 µg SWNTs film and 21µL polymer loaded. After 12 hours of continuous operation, film without SWNTs retained 68% of their original current, while films with SWNTs(7,6) film retained 78%. This result suggested that incorporation of SWNTs(7,6) film into electrodes, along with high polymer loading, increased the enzymatic stability of the films, which is in consistence with previous reports. According to recent studies[194, 195], because of the curvature of SWNTs, SWNTs can stabilize the enzyme activity to a greater extent than conventional flat supports by suppressing unfavorable protein-protein lateral interactions. Thus, in this study, the possible explanation is that the high surface SWNTs 3D network on GCE allows the adsorption of glucose oxidase to the top of nanotube surface, increasing enzymatic stability.

SWNTs (7,6) film modified Cl-Fc-LPEI/Laccase cathode electrode

Multicopper oxidases such as laccase or bilirubin oxidase are widely used for the bioelectrocatalytic reduction of dioxygen in biofuel cell cathodes. To investigate whether modification of electrodes with SWNTs(7,6) film can improve the performance of redox polymer mediated laccase based cathode, we prepared SWNTs (7,6) film modified Cl-Fc-LPEI/Laccase cathode electrode. Figure 4.7 shows the CVs of Cl-Fc-LPEI/Laccase electrodes without and with SWNTs (7,6) film. Similar to the results in Figure 4.4 (A), the incorporation of SWNTs(7,6) film into cathode electrode led to dramatic increase in the peak current (15 folds), as well as the broadening of redox peak separation.

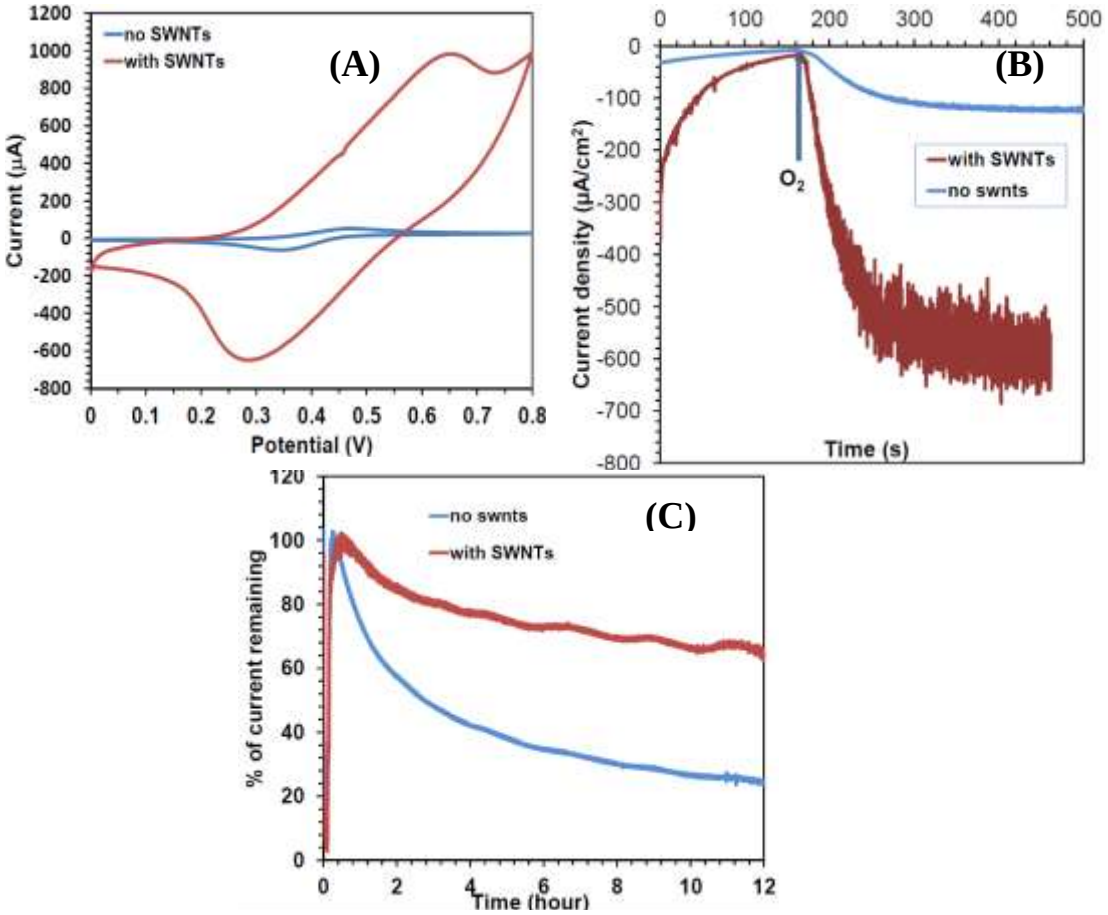


Figure 4.7 Effect of incorporating SWNTs films on the electrochemical and enzymatic response of Cl-Fc-LPEI/Laccase cathode electrodes. (A) Cyclic voltammetry of cross-linked Cl-Fc-LPEI/Laccase cathode electrodes with and without SWNTs film, scan rate = 50 mV/s. (B) Calibration curve of Cl-Fc-LPEI/Laccase cathode electrodes with and without SWNTs film. (C) Enzymatic stability of Cl-Fc-LPEI/Laccase cathode electrodes with and without SWNTs film. T=25^{o}C, pH=5.5 citric buffer

The corresponding enzymatic response of the prepared Cl-Fc-LPEI/Laccase electrodes with and without SWNTs film is shown in figure 4.7(B). Electrodes without SWNTs film exhibited low oxygen response, with a current density of around 120 μA/cm^2 at oxygen saturating condition. The incorporation of SWNTs(7,6) film into Cl-Fc-LPEI/Laccase electrodes resulted in ~ 5-fold increase in O_2 response, reaching 605 μA/cm^2. However, compared with the results in Figure 4.7(A), with the incorporation of nanotube film, the increase in the enzymatic response of electrode was not as significant as electrochemical performance, suggesting that the current output of electrode is limited by electron flow from the active sites of enzyme to

either SWNTs film or redox polymer limited the current output of electrodes, not the electron transfer in the redox polymer matrix.

The enzymatic stability of electrodes without and with incorporation of nanotube films was evaluated, as shown in figure 4.7(C). Similar to the results in figure 4.6, the incorporation of SWNTs film into electrodes improved the enzymatic stability of electrodes significantly. Electrodes with nanotube film retained 65% of their original current, while only 24% of original current was retained for Cl-Fc-LPEI/Laccase films without SWNTs(7,6) film. In conclusion, the modification of bare GCEs electrodes with a high surface area SWNTs (7,6) network is applicable to construct various redox polymer and enzyme based electrodes with improved electrochemical and enzymatic output and longer lifespan.

Glucose/O_2 biofuel cell

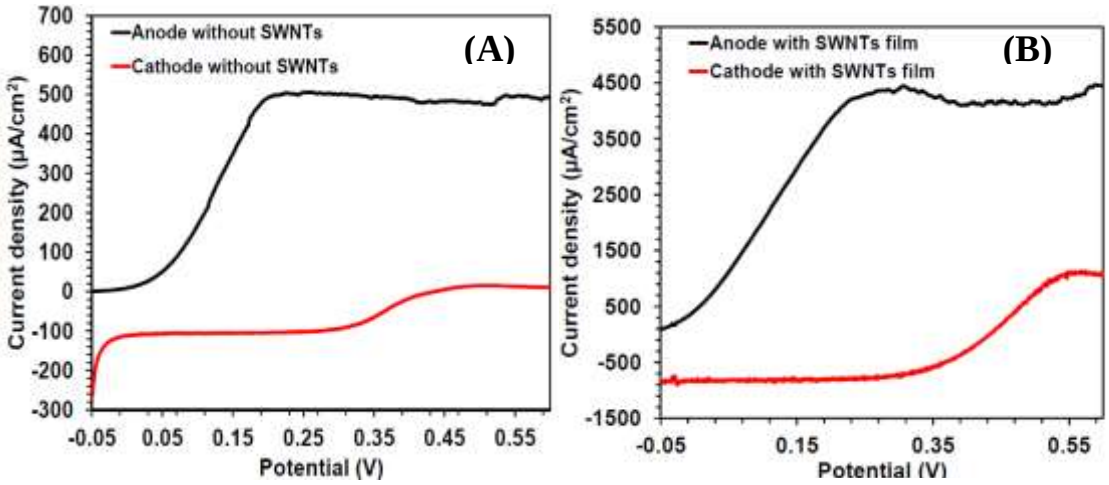


Figure 4.8 Polarization curves of $FcMe_2$-C_3-LPEI /GOX anode and Cl-Fc-LPEI/Laccase cathode without (A) and with SWNTs film (B). Stirred solution under air-saturating condition, citric buffer, pH 5.5, 60 mM glucose, scan rate 1 mV/s, 25°C.

From the above results, the incorporation of SWNTs film led to significant increase in the current density output of $FcMe_2$-C_3-LPEI mediated GOx electrodes and Cl-Fc-LPEI mediated laccase electrodes, as well as their enzymatic stability. In order to investigate whether the incorporation of nanotube film into biofuel cell would

increase the power density output and stability of biofuel cells, we constructed a one-chamber biofuel cells consisting of $FcMe_2$-C_3-LPEI / GOx anode and Cl-Fc-LPEI/laccase cathode without and with SWNTs films.

Figure 4.8 shows the polarization curves for anode and cathode without (A) and with SWNTs film (B). For electrodes without SWNTs film, the catalytic electro-oxidation current of glucose appeared at 0 V and reached maximum at 0.21 V. The catalytic electroreduction current of oxygen occurred at 0.49 V and maximized at 0.27 V. Comparing the midpoints of anodic polarization curve with the midpoint of cathodic polarization curve, the cell voltage of biofuel cell without SWNTs was 0.23 V at maximum power. The current density at the anode and cathode were 504 uA/cm^2 and 104 μA/cm^2, respectively. Since the current density of cathode was much lower than that of anode, the cathode reaction is the rate-determining factor of the maximum possible power output of biofuel cell. Figure 4.8 (B) shows the polarization curve for anode and cathode electrode with SWNTs film. Compared with the results of biofuel cell in Figure 4.8 (A), the incorporation of SWNTs increased the current density output of anode and cathode significantly. The current density of SWNTs film incorporated the $FcMe_2$-C_3-LPEI /GOx anode was 4377 μA/cm^2, which was around 8.7 times higher than electrodes without SWNTs film. Besides, the current density of Cl-Fc-LPEI/Laccase electrode with SWNTs film increased to 821 μA/cm^2. The cell voltage estimated from the polarization curves of biofuel cell with SWNTs was around 320 mV, which is higher than biofuel cell without nanotube film.

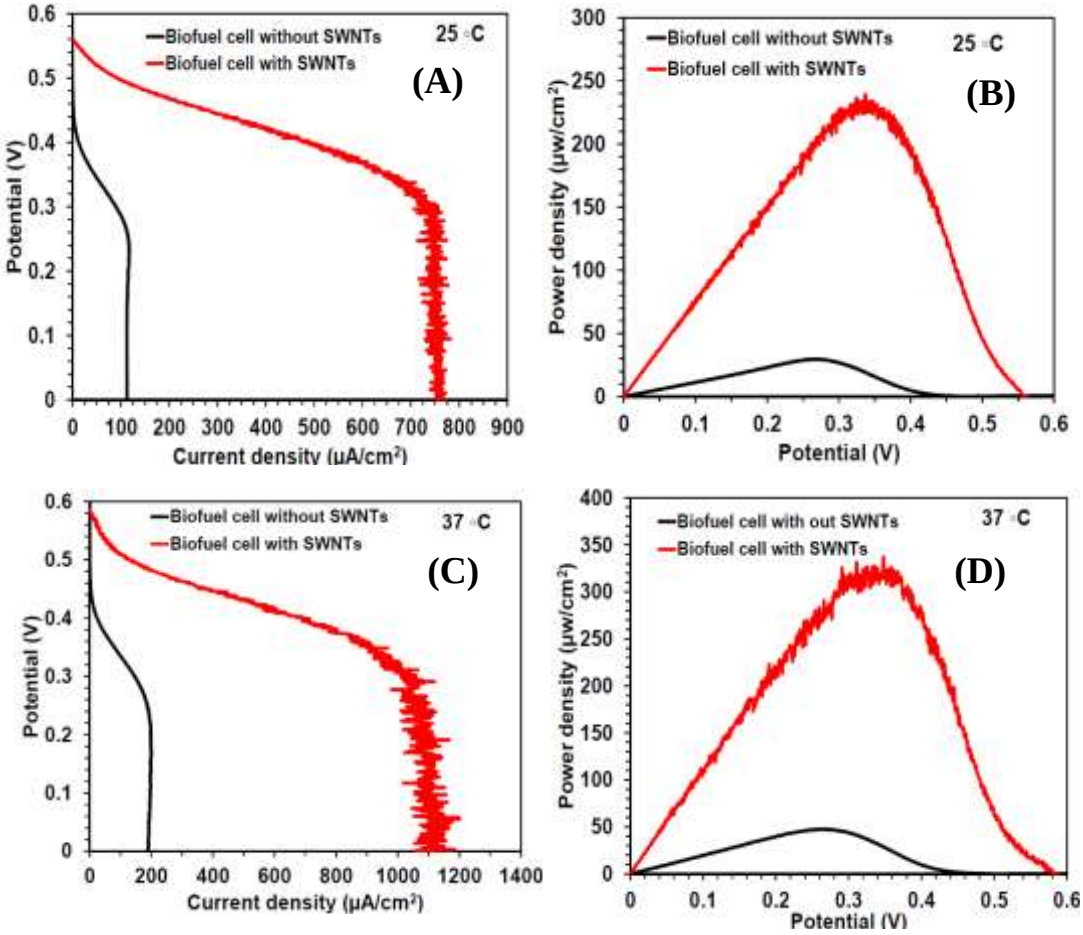


Figure 4.9 Effect of incorporating SWNTs on the performance of biofuel cell performance. A (C) and B (D) are the polarization and dependence of the biofuel cell without SWNTs and with SWNTs power density on cell voltage at 25 ^{o}C (at 37 ^{o}C), repectively. Bioanode and cathode films cast on a 3 mm GC electrodes. Stirred solution under air-saturating conditions, citric acid, pH 5.5, 60 mM glucose.

Figure 4.9 (A) and (C) shows the polarization of biofuel cells without or with SWNTs film at 25 ^{o}C and 37 ^{o}C. The corresponding dependence of the cell power densities on voltage at different temperature is in Figure 4.9 (B) and (D), and a summary of data from these biofuel cells is provided in Table 4.1. At 25 ^{o}C, comparing with biofuel cell without SWNTs film, the incorporation of SWNTs into biofuel cell resulted in 6.72 fold increase in the maximum current density output (760 μA/cm^2) and 8.03 fold increase in the maximum power density output (233 μw/ cm^2). Meanwhile, the incorporation of SWNTs film into biofuel cell shifted both of the

open-circuit voltage (OCVs) and cell voltage to higher value. The increase of cell voltage for biofuel cell with the incorporation of SWNTs was in consistence with the estimated value from the polarization curves in Figure 4.8(B). As expected, biofuel cell with and without SWNTs film exhibited higher current density and power density output at the optimal temperature (37 ^{o}C) for enzyme activity than as well as the OCVs value. The maximum current density and power density of biofuel cell with the modification of nanotube film were 1110 μA/cm^2 and 338 μw/ cm^2 at 37 ^{o}C, respectively, which are 1.46 fold and 1.45 fold higher than the performance of biofuel cells tested at room temperature. There was no obvious change in cell voltage tested under different temperatures, indicating that the increase in the power density output of biofuel cell was due to the significant increase in the current density of biofuel cell.

Table 4.1 Summary of biofuel cells without and with SWNTs(7,6) at 25 ^{o}C and 37 ^{o}C

Cell type	**Temperature**	**Open circuit voltage (mV)**	**Maximum current density (μA/cm^2)**	**Cell voltage (mV)**	**Maximum power density (μw/ cm^2)**
Biofuel cell no SWNTs	25 ^{o}C	340	113	267	29
Biofuel cell With SWNTs	25 ^{o}C	560	760	340	233
Biofuel cell no SWNTs	37 ^{o}C	450	187	265	48
Biofuel cell with SWNTs	37 ^{o}C	580	1110	338	324

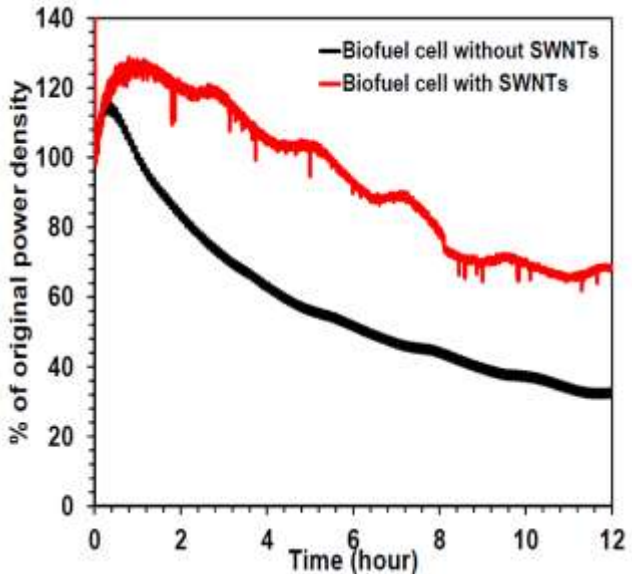


Figure 4.10 Biofuel cell stability. Biofuel cell with and without SWNTs were continuously operated at maximum power for 12 h at 25 ^{o}C. Citric acid buffer (0.05 M), pH 5.5, 60mM glucose, air saturating conditions, stirring.

Figure 4.10 shows the stability of the stationary biofuel cells without and with modification of SWNTs films at room temperature. After continuous operation at maximum power for 12 hours, the biofuel cell without SWNTs retained 33% of its original power density, while cell with SWNTs film retained 67% of its original power density, indicating that the modification of carbon nanotube film significantly improved cell stability. Taking the stability results of anode and cathode in Figure 4.6 and Figure 4.7(C) into consideration, since anode electrodes retained higher percentage of its original current density than cathode electrodes after operating for the same duration, we suspect that the limiting factor for the biofuel cell stability is the cathode electrodes. In all, it can be conclude that the incorporation of single wall carbon nanotube network into redox polymer mediated enzymatic biofuel cell led to more stable biofuel cell with higher current density and power density output.

CONCLUSIONS

In this study, we investigated the effect of incorporating single carbon nanotubes with different chirality on the electrochemical and enzymatic performance

of high surface carbon nanotube film modified redox polymer/glucose oxidase electrodes. We demonstrated that the chirality of carbon nanotube was an important factor affecting the electrochemical and enzymatic performance of redox hydrogel film. Redox hydrogel- enzyme electrodes with the incorporation of SWNTs(7,6) film showed higher glucose response (3326 uA/cm^2) than those with SWNTs(6,5) film .

We also observed that the nanotube film loading played an important role in determining the electrochemical and enzymatic output of electrodes. Electrodes with the SWNTs film loading of 30 μg showed the highest current density output at the glucose saturating concentration(5556 μA/cm^2). Furthermore, the redox polymer and enzyme hydrogel loading also affected the electrochemical and enzymatic performance of electrodes significantly. Electrodes with higher redox polymer hydrogel loading showed the highest limiting current density output of 11.2 mA/cm^2 at glucose saturating concentration, which was among the highest value reported for glucose electrodes with the incorporation of carbon nanotube. Moreover, our results showed improved enzymatic stability of glucose electrodes with the incorporation of nanotube film and higher redox polymer hydrogel loading. Similarly, the incorporation of SWNTs film into ferrocene redox polymer mediated laccase cathode electrodes led to obvious improvement of current density output and prolonged enzyme stability. Lastly, the effect of incorporating nanotube network on the performance of biofuel cell consisting of $FcMe_2$-C_3-LPEI / GOx anode and Cl-Fc-LPEI/laccase cathode without and with SWNTs films was evaluated. Our results showed that compared with cell without SWNTs, the incorporation of nanotube film into biofuel cell resulted in 8.03 fold increase in the maximum power density output of 233 μw/ cm^2 at 25 ^oC, and 338 μw/ cm^2 at 37 ^oC. Biofuel cells stability also improved. In conclusion, the incorporation of high surface SWNTs(7,6) film into

electrodes provides a clue to construct a wide range of enzymatic biosensor electrodes with high current density output and long lifespan, as well as biofuel cell with high power density output.

Acknowledgements:

I would like to thank David Hickey for synthesizing polymers for me. I would also like to thank Dr. Glatzhofer for all of his valuable insight and discussions.

Chapter 5:

Effect of SWNTs(7,6) Incorporating Methods on the Ferrocene-modified Linear Poly(ethylenimine) Hydrogel film for Biofuel Cell

INTRODUCTION

Nowadays, enzymatic biofuel cells (EBFCs) are drawing noticeable attention due to their potential application as alternative energy source for implantable electronic devices and portable electronics[1, 3]. EBFCs represent a new energy-conversion technology using renewable biocatalysts (enzymes) to oxidize/reduce substrates, and operate under mild conditions (25-40 ^{o}C, and near neutral pH). The specificity of immobilized enzymes in biofuel cells eliminates the need of a membrane to separate the anode and cathode, allowing construction of compartmentless and miniaturized biofuel cells. In addition, without membrane separation, oxidants and fuels from the surrounding environment, such as vegetal and body fluids, can be used by EBFCs. However, there are some obstacles limiting the practical implantation of EBFCs into mammals, including relatively low power density (in the range of $\mu W/cm^2$), a short lifetime due to the instability of enzymes, and inefficient electron communication. Various strategies have been introduced to address these problems, including using enzyme cascades,[13, 196] applying redox mediators [16, 56]and incorporating nanomaterials [9, 197]into biofuel cells.

Recently, semiconducting carbon nanotubes (CNTs) have been recognized as a very promising materials for the construction of high performing biosensors and biofuel cells, due to their excellent electrical conductivity and unique structural properties[6, 7, 27, 28]. Previously, we reported that incorporation of semi-conductive single wall carbon (SWNTs (6,5)) nanotubes into redox polymer hydrogel films either by directly mixing SWNTs into redox hydrogel film, or creating a high surface

SWNTs network led to a significant increase in the electrochemical and enzymatic performance of redox polymer/enzyme hydrogel film with glucose electro-oxidation current densities of ~ 3 mA/cm^2 [27, 28]. In this study, in order to taking full advantage of the two nanotube incorporation methods mentioned above, a novel method was developed by casting nanotube incorporated redox polymer and enzyme hydrogel film on top of high surface area nanotube film modified glassy carbon electrodes. The effect of incorporating single wall carbon nanotubes SWNs(7,6) on the electrochemical and enzymatic performance of $FcMe_2$-C_3-LPEI mediated glucose electrode and whether this method could be applicable to improve other enzyme based electrodes like laccase and fructose dehydrogenase (FDH), were investigated. Further, the effect of incorporating SWNTs (7,6) into redox polymer mediated enzymatic anode and cathode on the power density output and stability of biofuel cell were evaluated.

EXPERIMENTAL SECTION

Chemicals and solutions

Glucose oxidase from *Aspergillus niger* (EC 1.1.3.4, type X-S, 204.1 units/mg of solid), laccase from Trametes versicolor were purchased from Sigma Aldrich. Fructose dehydrogenase from Gluconobacter *sp.* (EC 1.1.99.11, grade III, 100 units/mg of solid) was purchased from TOYOBO. Triton X-100 was purchased from EM Science. Ethylene glycol diglycidyl ether (EGDGE) was purchased from Polysciences, Warrington, PA. All chemicals and solvents were used as received without further purification. $FcMe_2$-C_3-LPEI redox polymer and Cl-Fc-LPEI redox polymer were kindly provided by Dr.Glatzhofer's lab, and synthesized by David Hickey and Nick Godman in Glatzhofer lab, respectively [186, 187]. 50 mM phosphate buffer solution (pH=7) was prepared by dissolving 6g of NaH_2PO_4 in 1 L of nanopure

deionized water. 2M glucose solution was prepared in water 24 h before use and refrigerated at 4°C when not in use. Single-wall carbon nanotube (7,6) were purchased from South West Nanotechnologies. Nanotubes suspensions (3 mg/ml) were prepared by sonicating 9 mg nanotube in 3 ml of 5 g/L Triton X-100 aqueous solutions with a horn sonic dismembrator (Model 500, Fisher Scientific) running at 22% output for 1 hour.

Enzyme electrode construction

Glassy carbon electrodes (3 mm diameter stationary disk) were polished successively on three grades of alumina (5, 1, 0.3μm), and washed thoroughly with nanopure water after each polishing step.

Anodic enzyme electrodes:

Solutions of $FcMe_2$-C_3-LPEI were prepared by dissolving in water while adding 0.1 M HCl solution until the final concentration of the polymer solution was 10 mg/mL and pH was 5 (for glucose electrodes) or 4.2 (for fructose electrodes). The schematics of preparing electrodes with the incorporation of nanotube by two different strategies (type A and type B) are shown in Figure 5.1.

Control Anode electrodes

Electrodes without SWNTs were made by mixing the following solutions: 14 μL of $FcMe_2$-C_3-LPEI polymer solution (10 mg/mL in water), 6 μL of GOX (10 mg/mL) or FDH solution (60 mg/mL) and 0.75μL of EGDGE crosslinker solution. A 3 μL of mixture solution was then deposited onto the glassy carbon electrode surface and allowed to dry for at least 12 hours at room temperature.

Type A anode electrodes

First, 10μl of a SWNTs dispersion was cast on top of a polished glassy carbon electrode and allowed to dry overnight at room temperature to form a SWNTs film

modified GCE. Next, redox hydrogels were made from mixing 14 µL of $FcMe_2$-C_3-LPEI polymer solution (10 mg/mL in water), 6 µL of GOX (10 mg/mL) or FDH solution (60 mg/mL) and 0.75µL of EGDGE crosslinker solution. Finally, 21µL of the redox hydrogel mixture was then deposited on top of a SWNTs film coated GCEs and allowed to dry for at least 12 h.

Type B anode electrodes

Similar to type A electrodes, the first step in type B electrodes was to form SWNTs network on the GCEs. Then, a redox hydrogel film was made by mixing 14 µL of $FcMe_2$-C_3-LPEI polymer solution (10 mg/mL in water), 3 µL of GOX (20 mg/mL) or FDH solution (120 mg/mL), 3 µL of nanotube suspension (27.6 mg/ml) and 0.75µL of EGDGE crosslinker solution. Finally, 21µL of the redox hydrogel-SWNTs mixture was deposited on top of a SWNTs coated GCEs and allowed to dry for at least 12 h.

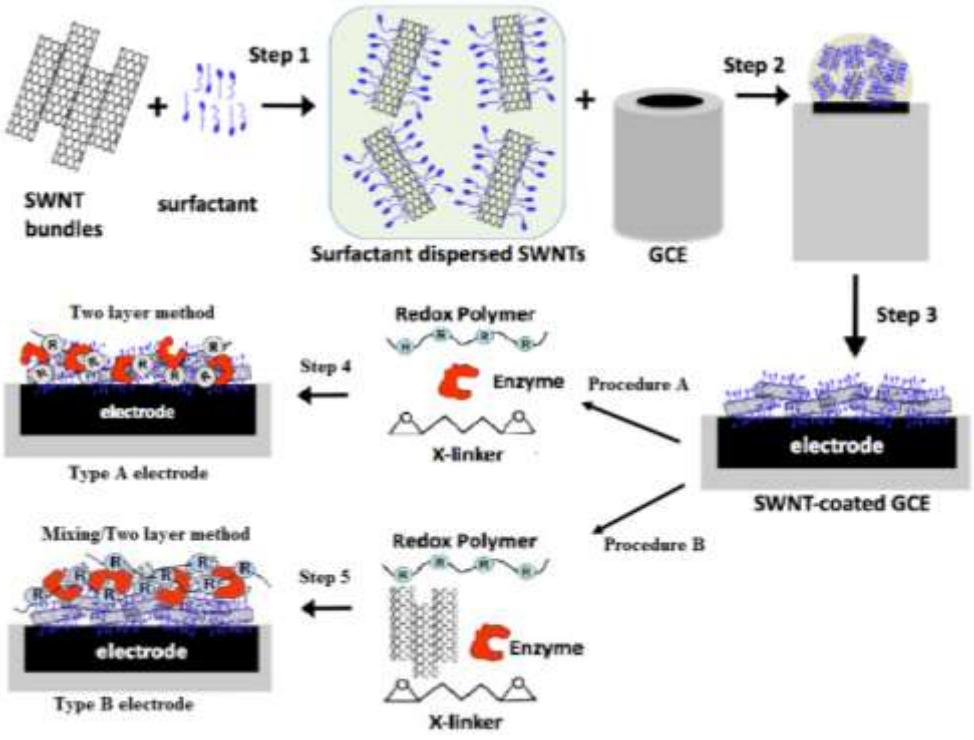


Figure 5.1 Schematic of the construction of redox polymer hydrogel film with the incorporation of SWNTs by different method: two layer method (procedure A) and mixing/two layer method (Procedure B)

Cathodic enzyme electrodes:

A 12 mg/ml Cl-Fc-LPEI polymer solution was prepared by dissolving Cl-Fc-LPEI polymer in water. Similar to the anodic electrodes we applied the methods shown in Figure 5.1 to prepare control electrodes, type A and type B cathodic electrodes. Control electrodes were prepared by mixing 4 µL of Cl-Fc-LPEI polymer solution, 6 µL of 35 mg/ml Laccase and 0.75 µL of EGDGE (adding 10 µL of crosslinker into 45 µl of H_2O)), and then depositing 3 µl of this mixture onto bare GCEs. Type A cathode electrodes were prepared by casting 21 µL of the redox polymer-enzyme solution using the same volume ratio of redox polymer, enzyme and crosslinker as in control cathode electrodes onto SWNTs film modified GCEs. Type B cathodic electrodes with the incorporation of SWNTs were prepared by mixing 14 µL of 12 mg/ml Cl-Fc-LPEI, 3 µL of 70 mg/ml Laccase, 3 µL of nanotube suspension (27.6 mg/ml) and 0.75 µL of EGDGE (adding 10 µL of crosslinker into 45 µl of H_2O) together, then casting 21 µL of the mixture solution onto SWNTs film modified glassy carbon electrode surface. All electrodes are allowed to dry overnight.

Electrochemical and Spectroscopic Measurement

Cyclic voltammetry and constant potential tests were performed with a CH Instruments model 832 bipotentiostatin using a three-electrode cell configuration with platinum wire as counter electrodes and saturated calomel electrodes as reference electrodes. The background electrolyte was 50 mM phosphate buffer solution (pH 7) for glucose electrodes or Mcilvaine buffer (pH=5) for fructose electrodes. The temperature was maintained at 25±1°C with a water-jacketed electrochemical cell. The calibration curve was measured by adding aliquots of a stock 2 M substrate solution (glucose or fructose) to a well-stirred cell with the working electrode poised at 50 mV higher than oxidation peak potential. Biofuel cells were assembled by

placing one anodic enzyme electrode and one cathodic enzyme electrode into a one-compartment electrochemical cell filled with citric buffer (pH 5.5) and 60 mM glucose or with Mcilvaine buffer pH 5.5 and 60 mM fructose.

Calculation and Statistics

Current densities were calculated using the geometric surface area of a 3-mm-diameter electrode. Values are presented as mean ± standard error of the mean (SEM) unless otherwise specified.

RESULTS AND DISCUSSION

Effect of SWNTs incorporating methods on the performance of $FcMe_2$-C_3-LPEI/GOX electrodes

Previously, we have demonstrated that the incorporation of semi-conducting SWNTs into linear polyethylenimine (Fc-C_6-LPEI) /glucose oxidase hydrogel film led to 4-5 fold increase in the redox peak currents in cyclic voltammetry, and 5 folds increase in enzymatic response[27]. We also demonstrated that modifying the surface of glassy carbon electrodes with a network of SWNTs prior to coating of a redox polymer hydrogel film led to significant increase in enzymatic response to glucose, reaching a current density of ~1.7–2.1 mA/cm^2 [24]. In order to take advantage of these two methods mentioned above, a novel method, type B method as shown in Figure 5.1, was developed by incorporating SWNTs into cross-linked redox polymer/enzyme hydrogel film on SWNTs-network modified GCEs. The effect of different SWNTs(7,6) incorporating methods on the electrochemical and enzymatic performance of $FcMe_2$-C_3-LPEI/GOx electrodes was investigated by cyclic voltammetry and constant potential experiments.

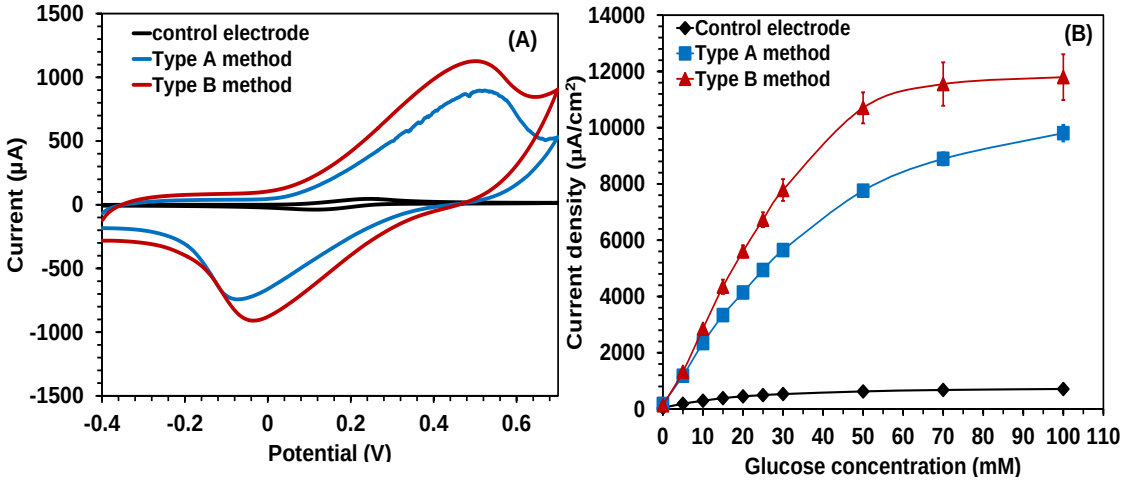


Figure.5.2 Cyclic voltammograms (A) and Glucose response (B) of GCE with redox polymer/enzyme film alone (control), type A electrodes, and type B electrodes. Scan rate=50 mV/s in 50 mM sodium phosphate (pH=7) at 25℃

Figure 5.2(A) shows the CVs of bare glassy carbon electrodes with $FcMe_2$-C_3-LPEI/GOx hydrogel film (control), SWNTs film modified GCEs with $FcMe_2$-C_3-LPEI/GOx film (type A electrodes), and SWNTs film modified GCEs with $FcMe_2$-C_3-LPEI/GOx/ SWNTs film (type B electrodes) in sodium phosphate buffer. For control electrodes without SWNTs, a pair of well-defined redox peaks corresponding to the oxidation and reduction of the redox polymer's methylated ferrocene complexes was observed at 244 and 116 mV versus SCE, respectively ($\Delta E_{control}$=108 mV). Compared with control electrodes, both type A and type B electrodes showed significant increase in their oxidation and reduction peak currents, as well as background currents. The increase of background current with the presence of nanotube is consistent with our previous reports and others[198, 199], due to increased electrode area undergoing double layer charging and background reaction from the high surface of SWNTs. The oxidation peak currents of type A electrodes and type B electrodes were 19.5 fold and 24 fold higher than control electrodes, suggesting that the incorporation of SWNTs by both methods made more redox polymer active sites electrochemically accessible. Moreover, compared with type A electrodes, type B electrodes showed further improvement in the electrochemical performance. Besides,

the incorporation of SWNTs into $FcMe_2$-C_3-LPEI/GOx electrodes by both type A and type B method shifted the oxidation and reduction peak potential, resulting in a large potential peak separation ($\Delta E_{\text{type A}}$ =609 mV, $\Delta E_{\text{type B}}$ =536 mV), which is consistent with our previous reports [27] and most likely due to the ability of carbon nanotubes to donate/ accept electrons (i) at the glassy carbon interface, (ii) junctions between interconnected SWNTs or (iii) ferrocene redox. Meanwhile, the presence of SWNTs broadened the oxidation and reduction peak of type A and type B electrodes, in contrast to the well-defined peaks in control electrodes.

To determine the effect of different SWNTs incorporation methods on enzymatic response of $FcMe_2$-C_3-LPEI/GO_X electrodes to glucose and evaluate its potential application as anode in the biofuel cell, constant potential amperometry was performed by poising the electrodes at 50mV higher than the oxidation peak potential, and measure the current output as a function of glucose concentration in well-stirred buffer solution. As shown in figure 5.2 (B), all electrodes displayed Michaelis-Menten-type behavior. The Michaelis constant value (K_m) of control electrodes, type A, and type B electrodes were 13.5 mM, 25 mM and 21 mM, respectively. The increased K_m value with the incorporation of SWNTs into redox hydrogel electrodes may be the result of increasing mass transfer resistance.

Incorporation of nanotubes into $FcMe_2$-C_3-LPEI/GO_X electrodes by type A and type B methods led to 13.7 fold and 16.5 fold increase in the maximum current density output under saturating glucose concentration, reaching 9.81 and 11.8 mA/cm^2, respectively. To date, the high current density of type B electrodes in this study is among the highest reported current densities for single enzyme mediated bioelectrodes constructed on glassy carbon electrodes. The above results suggest that the method to incorporate carbon nanotube has critical influence in determining the

electrochemical and enzymatic performance of electrodes. In order to obtain high performing enzymatic biofuel cell, type B method was chosen to prepare the anode and cathode electrodes of a biofuel cell in the following study.

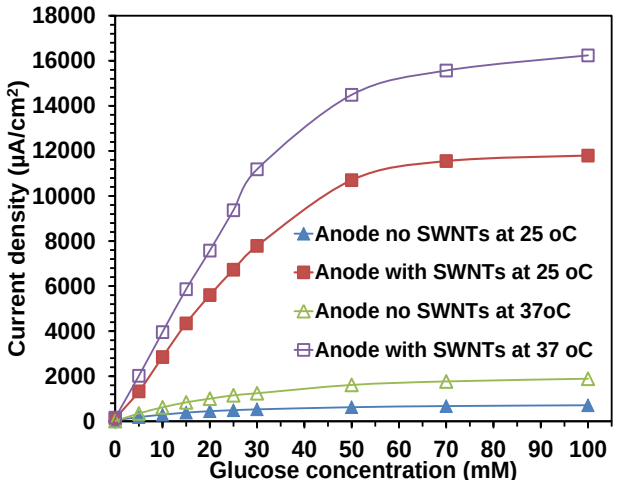


Figure 5.3 Glucose calibration curves of control electrodes (▲) and Type B electrodes (■) at 25◦C (No fill) and 37◦C (Solid filled). Sodium phosphate buffer, pH 7, E= 0.3V (FcMe2-C3-LPEI/GOX without SWNTs) or 0.55 V (FcMe2-C3-LPEI/GOX with SWNTs).

In order to evaluate the performance of the $FcMe_2$-C_3-LPEI/GO_X type B electrodes at physiological temperature for its potential application as anode of enzymatic biofuel cell, we measured the glucose response of $FcMe_2$-C_3-LPEI/GO_X electrode without SWNTs and type B electrodes at 37◦C. As shown in Figure 5.3,increasing temperature from 25◦C to 37 ◦C resulted in an obvious increase in current density, with a limiting current density of 1940 µA/cm^2 for electrodes without SWNTs, and 16.2 mA/cm^2 for SWNTs incorporated electrodes. The high current density output of $FcMe_2$-C_3-LPEI/GO_X electrodes with incorporation of SWNTs at both temperatures suggest the possibility of using these electrodes as anode in a biofuel cell producing high current and power densities, when coupled with proper bio-cathode with good electrochemical efficiency and high voltage. Meanwhile, the high current density achieved in this study provides the potential of constructing miniature and high sensitivity glucose biosensor.

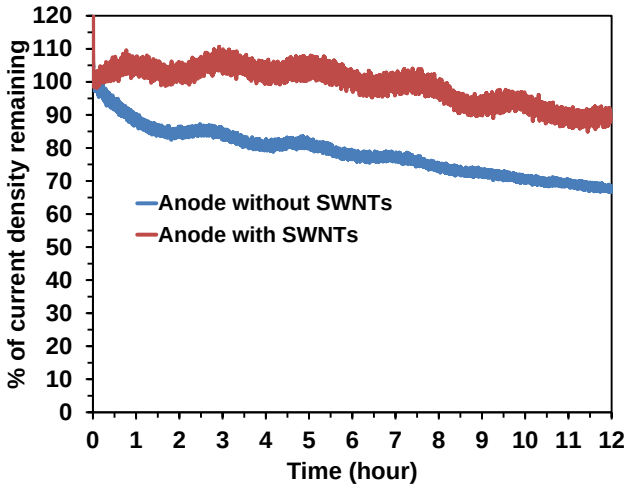


Figure 5.4 Enzymatic stabilities of $FcMe_2$-C_3-LPEI /GO_X electrodes without and with SWNTs (type B electrodes). Cross-linked films of GO_X and $FcMe_2$-C_3-LPEI films without and with SWNTs were operated continuously in sodium phosphate at pH 7 and 10 mM glucose, E= 0.3V ($FcMe_2$-C_3-LPEI/GO_X without SWNTs) or 0.55 V ($FcMe_2$-C_3-LPEI/GO_X with SWNTs), T=25 ℃

Stability tests were performed to determine the effect of incorporating SWNTs(7,6) on the enzymatic stability of $FcMe_2$-C_3-LPEI/GO_X electrodes. Figure 5.4 shows continuous operation stability tests for electrodes without SWNTs and electrodes with SWNTs. After 12 hours of continuous operation, films without SWNTs retained 68% of their original current density, while electrode with SWNTs(7,6) retained 90% of their initial current density, suggesting that incorporation of SWNTs(7,6) into electrodes improved the enzymatic stability of electrodes significantly. According to recent studies[194, 200, 201], smaller nanoparticles with high surface curvature promoted the retention of protein structure and function, as well as protein stability. Asuri et al. reported the ability of SWNTs to stabilize protein activity to a greater extent than conventional flat supports. He also suggested that lateral interactions between adjacent adsorbed proteins, causing protein deactivation, were suppressed on highly curved SWNTs relative to those on flat surfaces[194]. Therefore, in this study, we hypothesize that the inherent property of SWNTs incorporated in $FcMe_2$-C_3-LPEI/GO_X electrodes contributed to the increase

of enzymatic stability. The improvement in the enzymatic stability of $FcMe_2$-C_3-LPEI/GO_X electrodes prepared by type B method was favorable for the construction of enzymatic biofuel cell with long span life.

Effect of incorporating SWNTs (7,6) onto Cl-Fc-LPEI/Laccase cathode

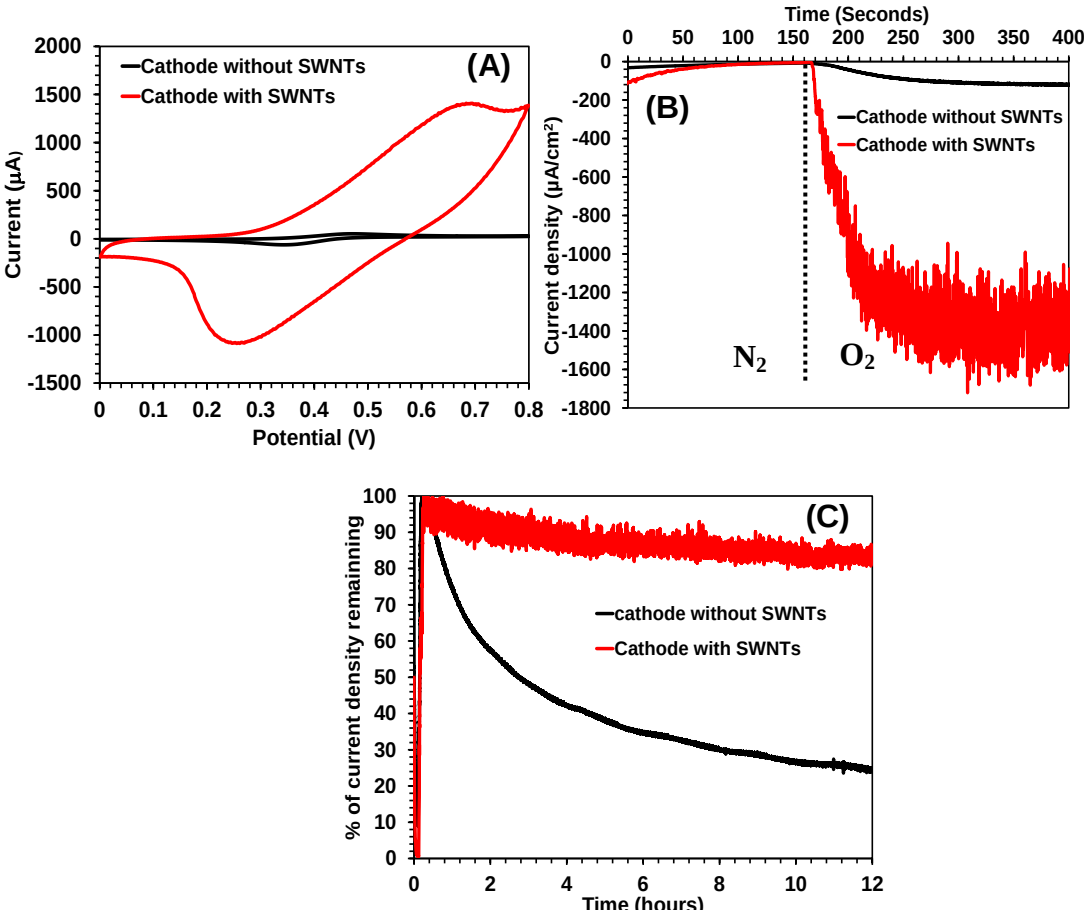


Figure 5.5 (A) Effect of incorporating SWNTs(7,6) on cyclic voltammetry curves of Cl-Fc-LPEI/Laccase electrodes without and with SWNTs. scan rate: 50 mv/s, in citric acid pH 5.5 at 25℃. (B) Glucose calibration curves of electrodes without and with SWNTs at 25◦C. citric acid buffer, pH 5.5, E= 0.29V (Cl-Fc-LPEI/Laccase without SWNTs) or 0.23 V (Cl-Fc-LPEI/Laccase with SWNTs). (C) Enzymatic stability of Cl-Fc-LPEI/Laccase cathode electrodes with and without SWNTs. T=25°C, pH=5.5 citric buffer

As a common biocatalyst applied to construct biofuel cell cathode, laccase can efficiently catalyze the reduction of molecular oxygen to water in either direct electron transfer mode or mediated electrode transfer mode. In this study, we use a Cl-Fc-LPEI redox polymer to prepare mediated laccase electrodes as cathode in the biofuel cell. To investigate whether the incorporation of SWNTs(7,6) by type B

method could improve the electrochemical and enzymatic performance of laccase electrodes, we prepared Cl-Fc-LPEI/Laccase electrodes without and with the incorporation of SWNTs. Figure 5.5(A) shows the CVs of Cl-Fc-LPEI/Laccase electrodes without and with the incorporation of SWNTs (7,6). Similar to aforementioned results in Figure 5.2 (A), the incorporation of SWNTs into cathode electrode led to a 15-fold increase in the oxidation and reduction peak current, as well as a large background current. The corresponding enzymatic response of the prepared Cl-Fc-LPEI/Laccase electrodes is shown in Figure 5.5(B). Compared with electrodes without SWNTs film, the incorporation of SWNTs into electrodes resulted in a 11.8-fold increase in oxygen response, reaching a current density of 1455.4 $\mu A/cm^2$. Figure 5.5(C) shows continuous operation stability tests for Cl-Fc-LPEI/Laccase electrodes without SWNTs and with SWNTs. After 12 hours continuous operation, film without SWNTs retained 24.3% of their original current density, while electrode with SWNTs(7,6) retained 83.2%, indicating that the incorporation of SWNTs into Cl-Fc-LPEI/Laccase electrodes improved the enzymatic stability significantly. From the above results, it can be concluded that incorporation of SWNTs into enzymatic electrodes by type B method is applicable to construct various enzyme and redox polymer based electrodes with high electrochemical and enzymatic performance output and good stability.

Glucose /O_2 biofuel cell

To determine the influence of incorporating SWNTs into redox polymer-enzyme coated cathodes and anodes on the performance of biofuel cell, we constructed compartment-less biofuel cells consisted of a $FcMe_2$-C_3-LPEI / GOx anode and a Cl-Fc-LPEI/laccase cathode both without and with the incorporation of SWNTs. Figure 5.6 shows the polarization curves for anodes and cathodes without

(Fig. 5.6(A)) and with SWNTs film (Fig. 5.6(B)). For biofuel cell without SWNTs, the catalytic electro-oxidation current of glucose appeared at 0 V and reached a maximum of 505 μA/cm^2 at 0.21 V, while the catalytic electro-reduction current of oxygen occurred at 0.49 V and reached a maximum of 110 μA/cm^2 at 0.24 V. Comparing the midpoints of anodic polarization curve with their counterparts of cathodic polarization curve, the cell voltage of biofuel cell without SWNTs was calculated to be 250 mV at the maximum power. Compared to the polarization curve in Figure 5.6 (A), incorporation of SWNTs into the anode and cathode increased the current density ouput, and shifted the electro-oxidation and reduction potential. For anode with SWNTs, the catalytic electro-oxidation current of glucose appeared at 0 V and reached a maximum at 0.48 V, while the catalytic electroreduction current of oxygen occurred at 0.56 V and reached a maximum at 0.24 V. The cell voltage estimated from the polarization curves of biofuel cell with SWNTs was around 302 mV. The current density at the anodes and cathodes with SWNTs were 14.6 mA/cm^2 and 1361 μA/cm^2, respectively, which are 29-fold and 12.4-fold higher than electrodes without SWNTs. Meanwhile, the current density output of the cathode was much lower than that of anode, indicating that in a biofuel cell with stationary electrodes of equivalent surface areas, it is the cathode that limits the maximum possible power output of biofuel cell.

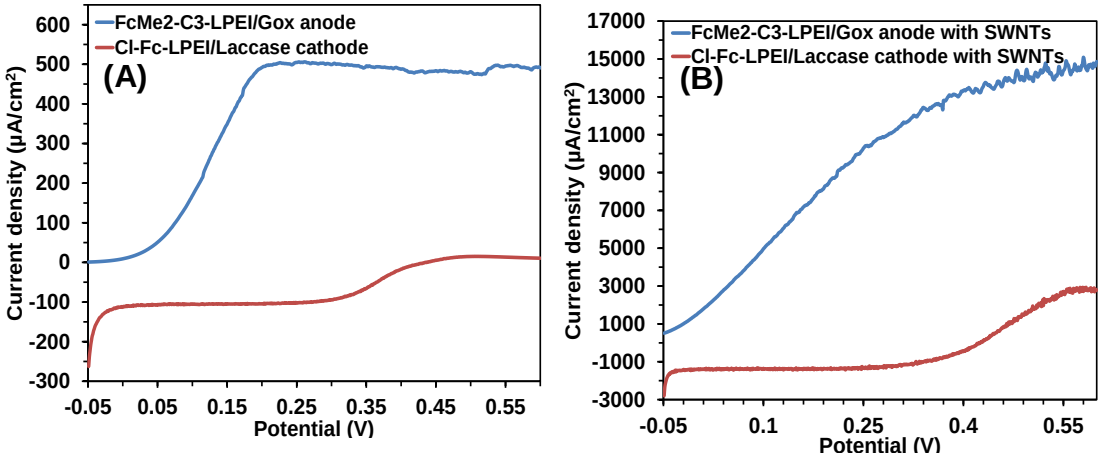


Figure 5.6 Polarization curves of $FcMe_2$-C_3-LPEI /GOX anode and Cl-Fc-LPEI/Laccase cathode without (A) and with SWNTs (B). Stirred solution under air-saturating condition, citric buffer, pH 5.5, 60 mM glucose, scan rate 1 mV/s, 25^{o}C.

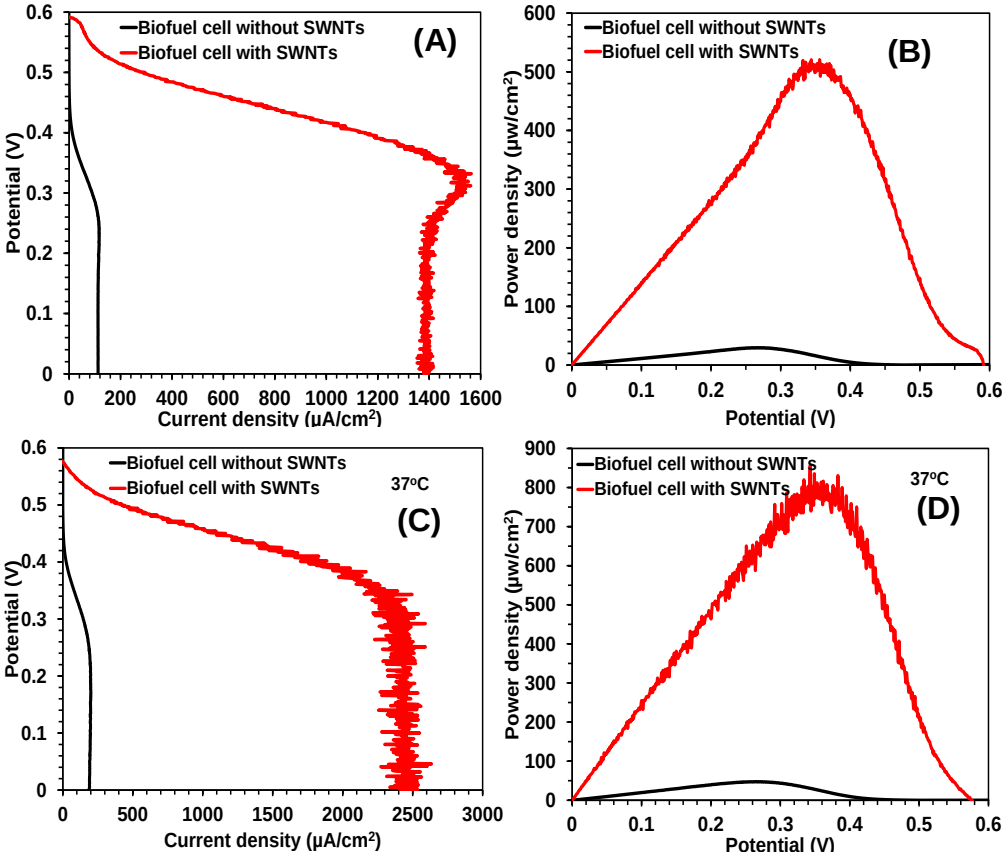


Figure 5.7 Effect of incorporating SWNTs on the performance of biofuel cell. A (C) and B (D) are the polarization and dependence of biofuel cell without and with SWNTs power density on cell voltage at 25 ^{o}C (at 37 ^{o}C), respectively. Bioanode and cathode films cast on a 3 mm GC electrodes. Stirred solution under air-saturating conditions, citric acid, pH 5.5, 60 mM glucose

Figure 5.7(A) and (C) shows the polarization curve of biofuel cells using $FcMe_2$-C_3-LPEI/GOx anode and Cl-Fc-LPEI/laccase cathode with or without SWNTs

at 25 ^{o}C or 37^{o}C. The dependence of the cell power densities on voltage at 25 ^{o}C and 37^{o}C is also shown in Figure 5.7(B) and (D), and a summary of data from biofuel cell with and without SWNTs is provided in Table 5.1. For biofuel cell without SWNTs film at 25 ^{o}C, the maximum current density was ~113 μA/cm^{2}, the maximum power density was 30 μW/cm^{2} at cell voltage of 267 mV and the open-circuit voltage (OCVs) was estimated to be 430 mV. At room temperature, the incorporation of SWNTs into both the anode and cathode resulted in a 12.3-fold increase in the maximum current density, reaching 1390 μA/cm^{2}, and 17-fold increase in the maximum power density output, to 510 μw/ cm^{2} at cell voltage of 350 mV. The biofuel cell with a SWNT film exhibited OCVs of 590 mV. Increasing the temperature from 25 ^{o}C to 37 ^{o}C resulted in increases of current density and power density output of biofuel cells both without and with SWNTs. The maximum current density and power density of biofuel cells with SWNTs were 2456 μA/cm^{2} and 802 μW/cm^{2}, respectively, which were 1.78-fold and 1.57-fold higher than at 25 ^{o}C. However, there was no obvious change in the open circuit potential and cell voltage. The power density output of nanostructured enzymatic biofuel cells in this study was the highest value for mediated enzymatic biofuel cells, higher than the power density of a recent report by Mano and coworkers using glucose oxidase as anode catalyst and bilirubin oxidase as cathode enzyme (740 μW/cm^{2} at 0.57 V)[202].

Table 5.1 Summary of biofuel cells without and with SWNTs at 25 ^{o}C and 37 ^{o}C

Biofuel cell type	temperature	Open circuit voltage (mV)	Maximum current density (μA/cm^2)	Cell voltage (mV)	Maximum power density (μW/ cm^2)
Biofuel cell no SWNTs	25 ^{o}C	430	113	267	30
Biofuel cell With SWNTs	25^{o}C	590	1390	350	510
Biofuel cell no SWNTs	37 ^{o}C	440	187	264	50
Biofuel cell With SWNTs	37 ^{o}C	580	2456	355	802

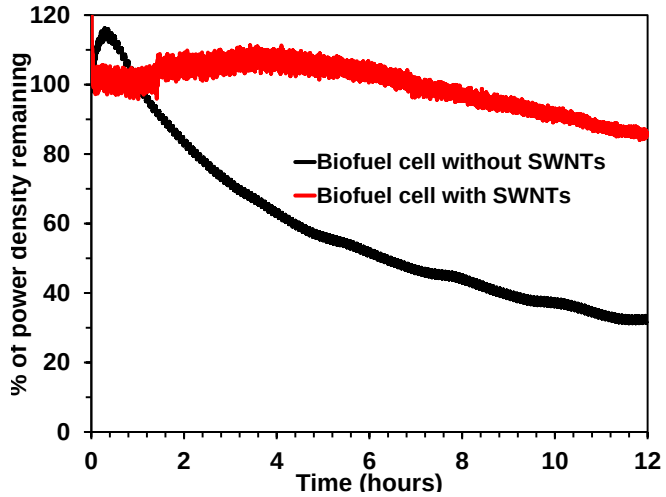


Figure 5.8 Biofuel cell stability. Biofuel cell with and without SWNTs were continuously operated at maximum power for 12 h at 25 ^{o}C. Citric acid buffer (0.05 M), pH 5.5, 60mM glucose, air saturating conditions, stirring.

Figure 5.8 shows the stability of the stationary biofuel cells without and with incorporation of SWNTs at room temperature. After continuous operation at maximum power for 12 hours, the biofuel cell without SWNTs retained 33% of its original power density, while cell with SWNTs film retained 86.3% of its original power density under the same conditions, indicating that the incorporation of carbon nanotube significantly improve the biofuel cell stability. In summary, it can be

concluded that the incorporation of single wall carbon nanotube into redox polymer mediated glucose/O_2 enzymatic biofuel cell led to dramatic increase in the current density and power density output, also significantly improved biofuel cell stability.

Fructose/O_2 biofuel cell

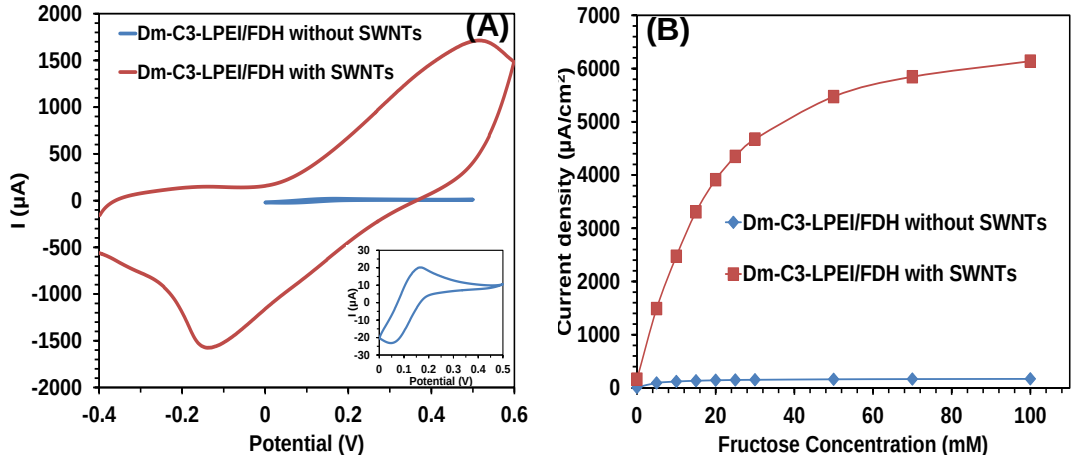


Figure.5.9 Cyclic voltammograms (A) and Fructose response (B) of $FcMe_2$-C_3-LPEI/FDH electrodes without SWNTs and with SWNTs (type B electodes) . Scan rate=50 mV/s, Mcilvaine buffer (pH=5), 60 mM fructose. Inset in (A) is the CV curves of $FcMe_2$-C_3-LPEI/FDH electrodes without SWNTs

In order to investigate whether the incorporation of SWNTs(7,6) can be applied to increase the current density output of other enzymatic electrodes, we constructed $FcMe_2$-C_3-LPEI mediated fructose dehydrogenase (FDH) electrodes with the incorporation of SWNTs using type B method aforementioned. The CV curves of $FcMe_2$-C_3-LPEI/FDH electrodes without and with SWNTs are shown in Figure 5.9 (A). Incorporation of SWNTs into $FcMe_2$-C_3-LPEI/FDH showed similar effect to that of glucose electrodes in Figure 5.2 (A), leading to dramatic increase in the oxidation and reduction peak current, background current and large peak separation. Compared with electrodes without SWNTs, presence of SWNTs resulted in 60-fold increase in the oxidation peak current, reaching 1710 μA. The fructose responses of $FcMe_2$-C_3-LPEI/FDH electrodes without and with SWNTs are shown in Figure 5.9(B). For control electrodes, the limiting current density at the glucose saturating concentration

was around 170μA/cm^2. The incorporation of SWNTs into $FcMe_2$-C_3-LPEI/FDH electrodes by type B method showed a limiting current density of 6138 μA/cm^2, 36-fold higher than electrodes without SWNTs. The current density of fructose electrodes in this study is significantly higher than the current density output of direct electron transfer fructose electrodes of 4 mA/cm^2 reported by Kano et al[9].

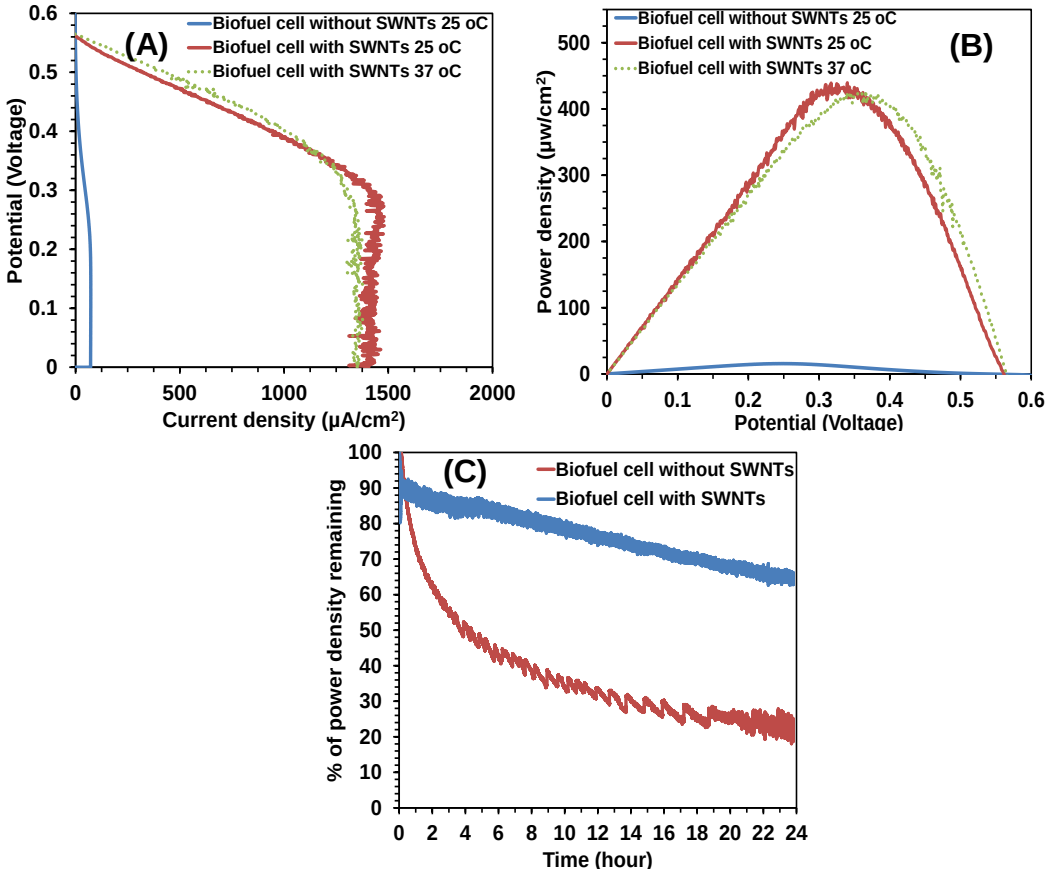


Figure 5.10 Biofuel cell Performance without SWNTs and with SWNTs. (A) and (B) are the polarization curves and dependence of biofuel cell without and with SWNTs power density on cell voltage at 25 ^oC (solid line) and at 37 ^oC (dot line), respectively. Bioanode and cathode films cast on a 3 mm GC electrodes. Stirred solution under air-saturating conditions, Mcilvaine buffer (pH=5), 60 mM fructose. (C) **S**tability of biofuel cell with and without SWNTs. Biofuel Cells was continuously operated at maximum power for 24 h at 25 ^oC. Mcilvaine buffer (pH=5), 60mM fructose, air saturating conditions, stirring.

The effect of incorporating SWNTs on the performance of Fructose/ O_2 biofuel cell was investigated by using $FcMe_2$-C_3-LPEI/ FDH electrodes as anode, and Cl-Fc-LPEI/Laccase electrodes aforementioned as cathode. The polarization curves and dependence of power density on cell voltage curves of biofuel cell with $FcMe_2$-

C_3-LPEI/FDH anode and a Cl-Fc-LPEI/laccase cathode with or without SWNTs at 25 ^oC are shown in Figure 5.10 (A) and Figure 5.10 (B). For biofuel cell without SWNTs film, the maximum current density was ~72 μA/cm^2, and the maximum power density was 15.5 μW/cm^2 at cell voltage of 245 mV. Similar to the results of glucose/O_2 biofuel cell, the incorporation of SWNTs into fructose/O_2 biofuel cell resulted in a 19.4-fold increase in the maximum current density, reaching 1400 μA/cm^2, and a 29-fold increase in the maximum power density output, to 450 μW/ cm^2 at cell voltage of 330 mV. For biofuel cell with SWNTs, increasing temperature from 25 ^oC to 37 ^oC did not lead to an increase in the current density and power density, suggesting that fructose/ O_2 biofuel cell are not catalytically limited, in which case an increase in enzymatic activity should result in a proportional increase in current output. The stability of fructose/O_2 biofuel cells without and with the incorporation of SWNTs at room temperature is shown in Figure 5.10(C). After continuous operation at maximum power for 24 hours, the biofuel cell without SWNTs retained 23% of its original power density, while cell with SWNTs film retained 66% of its original power density under the same conditions, indicating that the incorporation of carbon nanotube significantly improved the stability of fructose/O_2 biofuel cells. From these results, the incorporation of SWNTs into enzymatic electrodes by type B method was applicable to construct various enzymatic biofuel cell with dramatically increase in the current density and power density output, as well as prolonged stability, providing a clue to design a wide range of high performing nanostructured enzymatic biofuel cell.

CONCLUSIONS

In this study, we demonstrated that the method of incorporating SWNTs into $FcMe_2$-C-LPEI/GOx electrodes affected the electrochemical and enzymatic

performance of electrodes significantly. Incorporation of SWNTs by either type A method or type B method led to dramatic increase in enzymatic response to glucose, especially for type B method. Compared with control electrodes without SWNTs, incorporation of nanotube into electrodes by type B method resulted in a 24-fold increase in the oxidation peak current and a 16.5-fold increase in the maximum current density output under glucose saturating concentration, reaching 11.8 mA/cm^2 at 25 ^oC, and 16.2 mA/cm^2 at 37 ^oC, which was among the highest value reported for glucose nanostructured electrodes. In addition our results indicated that the enzymatic stability of glucose electrodes improved significantly with the incorporation of nanotube. Meanwhile, the feasibility of using this method to improve the electrochemical and enzymatic performance of other enzymatic electrodes and enzymatic biofuel cell was investigated. Similar to aforementioned results of glucose electrodes, the incorporation of SWNTs into chloride modified ferrocene redox polymer mediated laccase cathode electrodes lead to a 11.8- fold increase of the response to oxygen, reaching a current density of 1455.4 $\mu A/cm^2$ and much longer enzyme stability. Furthermore, the effect of incorporating nanotube on the performance of biofuel cell, consisting of $FcMe_2$-C_3-LPEI / GOx anode and Cl-Fc-LPEI/laccase cathode, was evaluated. Our results showed that compared with biofuel cell without SWNTs, incorporation of nanotube into biofuel cell resulted in 12.3-fold increase in the maximum current density reaching 1390 $\mu A/cm^2$, and a 17-fold increase in the maximum power density output to 510 $\mu w/ cm^2$ at 25 ^oC. When increasing temperature from 25 ^oC to 37 ^oC, biofuel cell with SWNTs exhibited a maximum current density of 2456 $\mu A/cm^2$ and power density of 802 $\mu W/cm^2$. The biofuel cells stability also improved dramatically. In addition, the feasibility of applying type B method to design other nanostructured enzymatic biofuel cell with

improved performance was investigated. The incorporation of SWNTs into anode and cathode electrodes of fructose/O_2 biofuel cell showed similar improvement in the performance of biofuel cell. Incorporation of SWNTs into fructose/O_2 biofuel cell resulted in a 19.4-fold increase in the maximum current density, reaching 1400 $\mu A/cm^2$, and a 29-fold increase in the maximum power density output of 450 $\mu W/cm^2$, as well as the improved stability of biofuel cell. In summary, the incorporation of SWNTs film into enzymatic electrodes or biofuel cell in this study provides a strategy to construct a wide range of enzymatic biosensor electrodes with high current density output and long lifespan, as well as high performing biofuel cell.

Acknowledgements:

I would like to thank David Hickey for preparing Cl-Fc-LPEI redox polymer and Nick Godman for preparing $FcMe_2$-C_3-LPEI polymer. I would especially like to thank Dr. Glatzhofer for all of his valuable insight and discussions.

Chapter 6:

Vertically-aligned MWCNTs forest based ferrocene redox polymer for glucose sensing

INTRODUCTION

Enzyme-based electrodes are the core components of bioelectronics devices such as biosensors and enzymatic biofuel cells[10, 60, 202, 203]. How to achieve efficient electron commuting between the active sites of enzymes and electrodes surface is an active focus area of research for developing high performing bioelectronics devices[7, 25, 204, 205]. Several strategies have been developed to establish electron communication between active sites of enzyme and electrodes, including introducing diffusion mediators[39, 75,206]or redox polymer[28, 207], tethering redox relay units to protein linked to the electrodes,[57, 208] reconstitution of apo-enzymes on a relay-cofactor unit associated with electrodes[209, 210], or applying nanomaterials[24, 211]. Among these methods, introducing carbon nanotubes is a versatile and effective way for constructing enzymatic electrodes with high current density output, due to their excellent electrical conductivity and large surface area.

Since the discovery of multiwall carbon nanotubes (MWCNTs) by lijima in 1993[212], extensive research has been done in designing nanostructured electrodes incorporated with carbon nanotubes for applications in electrochemical devices. Britto et al [213] first reported significant improvement in electrochemical performance of dopamine at MWCNTs electrodes using bromoform as a binder, and they suggested the superior property of carbon nanotube electrodes to other carbon based electrodes. Since then, several carbon nanotube based structures have been developed for biosensor and enzymatic biofuel cell applications, including carbon nanotube forests[84, 214], carbon nanotube/enzyme composites[27], bucky paper[26, 215], yarns[216].

Vertically aligned carbon nanotubes arrays are of great interest as a promising material for the construction of nano- electrodes for biosensors. G.D. Withey et al[89] prepared highly ordered arrays of carbon nanotubes as a nanoelectrode interface to immobilize glucose oxidase. Their results showed that the covalent docking of glucose oxidase on the tips of carbon nanotubes enhanced the electron transfer properties. However, this procedure was relatively complicated, with nanotube etching in acid solution to create carboxyl groups to attach enzymes. The maximum current density output of electrodes at glucose saturating concentration was relatively low (330 $\mu A/cm^2$).

Previously, we have reported that redox polymers based on coupling ferrocene to a linear poly(ethylenimine) (LPEI) backbone can efficiently wire the redox centers of glucose oxidase [162, 163, 217] to electrode surfaces, producing high current densities of ~1 mA/cm^2. We have also demonstrated that either (i) the direct incorporation of SWNTs into redox polymer-enzyme hydrogels[124, 125], or (ii) or deposition of the redox polymer-enzyme hydrogel onto an electrode modified with a SWNT film[164], also increases the signal output. In this study, we investigate the feasibility of applying high surface area multi-wall carbon nanotube arrays as electrode platform to construct redox polymer mediated enzyme electrodes. The effect of applying Triton X-100 surfactant on top of MWCNTs array to make array surface hydrophilic on the electrochemical and enzymatic performance of redox hydrogel film was also evaluated.

EXPERIMENTAL SECTION

Chemicals and solutions

Glucose oxidase (GOx) from *Aspergillus niger* (EC 1.1.3.4, type X-S, 204.1 units/mg of solid, 75% protein) was purchased from Sigma Aldrich. Triton X-100 was

purchased from EM Science. Ethylene glycol diglycidyl ether (EGDGE) was purchased from Polysciences, Warrington, PA. All chemicals and solvents were used as received without further purification. The redox polymer $FcMe_2$-C_3-LPEI was prepared as previously described. [186] Phosphate-buffered saline solution (PBS) pH 7.4, was prepared in nanopure deionized water as previously described. Stock solutions of glucose (2M) were prepared in water and refrigerated at 4°C when not in use. A range of aqueous solutions of Triton X-100 were prepared by adding well-defined volume of Triton X-100 into water. MWCNTs forest on silicon wafer was provided from Dr. Crossley's lab, and synthesized by Nicholas Briggs and Brandon Bonk in Crossley lab.

Enzyme electrode construction

Solutions of $FcMe_2$-C_3-LPEI were prepared by dissolving the polymer in water while adding 0.1 M HCl solution until the final concentration of the polymer solution was 10 mg/mL and pH was 5. The schematic of MWCNTs array electrodes is shown in Figure 6.1. The array electrode consists of three main parts colored differently: (i) the black area indicates coating with redox polymer and enzyme hydrogel film; (ii) the white area is coated with Paraffin wax layer; and (iii) the shaded area indicates the area electronic conduction between the MWCNTs and the copper wire via silver-paint epoxy. MWCNTs array working electrodes without Triton X-100 modification were prepared by depositing a redox hydrogels solution, made from mixing 14 µL of $FcMe_2$-C_3-LPEI polymer solution (10 mg/mL in water), 6 µL of GOX solution (10 mg/mL), and 0.75µL of EGDGE crosslinker solution, on top of the white area of MWCNTs array, and allowed to dry for at least 12 hours. The amount of redox polymer and enzyme hydrogel mixture is calculated based on the area of electrodes. In order to increase the wettability of redox polymer and enzyme

hydrogel solution on MWCNTs array electrodes, the nonionic surfactant Triton X-100 was applied to make the MWCNTs array surface hydrophilic. The amount of Triton X-100 deposited on top of MWCNTs electrode is estimated based on the area of electrodes. Then the electrodes were allowed to dry for at least 12 h, before coating with redox polymer-enzyme hydrogel solution.

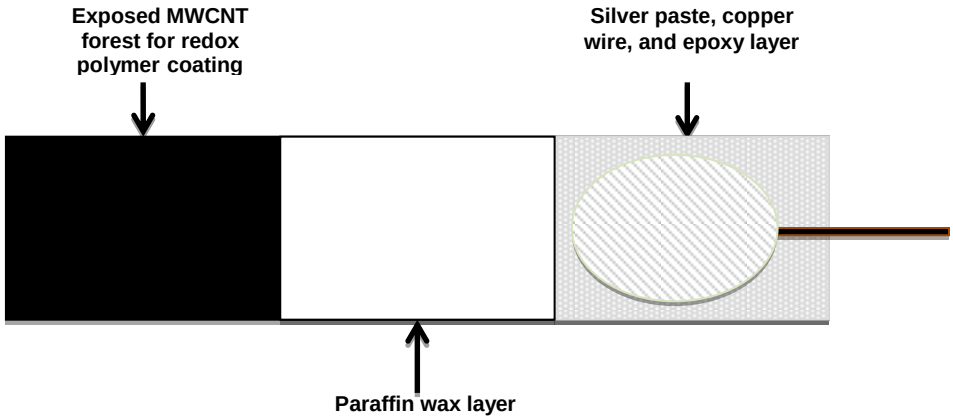


Figure 6.1 Schematic of MWCNTs array electrode.

Electrochemical Measurement

Electrochemical characterization (i.e. cyclic voltammetry and constant potential experiments) was performed in a three-electrode cell configuration (counter electrode = platinum wire, reference electrode = saturated calomel electrode, SCE) with a CH Instruments model 832 bipotentiostat. The temperature was maintained at 25±1°C with a water-jacketed electrochemical cell unless specified otherwise.

Cyclic voltammetry and constant potential tests were performed with a CH Instruments model 832 bipotentiostation using a three-electrode cell configuration, with platinum wire as counter electrodes and saturated calomel electrodes as reference electrodes. The background electrolyte was phosphate buffer saline (PBS), pH 7.4.. Glucose response was measured by adding aliquots of a stock 2 M glucose solution to a well-stirred cell with the MWCNTs array working electrode poised at 500 mV vs. SCE.

Characterization of MWCNTs forest

The morphology and height of MWCNTs forest were characterized using a Zeis NEON 40 EsB scanning electronic microscope.

Calculation and Statistics

Current densities were calculated using the geometric surface area of white area in the MWCNTs array electrode. Values are presented as mean ± standard error of the mean (SEM) unless otherwise specified.

RESULTS AND DISCUSSION

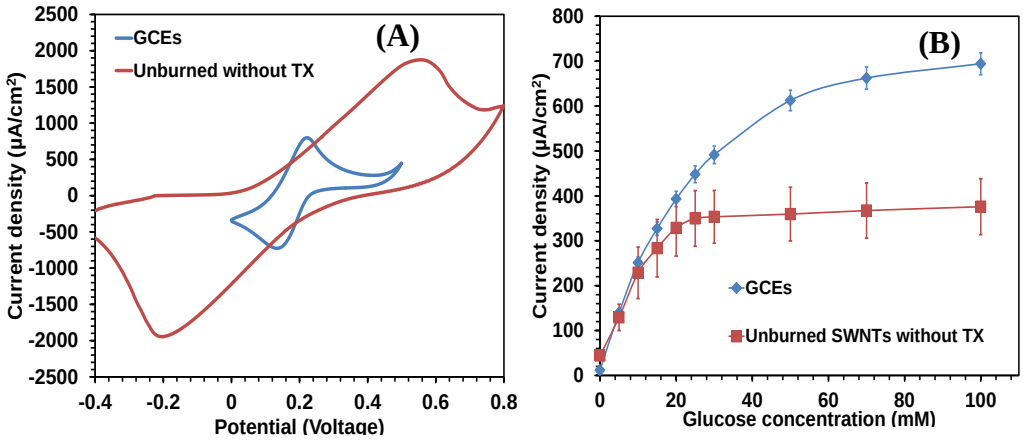


Figure 6.2 (A) Cyclic voltammograms and glucose calibration curves (B) of GCEs and MWCNTs array electrodes modified with $FcMe_2$-C_3-LPEI and GOx hydrogel film. For CV test, scan rate=50 mV/s in PBS at 25°C. For glucose response, E=0.5 V vs. SCE

The electrochemical performance of MWCNTs array based cross-linked redox polymer/enzyme hydrogel was investigated through cyclic voltammetry (CV). Figure 6.2A shows the CVs of bare glassy carbon electrodes (GCEs) and MWCNTs array coated with $FcMe_2$-C_3-LPEI /GOx film in the phosphate buffered saline (PBS) buffer. For the GCEs modified with a $FcMe_2$-C_3-LPEI /GOx hydrogel film, a pair of well-defined redox peaks corresponding to the oxidation and reduction of the redox

polymer's ferrocene complexes was observed at 221 and 149 mV versus SCE, respectively (ΔE=27 mV).

For MWNTs array electrodes, there were significant increase in both the redox peak current and background currents. Compared with GCEs with redox hydogel film, MWCNTs array based redox polymer/enzyme electrodes resulted in a 2.4-fold increase in the oxidation and reduction peak current. Interestingly, incorporation of MWCNTs shifted both oxidation and reduction peak potential (ΔE=760 mV), resulting in a much broader potential separation than GCEs (ΔE=27 mV). The phenomenon is characteristic of sluggish electron transfer kinetics, which might result from the fact that redox polymer and enzyme hydrogel solution did not spread over on the hydrophobic surface of MWCNTs array electrodes, thus creating increased diffusion resistance.

To determine the effect of using high surface MWCNTs array on the performance of crosslinked redox polymer hydrogel film, we performed constant potential amperometry by poising the electrodes at 0.5 V vs SCE, and measuring the output current as 2M glucose solution was added into buffer solution. As shown in Figure 6.2(B), all GCEs and MWCNTs forest electrodes showed Michaelis-Menten behavior. Surprisingly, the maximum current density (376 $\mu A/cm^2$) of MWCNTs forest electrodes at glucose saturating concentration was 54% of GCEs (694 $\mu A/cm^2$). Since MWCNTs array electrodes exhibited higher electrochemical performance than GCEs, this result suggests that the glucose response on MWCNTs array electrodes is not limited by the electron transfer through the redox polymer matrix to the electrode surface, but the electron transfer from enzyme active sites to redox polymer active sites, or electrode surface.

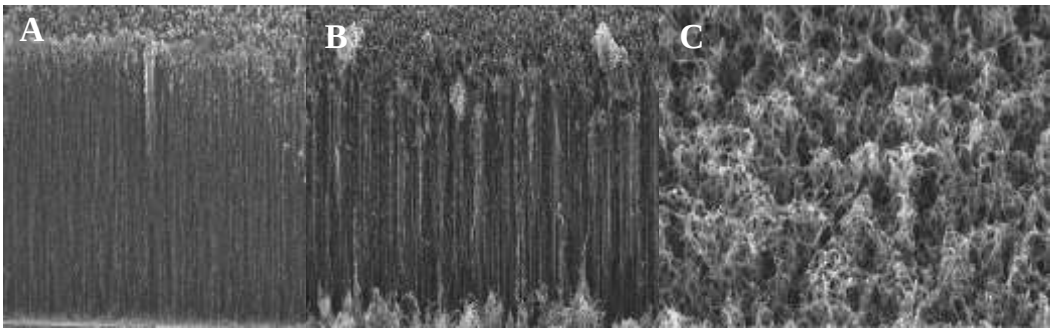


Figure 6.3 Scanning microscope image (SEM) of vertically alligned MWCNT forest before (A) and after oil burn off (B). (C) Magnified SEM images of MWCNTs forest electrodes after burning.

To investigate whether the low glucose response of MWCNTs array electrodes is associated to the MWCNTs forest structure, we performed scanning microscope microscopy (SEM) under different magnifications. As shown in Figure 6.3(A), the MWCNTs forest consists of densely packed vertical oriented MWCNTs with height of around 20 um. An oily stain was observed on top of MWNTs forest, which due to the pyrolysis of ethylene (carbon source to make MWCNTs) during the growth of MWCNTs array. The presence of this oily layer on top of nanotube forest may inhibit electron communication between the active sites of enzyme and electrode surface, resulting in relatively low enzymatic response.

To test this, the MWCNTs forest was burned under high temperature to remove the residue on top of the MWCNTs forest. The SEM images of burned MWCNTs forests with low and high magnification are shown in Figure 6.3(B) and (C), respectively. As shown in Figure 6.3(B), after burning, the residue at the top of MWCNTs forest was removed, and there was no obvious change or shortening in the height of nanotube forest. From Figure 6.3(C), the mean average diameter of multiwall carbon nanotube was 30 nm, and the nanotube on top of MWCNTs forest were not perfectly vertically aligned, but were bent and entangled, making the forest surface rough. Some porous structures were observed in the MWCNTs forest.

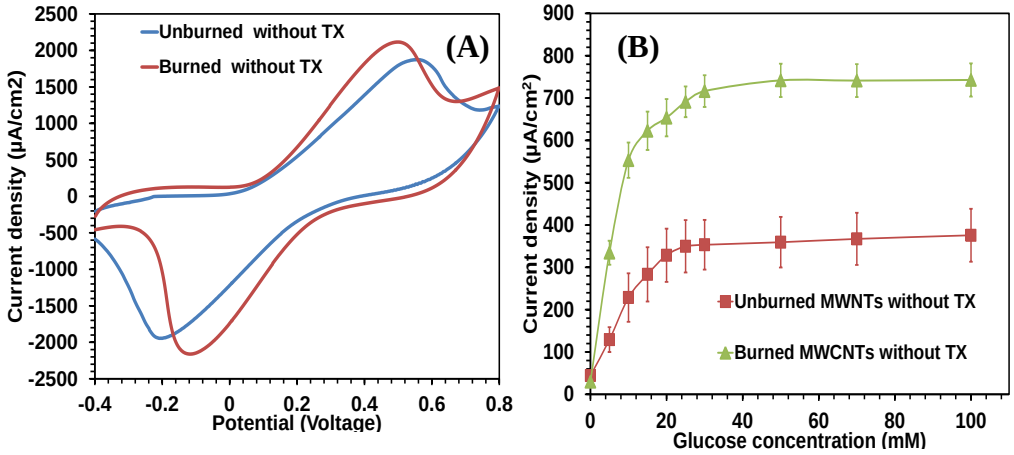


Figure 6.4 (A) Cyclic voltammograms and glucose calibration curves (B) of unburned and burned MWCNTs array electrodes modified with $FcMe_2$-C_3-LPEI and GOx hydrogel film. For CV test, scan rate=50 mV/s in PBS at 25°C. For glucose response, E=0.5 V vs. SCE

In order to remove the oily residue and determine the effect of its presence on the electrochemical and enzymatic performance of MWCNTs forest electrodes with a $FcMe_2$-C_3-LPEI /GOx hydrogel film, we burned MWCNTs array and applied these electrodes to construct redox polymer-enzyme hydrogel electrodes. Figure 6.4(A) compared the CV curves of unburned and burned MWCNTs forest electrodes with $FcMe_2$-C_3-LPEI /GOx film. Burning did not result in significant change in the oxidation and reduction peak currents. The separation between oxidation and reduction peak decreased slightly, which may due to the change in the ability of carbon nanotubes to donate or accept electrons from the active sites of redox polymer to electrode surface. Burning at high temperature might also create oxygen-containing groups such as hydroxyl and carboxylic acid groups on the top or surface of nanotube forest, which may affect the electron transfer process.[20]

The glucose response of unburned and burned MWCNTs array electrodes with $FcMe_2$-C_3-LPEI and GOx hydrogel film are shown in Figure 6.4(B). Compared with unburned electrodes, burning nanotube forest resulted in 1.97-fold increase in the maximum current density, reaching 741μA/cm^2. The increase in the maximum current density of burned MWCNTs forest electrodes may result from the removal of

oily residue. Besides, burned MWCNTs array electrodes exhibited a slightly higher maximum current density than GCEs, although the redox polymer hydrogel solution did not spread over the top surface of MWCNTs forest electrodes. Therefore, we then tested the possibility that improving the wettability of redox polymer hydrogel solution on MWCNTs forest electrodes would boost electrochemical and enzymatic performance of electrodes.

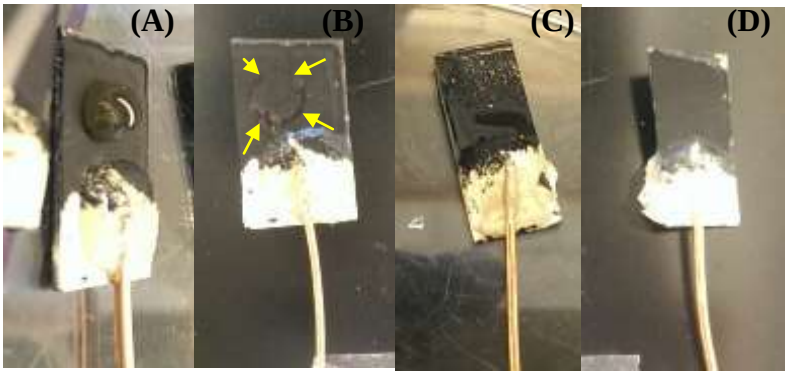


Figure 6.5 Optical images of burned MWCNTs forest electrodes without (A) and with the modification of 1% Triton X-100 (B) with the addition of redox polymer hydrogel solution. (C) and (D) are optical images of burned MWCNTs forest without and with the modification of 1% Triton X-100, when the redox hydrogel get dried.

Previously, we have demonstrated that modification of glassy carbon electrodes with high surface nanotube network by casing nanotube aqueous solution dispersed by Triton X-100, followed by redox polymer and enzyme hydrogel film, resulted in significant increase in the electrochemical and enzymatic performance of electrodes[24]. In order to improve the wettability of redox polymer hydrogel solution on MWCNTs forest, different concentrations of Triton X-100 aqueous solutions were applied to change the surface property of nanotube forest from hydrophobic to hydrophilic before the coating of redox polymer hydrogel film, the optical images of burned MWCNTs forest electrodes without and with the treatment of 1% Triton X-100 solution when redox polymer hydrogel solution was added, are shown in Figure 6.5 (A) and (B). From figure 6.5(A), the redox hydrogel solution did not spread over

the surface of MWCNTs forest because of high surface tension and resulted in a ring structure remaining on the surface of MWCNTs forest after air dry for 12 hours. For MWCNTs array electrodes treated with 1% Triton X-100(Figure 6.5(B)), the redox polymer hydrogel solution spread over the entire surface area quickly, due to reduced surface tension by surfactant. After drying in air for 12 hours, there is a uniform film of redox polymer hydrogel film formed on MWCNTs electrodes. Therefore, addition of surfactant solution facilitated even spreading of redox hydrogel solution on the surface of MWCNTs forest electrodes.

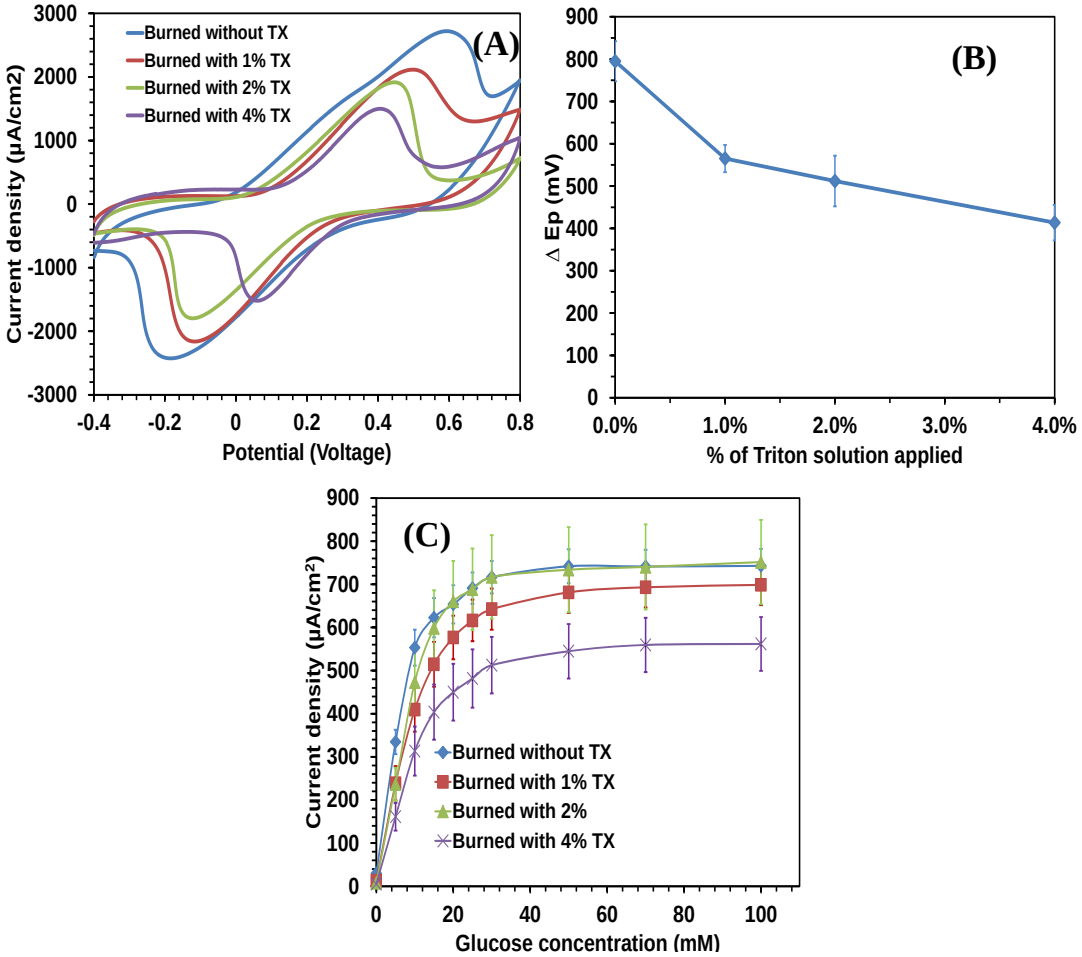


Figure 6.6 (A) Cyclic voltammograms and glucose calibration curves (C) of burned MWCNTs array electrodes without and with the modification of Triton X-100 surfactant, followed by $FcMe_2$-C_3-LPEI and GOx hydrogel film . For CV test, scan rate=50 mV/s in PBS at 25°C. For glucose response, E=0.5 V vs. SCE; (B) The relationship between redox peak separation (ΔE_p)and surfactant amount applied on to MWCNTs array surface

To evaluate the effect evenly spread of redox polymer hydrogel film and the surfactant loading on the electrochemical performance of MWCNTs array electrodes, cyclic voltammetry was performed and is shown in Figure 6.6 (A). Surprisingly, the oxidation and reduction peak current of MWCNTs electrodes decreased with the treatment of Triton X-100 aqueous solution, although the wettability of redox polymer hydrogel solution on MWCNTs electrodes improved. With the increase of surfactant loading on MWCNTs array surface, there was an obvious decrease in peak current. One possible explanation for this decrease is that that the presence of surfactant film inhibited electron transport from polymer active sites to electrode surface. The relationship between redox peak separation and the surfactant amount applied onto MWCNTs array is shown in Figure 6.6 (B). From this figure, peak separation between oxidation and reduction peak of MWCNTs forest electrodes decreased with surfactant treatment. The glucose responses of MWCNTs array electrodes without and with different loading of Triton X-100 are shown in Figure 6.6 (C). As shown in this figure, modification of MWCNTs array electrodes with low loading of Triton X-100 surfactant (<2%) did not change the limiting current density output obviously. However, further increase in the surfactant solution loading decreased the glucose response.

The glucose response of MWCNTs electrodes with modification of Triton X-100 surfactant are not consistent with the electrochemical response showed in Figure 6.6(A), suggesting that the electron transport process is not limited by electron transport from the actives sites of redox polymer network to electrode surface. Besides, from the above results, it can be concluded that the spread of redox polymer hydrogel solution over MWCNTs array forest with the treatment of surfactant did not improve the electrochemical and enzymatic performance of electrodes. There are two

possible reasons. One is that the presence of surfactant affected electron transport process between redox hydrogel films to electrode surface. Another possibility is that only a small proportion of the nanotube forest surface is electrochemically accessible.

In order to estimate the percentage of MWCNTs forest electrodes electrochemically accessible, we performed cyclic voltammetry of burned MWCNTs forest electrodes, without the modification of surfactant and redox polymer hydrogel film, in an aqueous solution with a well characterized redox couple of $Fc(CN)_6^{4-}$/ $Fc(CN)_6^{3-}$. By applying Randles-Sevcik equation, the effective electrochemical surface area of MWCNTs forest electrodes was estimated to be 0.6555 cm^2. Using Xiong et al's method, the total theoretical geometric area of the same MWCNTs electrodes was determined to be 418.93 cm^2. Therefore, the majority (99.8%) of nanotube forest surface is electrochemically inaccessible. The extremely low proportion of electrochemically accessible nanotube forest surface may due to the poor interconnection between nanotubes, resulting in some portion of nanotube forest to be electrochemically isolated. Besides, since the MWCNTs forests were grown on a silicon substrate, a thin insulating layer of silicon dioxide may have formed between nanotube forests and substrate, inhibiting electron transport from nanotube to the external electron circuit. The electron transport from the redox polymer hydrogel film to external electron circuit was mainly achieved via the partially interconnected nanotube via amorphous carbon. Therefore, how to create an effective electron transport network between nanotubes or between nanotubes forest to substrate is of great importance to achieve high current density output of redox polymer hydrogel film modified electrodes. There is great potential to get high current density output of MWCNTs array electrodes if most of the nanotube forest is electrochemically wired.

CONCLUSIONS

Vertical oriented MWCNTs forest was successfully prepared on silicon substrate by chemical vapor deposition. SEM images indicate that the length of MWCNTs forests was around 20 μm with an average diameter of 30 nm. The potential application of using high surface MWCNTs forest as substrate to construct redox polymer and enzyme hydrogel film was evaluated by cyclic voltammetry and constant potential measurement. Our results indicated that incorporating high surface MWCNTs forest into redox polymer hydrogel electrodes resulted in significant increase in redox peak current and background current, but lower glucose response. Burning nanotube forest led to an obvious increase in the limiting current density, reaching 741μA/cm^2 at glucose saturating concentration of 100 mM. In order to improve the wettability of MWCNTs forest electrodes, Triton X-100 aqueous solution was applied to treat MWCNTs forest surface, prior to the coating of redox polymer and enzyme hydrogel solution. However, increasing wettability of redox polymer and enzyme hydrogel solution on top of MWCNTs forest did not enhance the electrochemical and enzymatic performance significantly, which may due to that the majority of MWCNTs (>99%) was electrochemically inaccessible. Therefore, how to improve the electrical interconnection between nanotubes or between nanotube and substrate to take full advantage of the high surface of nanotube forest provide a great potential to prepare electrodes with high current density output.

Acknowledgements:

I would like to thank Nicholas Briggs and Brandon Bonk for preparing MWCNTs forest and taking SEM images and Nick Godman for preparing $FcMe_2$-C_3-LPEI redox polymer. I would especially like to thank Dr. Crossley for all of his valuable insight and discussions.

Chapter 7:

Conclusions and Recommendations for Future Work

CONCLUSIONS

This dissertation examined the construction of various carbon nanotube based structures to fabricate high powered and stable enzymatic biofuel cells. The effects of (i) dispersing carbon nanotubes with different surfactants; (ii) varying the type of carbon nanotube type; (iii) varying the carbon nanotube loading; and (iv) varying the method of carbon nanotube incorporation on the electrochemical and enzymatic performance of redox polymer-enzyme electrodes and biofuel cells was investigated.

In chapter 2 it was demonstrated that the type of surfactant used to disperse single-walled carbon nanotubes (SWNTs) and form high surface area SWNT networks on glassy carbon electrodes was an important parameter in the electrochemical and enzymatic performance of redox polymer-enzyme films. The use of non-ionic surfactants, such as Triton X-100 and Tween 20, to disperse (6,5) SWNTs and form SWNT networks resulted in an increased response to glucose ($\sim$ 1.7$-$ 2.1 mA/cm^2), while SNWTs dispersed with anionic surfactants (e.g. sodium cholate or NaDDBS) significantly reduced the enzymatic response (>0.4 mA/cm^2). The fact that similar results were observed when three different redox polymers (PVP-Os, Fc-C_6-LPEI, Fc-C_3-LPEI) were used demonstrated the importance of surfactant type.

In Chapter 3 it was demonstrated that the method of fabricating high surface area SWNT networks could not only improve the performance of glucose oxidase based films, but could be used with other redox polymer-enzyme films. Both the electrochemical and enzymatic performance of anodic films made with the enzyme fructose dehydrogenase or cathodic films made with laccase was also improved

through the use of the SWNT networks. The maximum current density of fructose sensitive films (Fc-C_6-LPEI/FDH) increased from 245 μA/cm^2 without any SWNTs to ~1 mA/cm^2 with (6,5) SWNTs films. Similarly the response of laccase based films (PVP-Os/Laccase) increased from ~160 μA/cm^2 (without SWNTs) to 366 μA/cm^2 (with SWNTs) in response to oxygen.

In Chapter 4 it was demonstrated that the type of single-walled carbon nanotubes used to form the SWNT network and the loading of the SWNTs had a significant effect on the enzymatic and electrochemical performance. In specific it was demonstrated that electrodes coated with a network of conductive (7,6) SWNTs exhibited higher current responses then electrodes coated with a network of semi-conducting (6,5) SWNTs. In addition, increasing the amount of SWNTs deposited in the formation of the SWNT networks and the amount of redox polymer-enzyme solution deposited also increased the response to glucose producing current densities of ~11 mA/cm^2. Similarly, the response of laccase films was also increased with the use of (7,6) SWNT networks producing a response to oxygen of 605 μA/cm^2.

In chapter 5, it was demonstrated that the method of incorporating SWNTs into the nanostructured composite films was an important parameter. In specific, a novel method of preparing the nanostructured electrodes was developed by adding conductive (7,6) SWNTs into the redox polymer-enzyme films that were deposited onto a glassy carbon electrode previously modified with a high-surface area network of (7,6) SWNTs. This novel method produced glucose electrodes which produced current outputs of 16.2 mA/cm^2 at 37 °C which are among the highest reported among nanostructured glucose electrodes. Similar increases were observed when this method was applied to construct fructose dehydrogenase based electrodes resulting in current outputs of 6.1 mA/cm^2.

Finally in chapter 6, it was demonstrated that high surface area vertically aligned MWCNTs forest can serve as a platform to construct redox polymer-enzyme based electrodes. Although the current density output of MWCNTs forest based electrodes was relatively low at this stage, there is a great potential to increase the current density of electrodes by making more carbon nanotubes electrochemical accessible. The results showed that the majority of MWCNTs forest (>99%) was isolated and electrochemically inaccessible in this study.

RECOMMENDATIONS FOR FUTURE WORK

There are three issues of particular importance to be addressed in future studies. First, increasing the current density output of the cathode is critical to construct enzymatic biofuel cell with high power densities. According to our results, the current density output of the cathode is significantly lower than that of anode, and thus limiting the power density output of biofuel cell. We proposed several strategies to increase the current density output of the cathode. The first strategy is to improve the purity of redox enzymes. Generally, commercially available enzymes have a large amount of impurities, including support materials and stabilizers, which can impair the enzymatic activity. For example, the laccase we purchased and applied in the construction of the cathode electrodes had a low activity of 13.6 unit/mg. Therefore, increasing the activity of enzyme by purification might be a promising way to increase the current density of the cathodes. The second strategy is to employ air breathing enzymatic biocathodes. The low solubility and slow diffusion rate of O_2 in aqueous solutions are the two significant factors affecting the current density output of cathode electrodes immersed in aqueous solutions. Designing air-breathing enzymatic biocathodes that can operate using gas phase O_2 would be a promising way to eliminate these two issues mentioned above, since the concentration of oxygen in

air is much higher than water [4]. Nicholas et al [218] prepared osimum redox polymer mediated biocatalytic air breathing cathodes, producing current densities of 1 mA/cm^2. However, the electrodes were not stable due to water loss from the cathode. Later, Gellett et al [219] prepared air breathing laccase electrodes based on direct electron transfer, the biocathode produced a high current density of 50 mA/cm^2 , and exhibited a lifetime of 290 h in a direct methanol fuel cell.

The third strategy is to apply high surface area, 3-dimensional carbon substrate such as hybrid nanotube microfibers, carbon nanotube forest, or carbon nanotube disks to construct cathode electrodes with high current density output. Feng Gao et al [202] prepared hybrid carbon nanotube wires for the preparation of redox polymer mediated enzyme electrodes for enzymatic biofuel cell application with a power density of 740 $\mu W/cm^2$ at 0.57 V. In our study, all electrodes were constructed on glassy carbon electrodes with the modification of carbon nanotube. Applying 3D carbon nanotube substrate with high porosity to construct cathode electrodes using the strategy developed in our study might increase the current density output of cathode, hence the power density of enzymatic biofuel cell. In chapter 7, we applied MWCNTs array to construct enzyme electrodes, but the majority of MWCNTs nanotubes were electrochemically inaccessible. Therefore, improving the electrical interconnection between nanotubes or between nanotube and the substrate should allow one to take to take full advantage of the high surface area of the nanotube forests and thereby prepare electrodes with high current density output.

Aside from optimization of cathode, the current density output of the anode can be further increased by utilizing enzyme cascades to completely oxidize glucose and collect all of the available electrons. In the study of this dissertation, the anode electrodes used a single enzyme (glucose oxidase) to oxidase glucose to

gluconolactone, generating 2 electrons. However, there are 22 more electrons that can potentially be extracted through the complete oxidation of glucose. The complete oxidation of glucose by applying an enzyme cascade, while using the nanostructured strategy we designed in this study, should further improve the current density output of glucose electrodes.

The cell voltage of biofuel cell will also need to be improved in order to achieve real application of enzymatic biofuel cells. For direct enzymatic biofuel cell without mediator, the cell voltage of the biofuel cell is normally determined by the redox potential difference between the redox enzymes at the anode and cathode. Taking glucose/O_2 biofuel cell constructed in this study for example, the cell potential is equal to the potential difference between the reduction potential of T1 copper center of laccase (0.539 V vs SCE) and the oxidation potential of FAD actives of GO_x (-0.21 V vs SCE), which should theoretically produce a cell potential of 0.749 V. However, the cell voltage of the enzymatic biofuel cells in our study was much lower (0.35 mV) than the theoretical value (0.749V), due to the presence of over-potential resulting from the potential difference between enzyme and redox mediators, ohmic resistance and mass transfer loss. In order to improve the cell potential of biofuel cell, efforts should be made in developing new redox mediators to minimize the overpotential.

The lifetime of enzymatic biofuel cell needs to be increased to the time frame of years to achieve real world application of enzymatic biofuel cells as power sources for implantable biomedical devices. Currently, the lifetime of enzymatic biofuel cells is around several weeks. From our results, the incorporation of carbon nanotube into enzymatic biofuel cell in this study significantly improved the stability of cell, but efforts need to be made to further increase the lifetime of enzymatic biofuel cells. One approach would be to chemical crosslink a highly concentration of enzymes onto

the nanostructures materials. Byoung Chan Kim et al [220] prepared highly stable enzyme precipitate coating of glucose oxidase by precipitating GOx molecules in the presence of ammonium sulfate, then crosslinking the precipitated GOx aggregates on the surface of electronspun polymer nanofibers with carbon nanotubes. The enzyme activity was maintained with negligible loss for 200 days.

BIBLOGRAPHY

1. Davis, F.; Higson, S. P. J. Biofuel cells - Recent advances and applications. *Biosens Bioelectron* **2007,** *22* (7), 1224-1235.

2. Minteer, S. D.; Liaw, B. Y.; COoney, M. J. Enzyme-based biofuel cells. *Curr Opin Biotech* **2007,** *18* (3), 228-234.

3. Barton, S. C.; Gallaway, J.; Atanassov, P. Enzymatic biofuel cells for Implantable and microscale devices. *Chem Rev* **2004,** *104* (10), 4867-4886.

4. Meredith, M. T.; Minteer, S. D. Biofuel Cells: Enhanced Enzymatic Bioelectrocatalysis. *Annu Rev Anal Chem* **2012,** *5*, 157-179.

5. Yahiro, A. T.; Lee, S. M.; Kimble, D. O. Bioelectrochemistry .I. Enzyme Utilizing Bio-Fuel Cell Studies. *Biochimica et biophysica acta* **1964,** *88* (2), 375-&.

6. Ivnitski, D.; Branch, B.; Atanassov, P.; Apblett, C. Glucose oxidase anode for biofuel cell based on direct electron transfer. *Electrochem Commun* **2006,** *8* (8), 1204-1210.

7. Zebda, A.; Gondran, C.; Le Goff, A.; Holzinger, M.; Cinquin, P.; Cosnier, S. Mediatorless high-power glucose biofuel cells based on compressed carbon nanotube-enzyme electrodes. *Nat Commun* **2011,** *2*.

8. Barriere, F.; Kavanagh, P.; Leech, D. A laccase-glucose oxidase biofuel cell prototype operating in a physiological buffer. *Electrochim Acta* **2006,** *51* (24), 5187-5192.

9. Kamitaka, Y.; Tsujimura, S.; Setoyama, N.; Kajino, T.; Kano, K. Fructose/dioxygen biofuel cell based on direct electron transfer-type bioelectrocatalysis. *Phys Chem Chem Phys* **2007,** *9* (15), 1793-1801.

10. Miyake, T.; Yoshino, S.; Yamada, T.; Hata, K.; Nishizawa, M. Self-Regulating Enzyme-Nanotube Ensemble Films and Their Application as Flexible Electrodes for Biofuel Cells. *J Am Chem Soc* **2011,** *133* (13), 5129-5134.

11. Topcagic, S.; Minteer, S. D. Development of a membraneless ethanol/oxygen biofuel cell. *Electrochim Acta* **2006,** *51* (11), 2168-2172.

12. Moore, C. M.; Minteer, S. D.; Martin, R. S. Microchip-based ethanol/oxygen biofuel cell. *Lab Chip* **2005,** *5* (2), 218-225.

13. Arechederra, R. L.; Minteer, S. D. Complete Oxidation of Glycerol in an Enzymatic Biofuel Cell. *Fuel Cells* **2009,** *9* (1), 63-69.

14. Sokic-Lazic, D.; Minteer, S. D. Pyruvate/Air Enzymatic Biofuel Cell Capable of Complete Oxidation. *Electrochem Solid St* **2009,** *12* (9), F26-F28.

15. Nadia Grossiord, M. C. H., and Cor Koning. *Polymer Carbon Nanotube Composites: The Polymer Latex Concept* 2012.

16. Meredith, M. T.; Kao, D. Y.; Hickey, D.; Schmidtke, D. W.; Glatzhofer, D. T. High Current Density Ferrocene-Modified Linear Poly(ethylenimine) Bioanodes and Their Use in Biofuel Cells. *J Electrochem Soc* **2011,** *158* (2), B166-B174.

17. Bullen, R. A.; Arnot, T. C.; Lakeman, J. B.; Walsh, F. C. Biofuel cells and their development. *Biosens Bioelectron* **2006,** *21* (11), 2015-2045.

18. Soukharev, V.; Mano, N.; Heller, A. A four-electron O-2-electroreduction biocatalyst superior to platinum and a biofuel cell operating at 0.88 V. *J Am Chem Soc* **2004,** *126* (27), 8368-8369.

19. Holzinger, M.; Le Goff, A.; Cosnier, S. Carbon nanotube/enzyme biofuel cells. *Electrochim Acta* **2012,** *82*, 179-190.

20. Sotiropoulou, S.; Chaniotakis, N. A. Carbon nanotube array-based biosensor. *Anal Bioanal Chem* **2003,** *375* (1), 103-105.

21. Gooding, J. J.; Wibowo, R.; Liu, J. Q.; Yang, W. R.; Losic, D.; Orbons, S.; Mearns, F. J.; Shapter, J. G.; Hibbert, D. B. Protein electrochemistry using aligned carbon nanotube arrays. *J Am Chem Soc* **2003,** *125* (30), 9006-9007.

22. Zhu, Z. G.; Garcia-Gancedo, L.; Flewitt, A. J.; Moussy, F.; Li, Y. L.; Milne, W. I. Design of carbon nanotube fiber microelectrode for glucose biosensing. *J Chem Technol Biot* **2012,** *87* (2), 256-262.

23. Zhu, Z. G.; Song, W. H.; Burugapalli, K.; Moussy, F.; Li, Y. L.; Zhong, X. H. Nano-yarn carbon nanotube fiber based enzymatic glucose biosensor. *Nanotechnology* **2010,** *21* (16).

24. Chen, J.; Tran, T. O.; Ray, M. T.; Brunski, D. B.; Keay, J. C.; Hickey, D.; Johnson, M. B.; Glatzhofer, D. T.; Schmidtke, D. W. Effect of Surfactant Type and Redox Polymer Type on Single-Walled Carbon Nanotube Modified Electrodes. *Langmuir* **2013,** *29* (33), 10586-10595.

25. Scherbahn, V.; Putze, M. T.; Dietzel, B.; Heinlein, T.; Schneider, J. J.; Lisdat, F. Biofuel cells based on direct enzyme-electrode contacts using PQQ-dependent glucose dehydrogenase/bilirubin oxidase and modified carbon nanotube materials. *Biosens Bioelectron* **2014,** *61*, 631-638.

26. Strack, G.; Babanova, S.; Farrington, K. E.; Luckarift, H. R.; Atanassov, P.; Johnson, G. R. Enzyme-Modified Buckypaper for Bioelectrocatalysis. *J Electrochem Soc* **2013,** *160* (7), G3178-G3182.

27. Tran, T. O.; Lammert, E. G.; Chen, J.; Merchant, S. A.; Brunski, D. B.; Keay, J. C.; Johnson, M. B.; Glatzhofer, D. T.; Schmidtke, D. W. Incorporation of Single-Walled Carbon Nanotubes into Ferrocene-Modified Linear Polyethylenimine Redox Polymer Films. *Langmuir* **2011,** *27* (10), 6201-6210.

28. Joshi, P. P.; Merchant, S. A.; Wang, Y. D.; Schmidtke, D. W. Amperometric biosensors based on redox polymer-carbon nanotube-enzyme composites. *Anal Chem* **2005,** *77* (10), 3183-3188.

29. Mateo, C.; Palomo, J. M.; Fernandez-Lorente, G.; Guisan, J. M.; Fernandez-Lafuente, R. Improvement of enzyme activity, stability and selectivity via immobilization techniques. *Enzyme Microb Tech* **2007,** *40* (6), 1451-1463.

30. Kim, J.; Jia, H. F.; Wang, P. Challenges in biocatalysis for enzyme-based biofuel cells. *Biotechnol Adv* **2006,** *24* (3), 296-308.

31. Mann, B.; Kuhn, H. Tunneling through Fatty Acid Salt Monolayers. *J Appl Phys* **1971,** *42* (11), 4398-&.

32. Li, T. T. T.; Weaver, M. J. Intramolecular Electron-Transfer at Metal-Surfaces .4. Dependence of Tunneling Probability Upon Donor-Acceptor Separation Distance. *J Am Chem Soc* **1984,** *106* (20), 6107-6108.

33. Degani, Y.; Heller, A. Direct Electrical Communication between Chemically Modified Enzymes and Metal-Electrodes .1. Electron-Transfer from Glucose-Oxidase to Metal-Electrodes Via Electron Relays, Bound Covalently to the Enzyme. *J Phys Chem-Us* **1987,** *91* (6), 1285-1289.

34. Shleev, S.; Jarosz-Wilkolazka, A.; Khalunina, A.; Morozova, O.; Yaropolov, A.; Ruzgas, T.; Gorton, L. Direct electron transfer reactions of laccases from different origins on carbon electrodes. *Bioelectrochemistry* **2005,** *67* (1), 115-124.

35. Shleev, S.; Tkac, J.; Christenson, A.; Ruzgas, T.; Yaropolov, A. I.; Whittaker, J. W.; Gorton, L. Direct electron transfer between copper-containing proteins and electrodes. *Biosens Bioelectron* **2005,** *20* (12), 2517-2554.

36. Gorton, L.; Lindgren, A.; Larsson, T.; Munteanu, F. D.; Ruzgas, T.; Gazaryan, I. Direct electron transfer between heme-containing enzymes and electrodes as basis for third generation biosensors. *Anal Chim Acta* **1999,** *400*, 91-108.

37. Wilson, R.; Turner, A. P. F. Glucose-Oxidase - an Ideal Enzyme. *Biosens Bioelectron* **1992,** *7* (3), 165-185.

38. Osman, M. H.; Shah, A. A.; Walsh, F. C. Recent progress and continuing challenges in bio-fuel cells. Part I: Enzymatic cells. *Biosens Bioelectron* **2011,** *26* (7), 3087-3102.

39. Heller, A. Electrical Connection of Enzyme Redox Centers to Electrodes. *J Phys Chem-Us* **1992,** *96* (9), 3579-3587.

40. Liu, Y.; Wang, M. K.; Zhao, F.; Xu, Z. A.; Dong, S. J. The direct electron transfer of glucose oxidase and glucose biosensor based on carbon nanotubes/chitosan matrix. *Biosens Bioelectron* **2005,** *21* (6), 984-988.

41. Zhao, S.; Zhang, K.; Bai, Y.; Yang, W. W.; Sun, C. Q. Glucose oxidase/colloidal gold nanoparticles immobilized in Nafion film on glassy carbon electrode: Direct electron transfer and electrocatalysis. *Bioelectrochemistry* **2006,** *69* (2), 158-163.

42. Yu, Y. Y.; Chen, Z. G.; He, S. J.; Zhang, B. B.; Li, X. C.; Yao, M. C. Direct electron transfer of glucose oxidase and biosensing for glucose based on PDDA-capped gold nanoparticle modified graphene/multi-walled carbon nanotubes electrode. *Biosens Bioelectron* **2014,** *52*, 147-152.

43. Tominaga, M.; Nomura, S.; Taniguchi, I. Bioelectrocatalytic current based on direct heterogeneous electron transfer reaction of glucose oxidase adsorbed onto multi-walled carbon nanotubes synthesized on platinum electrode surfaces. *Electrochem Commun* **2008,** *10* (6), 888-890.

44. Guiseppi-Elie, A.; Lei, C. H.; Baughman, R. H. Direct electron transfer of glucose oxidase on carbon nanotubes. *Nanotechnology* **2002,** *13* (5), 559-564.

45. Milton, R. D.; Giroud, F.; Thumser, A. E.; Minteer, S. D.; Slade, R. C. T. Hydrogen peroxide produced by glucose oxidase affects the performance of laccase cathodes in glucose/oxygen fuel cells: FAD-dependent glucose dehydrogenase as a replacement. *Phys Chem Chem Phys* **2013,** *15* (44), 19371-19379.

46. Zayats, M.; Katz, E.; Baron, R.; Willner, I. Reconstitution of apo-glucose dehydrogenase on pyrroloquinoline quinone-functionalized Au nanoparticles yields an electrically contacted biocatalyst. *J Am Chem Soc* **2005,** *127* (35), 12400-12406.

47. Long, Y. T.; Zou, J.; Chen, H. Y. Electrocatalytic oxidation and flow detection of NAD(P)H at a histidine modified silver electrode. *Anal Lett* **1997,** *30* (15), 2691-2703.

48. Tsujimura, S.; Kojima, S.; Kano, K.; Ikeda, T.; Sato, M.; Sanada, H.; Omura, H. Novel FAD-dependent glucose dehydrogenase for a dioxygen-insensitive glucose biosensor. *Biosci Biotech Bioch* **2006,** *70* (3), 654-659.

49. Dcosta, E. J.; Higgins, I. J.; Turner, A. P. F. Quinoprotein Glucose-Dehydrogenase and Its Application in an Amperometric Glucose Sensor. *Biosensors* **1986,** *2* (2), 71-87.

50. Frias, J. P.; Lim, C. G.; Ellison, J. M.; Montandon, C. M. Review of Adverse Events Associated With False Glucose Readings Measured by GDH-PQQ-Based Glucose Test Strips in the Presence of Interfering Sugars. *Diabetes Care* **2010,** *33* (4), 728-729.

51. Kim, D. M.; Kim, M. Y.; Reddy, S. S.; Cho, J.; Cho, C. H.; Jung, S.; Shim, Y. B. Electron-Transfer Mediator for a NAD-Glucose Dehydrogenase-Based Glucose Sensor. *Anal Chem* **2013,** *85* (23), 11643-11649.

52. Milburn, C. C.; Lamble, H. J.; Theodossis, A.; Bull, S. D.; Hough, D. W.; Danson, M. J.; Taylor, G. L. The structural basis of substrate promiscuity in glucose dehydrogenase from the hyperthermophilic archaeon Sulfolobus solfataricus. *J Biol*

Chem **2006,** *281* (21), 14796-14804.

53. Quintanar, L.; Stoj, C.; Taylor, A. B.; Hart, P. J.; Kosman, D. J.; Solomon, E. I. Shall we dance? How a multicopper oxidase chooses its electron transfer partner. *Accounts Chem Res* **2007,** *40* (6), 445-452.

54. Lee, S. K.; George, S. D.; Antholine, W. E.; Hedman, B.; Hodgson, K. O.; Solomon, E. I. Nature of the intermediate formed in the reduction of O-2 to H2O at the trinuclear copper cluster active site in native laccase. *J Am Chem Soc* **2002,** *124* (21), 6180-6193.

55. Clauwaert, P.; Aelterman, P.; Pham, T. H.; De Schamphelaire, L.; Carballa, M.; Rabaey, K.; Verstraete, W. Minimizing losses in bio-electrochemical systems: the road to applications. *Appl Microbiol Biot* **2008,** *79* (6), 901-913.

56. Barriere, F.; Ferry, Y.; Rochefort, D.; Leech, D. Targetting redox polymers as mediators for laccase oxygen reduction in a membrane-less biofuel cell. *Electrochem Commun* **2004,** *6* (3), 237-241.

57. Schuhmann, W.; Ohara, T. J.; Schmidt, H. L.; Heller, A. Electron-Transfer between Glucose-Oxidase and Electrodes Via Redox Mediators Bound with Flexible Chains to the Enzyme Surface. *J Am Chem Soc* **1991,** *113* (4), 1394-1397.

58. Salimi, A.; Compton, R. G.; Hallaj, R. Glucose biosensor prepared by glucose oxidase encapsulated sol-gel and carbon-nanotube-modified basal plane pyrolytic graphite electrode. *Anal Biochem* **2004,** *333* (1), 49-56.

59. Sokic-Lazic, D.; Minteer, S. D. Citric acid cycle biomimic on a carbon electrode. *Biosens Bioelectron* **2008,** *24* (4), 939-944.

60. Gooding, J. J. Nanostructuring electrodes with carbon nanotubes: A review on electrochemistry and applications for sensing. *Electrochim Acta* **2005,** *50* (15), 3049-3060.

61. Cass, A. E. G.; Davis, G.; Francis, G. D.; Hill, H. A. O.; Aston, W. J.; Higgins, I. J.; Plotkin, E. V.; Scott, L. D. L.; Turner, A. P. F. Ferrocene-Mediated Enzyme Electrode for Amperometric Determination of Glucose. *Anal Chem* **1984,** *56* (4), 667-671.

62. Bastos, A. C.; Simoes, A. M.; Gonzalez, S.; Gonzalez-Garcia, Y.; Souto, R. M.

Application of the scanning electrochemical microscope to the examination of organic coatings on metallic substrates. *Prog Org Coat* **2005,** *53* (3), 177-182.

63. Heller, A. Electron-conducting redox hydrogels: design, characteristics and synthesis. *Curr Opin Chem Biol* **2006,** *10* (6), 664-672.

64. Gregg, B. A.; Heller, A. Redox Polymer-Films Containing Enzymes .1. A Redox-Conducting Epoxy Cement - Synthesis, Characterization, and Electrocatalytic Oxidation of Hydroquinone. *J Phys Chem-Us* **1991,** *95* (15), 5970-5975.

65. Gregg, B. A.; Heller, A. Redox Polymer-Films Containing Enzymes .2. Glucose-Oxidase Containing Enzyme Electrodes. *J Phys Chem-Us* **1991,** *95* (15), 5976-5980.

66. Merchant, S. A.; Meredith, M. T.; Tran, T. O.; Brunski, D. B.; Johnson, M. B.; Glatzhofer, D. T.; Schmidtke, D. W. Effect of Mediator Spacing on Electrochemical and Enzymatic Response of Ferrocene Redox Polymers. *J Phys Chem C* **2010,** *114* (26), 11627-11634.

67. Park, T. M.; Iwuoha, E. I.; Smyth, M. R.; Freaney, R.; McShane, A. J. Sol-gel based amperometric biosensor incorporating an osmium redox polymer as mediator for detection of L-lactate. *Talanta* **1997,** *44* (6), 973-978.

68. Park, T. M.; Iwuoha, E. I.; Smyth, M. R.; MacCraith, B. D. Sol-gel-based amperometric glucose biosensor incorporating an osmium redox polymer as mediator. *Anal Commun* **1996,** *33* (8), 271-273.

69. Foulds, N. C.; Lowe, C. R. Immobilization of Glucose-Oxidase in Ferrocene-Modified Pyrrole Polymers. *Anal Chem* **1988,** *60* (22), 2473-2478.

70. Gallaway, J. W.; Barton, S. A. C. Kinetics of redox polymer-mediated enzyme electrodes. *J Am Chem Soc* **2008,** *130* (26), 8527-8536.

71. Pickup, P. G.; Kutner, W.; Leidner, C. R.; Murray, R. W. Redox Conduction in Single and Bilayer Films of Redox Polymer. *J Am Chem Soc* **1984,** *106* (7), 1991-1998.

72. Gregg, B. A.; Schmidt, H. L.; Schuhmann, W.; Ye, L.; Heller, A. Electrical Wiring of Redox Enzymes. *Abstr Pap Am Chem S* **1991,** *201*, 188-PMSE.

73. Merchant, S. A.; Glatzhofer, D. T.; Schmidtke, D. W. Effects of electrolyte and pH on the behavior of cross-linked films of ferrocene-modified poly(ethylenimine). *Langmuir* **2007,** *23* (22), 11295-11302.

74. Kavanagh, P.; Jenkins, P.; Leech, D. Electroreduction of O-2 at a mediated Melanocarpus albomyces laccase cathode in a physiological buffer. *Electrochem Commun* **2008,** *10* (7), 970-972.

75. Palmore, G. T. R.; Bertschy, H.; Bergens, S. H.; Whitesides, G. M. A methanol/dioxygen biofuel cell that uses NAD(+)-dependent dehydrogenases as catalysts: application of an electro-enzymatic method to regenerate nicotinamide adenine dinucleotide at low overpotentials. *J Electroanal Chem* **1998,** *443* (1), 155-161.

76. Seisser, B.; Lavandera, I.; Faber, K.; Spelberg, J. H. L.; Kroutil, W. Stereo-complementary two-step cascades using a two-enzyme system leading to enantiopure epoxides. *Adv Synth Catal* **2007,** *349* (8-9), 1399-1404.

77. Shi, J. F.; Wang, X. L.; Zhang, W. Y.; Jiang, Z. Y.; Liang, Y. P.; Zhu, Y. Y.; Zhang, C. H. Synergy of Pickering Emulsion and Sol-Gel Process for the Construction of an Efficient, Recyclable Enzyme Cascade System. *Adv Funct Mater* **2013,** *23* (11), 1450-1458.

78. Xu, S.; Minteer, S. D. Enzymatic Biofuel Cell for Oxidation of Glucose to CO2. *Acs Catal* **2012,** *2* (1), 91-94.

79. Jiang, K. Y.; Schadler, L. S.; Siegel, R. W.; Zhang, X. J.; Zhang, H. F.; Terrones, M. Protein immobilization on carbon nanotubes via a two-step process of diimide-activated amidation. *J Mater Chem* **2004,** *14* (1), 37-39.

80. Trancik, J. E.; Barton, S. C.; Hone, J. Transparent and catalytic carbon nanotube films. *Nano Lett* **2008,** *8* (4), 982-987.

81. Ahmadalinezhad, A.; Wu, G. S.; Chen, A. C. Mediator-free electrochemical biosensor based on buckypaper with enhanced stability and sensitivity for glucose detection. *Biosens Bioelectron* **2011,** *30* (1), 287-293.

82. Hussein, L.; Rubenwolf, S.; von Stetten, F.; Urban, G.; Zengerle, R.; Krueger, M.; Kerzenmacher, S. A highly efficient buckypaper-based electrode material for mediatorless laccase-catalyzed dioxygen reduction. *Biosens Bioelectron* **2011,** *26* (10), 4133-4138.

83. Yu, X.; Chattopadhyay, D.; Galeska, I. E.; Papadimitrakopoulos, F.; Rusling, J. F. Peroxidase activity of enzymes bound to the ends of single-wall carbon nanotube forest electrodes. *Abstr Pap Am Chem S* **2003,** *226*, U465-U465.

84. Yu, X.; Kim, S. N.; Patel, V.; Gutkind, S.; Gong, J.; Bhirde, A.; Papadimitrakopoulos, F.; Rusling, J. F. Protein immunosensor using single-wall carbon nanotube forests with electrochemical detection of enzyme labels. *Abstr Pap Am Chem S* **2005,** *230*, U1053-U1053.

85. Zhu, L. D.; Li, Y. X.; Tian, F. M.; Xu, B.; Zhu, G. Y. Electrochemiluminescent determination of glucose with a sol-gel derived ceramic-carbon composite electrode as a renewable optical fiber biosensor. *Sensor Actuat B-Chem* **2002,** *84* (2-3), 265-270.

86. Wang, J.; Musameh, M. Carbon nanotube/teflon composite electrochemical sensors and biosensors. *Anal Chem* **2003,** *75* (9), 2075-2079.

87. Lim, S. H.; Wei, J.; Lin, J. Y.; Li, Q. T.; KuaYou, J. A glucose biosensor based on electrodeposition of palladium nanoparticles and glucose oxidase onto Nafion-solubilized carbon nanotube electrode. *Biosens Bioelectron* **2005,** *20* (11), 2341-2346.

88. Zhang, M. G.; Smith, A.; Gorski, W. Carbon nanotube-chitosan system for electrochemical sensing based on dehydrogenase enzymes. *Anal Chem* **2004,** *76* (17), 5045-5050.

89. Withey, G. D.; Lazareck, A. D.; Tzolov, M. B.; Yin, A.; Aich, P.; Yeh, J. I.; Xu, J. M. Ultra-high redox enzyme signal transduction using highly ordered carbon nanotube array electrodes. *Biosens Bioelectron* **2006,** *21* (8), 1560-1565.

90. Zhou, Y. G.; Yang, S.; Qian, Q. Y.; Xia, X. H. Gold nanoparticles integrated in a nanotube array for electrochemical detection of glucose. *Electrochem Commun* **2009,** *11* (1), 216-219.

91. Rubianes, M. D.; Rivas, G. A. Carbon nanotubes paste electrode. *Electrochem Commun* **2003,** *5* (8), 689-694.

92. Nguyen, C. V.; Delzeit, L.; Cassell, A. M.; Li, J.; Han, J.; Meyyappan, M. Preparation of Nucleic Acid Functionalized Carbon Nanotube Arrays. *Nano Lett.* **2002,** *2* (10), 1079-1081.

93. Yun, Y. H.; Bange, A.; Heineman, W. R.; Halsall, H. B.; Shanov, V. N.; Dong,

Z. Y.; Pixley, S.; Behbehani, M.; Jazieh, A.; Tu, Y.; Dong, D. K. Y.; Bhattacharya, A.; Schulz, M. J. A Nanotube Array Immunosensor for Direct Electrochemical Detection of Antigen-Antibody Binding. *Sens. Actuators B* **2007,** *123* (1), 177-182.

94. Barisci, J. N.; Tahhan, M.; Wallace, G. G.; Badaire, S.; Vaugien, T.; Maugey, M.; Poulin, P. Properties of Carbon Nanotube Fibers Spun from DNA-Stabilized Dispersions. *Adv. Funct. Mater.* **2004,** *14* (2), 133-138.

95. Lynam, C.; Moulton, S. E.; Wallace, G. G. Carbon-Nanotube Biofibers. *Adv. Mater.* **2007,** *19* (9), 1244-1248.

96. Jung, D. H.; Kim, B. H.; Ko, Y. K.; Jung, M. S.; Jung, S.; Lee, S. Y.; Jung, H. T. Covalent attachment and hybridization of DNA oligonucleotides on patterned single-walled carbon nanotube films. *Langmuir* **2004,** *20* (20), 8886-8891.

97. Kalbacova, M.; Kalbac, M.; Dunsch, L.; Kataura, H.; Hempel, U. The Study of the Interaction of Human Mesenchymal Stem Cells and Monocytes/Macrophages with Single-Walled Carbon Nanotube Films. *Physica Status Solidi B - Basic Solid State Physics* **2006,** *243* (13), 3514-3518.

98. Akasaka, T.; Yokoyama, A.; Matsuoka, M.; Hashimoto, T.; Abe, S.; Uo, M.; Watari, F. Adhesion of Human Osteoblast-like cells (Saos-2) to Carbon Nanotube Sheets. *Bio-Medical Materials and Engineering* **2009,** *19*, 147-153.

99. Shim, B. S.; Chen, W.; Doty, C.; Xu, C. L.; Kotov, N. A. Smart Electronic Yarns and Wearable Fabrics for Human Biomonitoring Made by Carbon Nanotube Coating with Polyelectrolytes. *Nano Lett.* **2008,** *8* (12), 4151-4157.

100. Edwards, S. L.; Church, J. S.; Werkmeister, J. A.; Ramshaw, J. A. M. Tubular Micro-Scale Multiwalled Carbon Nanotube-Based Scaffolds for Tissue Engineering. *Biomaterials* **2009,** *30* (9), 1725-1731.

101. Jia, G.; Wang, H. F.; Yan, L.; Wang, X. J.; Pei, R. J.; Yan, T.; Zhao, Y. L.; Guo, X. B. Cytotoxicity of Carbon Nanomaterials: Single-Wall Nanotube, Multi-Wall Nanotube, and Fullerene. *Environ. Sci. & Tech.* **2005,** *39* (5), 1378-1383.

102. Bocanegra-Bernal, M. H.; Echeberria, J.; Oilo, J.; Garcia-Reyes, A.; Dominguez-Rios, C.; Reyes-Rojas, A.; Aguilar-Elguezabal, A. A Comparison of the Effects of Multi-Wall and Single-Wall Carbon Nanotube Additions on the Properties of Zirconia Toughened Alumina Composites. *Carbon* **2011,** *49* (5), 1599-1607.

103. Blackburn, J. L.; Barnes, T. M.; Beard, M. C.; Kim, Y. H.; Tenent, R. C.; McDonald, T. J.; To, B.; Coutts, T. J.; Heben, M. J. Transparent conductive single-walled carbon nanotube networks with precisely tunable ratios of semiconducting and metallic nanotubes. *Acs Nano* **2008,** *2* (6), 1266-1274.

104. Yanagi, K.; Udoguchi, H.; Sagitani, S.; Oshima, Y.; Takenobu, T.; Kataura, H.; Ishida, T.; Matsuda, K.; Maniwa, Y. Transport Mechanisms in Metallic and Semiconducting Single-Wall Carbon Nanotube Networks. *Acs Nano* **2010,** *4* (7), 4027-4032.

105. Cambre, S.; Wenseleers, W.; Goovaerts, E.; Resasco, D. E. Determination of the Metallic/Semiconducting Ratio in Bulk Single-Wall Carbon Nanotube Samples by Cobaly Poryphyrin Probe Electron Paramagnetic Resonance Spectroscopy. *Acs Nano* **2010,** *4* (11), 6717-6724.

106. Veedu, V. P.; Askari, D.; Ghasemi-Nejhad, M. N. Chirality Dependence of Carbon Single-Walled Nanotube Material Properties: Axial Young's Modulus. *J. Nanosci. Nanotech.* **2006,** *6* (7), 2159-2166.

107. Qu, G. B.; Bai, Y. Y.; Zhang, Y.; Jia, Q.; Zhang, W. D.; Yan, B. The Effect of Multiwalled Carbon Nanotube Agglomeration on Their Accumulation in and Damage to Organs in Mice. *Carbon* **2009,** *47* (8), 2060-2069.

108. Park, J. G.; Smithyman, J.; Lin, C. Y.; Cooke, A.; Kismarahardja, A. W.; Li, S.; Liang, R.; Brooks, J. S.; Zhang, C.; Wang, B. Effects of Surfactants and Alignment on the Physical Properties of Single-Walled Carbon Nanotube Buckypaper. *J. Appl. Phys.* **2009,** *106* (10), 104310.

109. Behnam, A.; Guo, J.; Ural, A. Effects of Nanotube Alignment and Measurement Direction on Percolation Resistivity in Single-Walled Carbon Nanotube Films. *J. Appl. Phys.* **2007,** *102* (4), 044313.

110. Du, F. M.; Fischer, J. E.; Winey, K. I. Effect of Nanotube Alignment on Percolation Conductivity in Carbon Nanotube/Polymer Composites. *Phys. Rev. B* **2005,** *72* (12), 121404.

111. Wang, Z. L.; Tang, D. W.; Li, X. B.; Zheng, X. H.; Zhang, Z. W.; Zheng, L. X.; Zhu, Y. T.; Jin, A. Z.; Yang, H. F.; Gu, C. Z. Length-Dependent Thermal Conductivity of an Individual Single-Wall Carbon Nantube. *Appl. Phys. Lett.* **2007,** *91* (12), 123119.

112. Rahatekar, S. S.; Koziol, K. K.; Kline, S. R.; Hobbie, E. K.; Gilman, J. W.; Windle, A. H. Length-Dependent Mechanics of Carbon-Nanotube Networks. *Adv.*

Mater. **2009,** *21* (8), 874-878.

113. Tasis, D.; Tagmatarchis, N.; Georgakilas, V.; Prato, M. Soluble Carbon Nanotubes. *Chem. Eur. J.* **2003,** *9*, 4000-4008.

114. Britz, D. A.; Khlobystov, A. N. Noncovalent interactions of molecules with single walled carbon nanotubes. *Chem. Soc. Rev.* **2006,** *35*, 637-759.

115. Pedrosa, V. A.; Paliwal, S.; Balasubramanian, S.; Nepal, D.; Davis, V.; Wild, J.; Ramanculov, E.; Simonian, A. Enhanced stability of enzyme organophosphate hydrolase interfaced on the carbon nanotubes. *Colloids Surf B Biointerfaces* **2010,** *77* (1), 69-74.

116. Kum, M. C.; Joshi, K. A.; Chen, W.; Myung, N. V.; Mulchandani, A. Biomolecules-carbon nanotubes doped conducting polymer nanocomposites and their sensor application. *Talanta* **2007,** *74* (3), 370-5.

117. Asuri, P.; Bale, S. S.; Pangule, R. C.; Shah, D. A.; Kane, R. S.; Dordick, J. S. Structure, function, and stability of enzymes covalently attached to single-walled carbon nanotubes. *Langmuir* **2007,** *23* (24), 12318-21.

118. Tan, Y. Q.; Resasco, D. E. Dispersion of single-walled carbon nanotubes of narrow diameter distribution. *J. Phys. Chem. B* **2005,** *109* (30), 14454-14460.

119. Deheer, W. A.; Bacsa, W. S.; Chatelain, A.; Gerfin, T.; Humphrey-Baker, R.; Forro, L.; Ugarte, D. Aligned carbon nanotube films: production and optical and electronic properties. *Science* **1995,** *268* (5212), 845-7.

120. Bahr, J. L.; Yang, J.; Kosynkin, D. V.; Bronikowski, M. J.; Smalley, R. E.; Tour, J. M. Functionalization of carbon nanotubes by electrochemical reduction of aryl diazonium salts: a bucky paper electrode. *J Am Chem Soc* **2001,** *123* (27), 6536-42.

121. Wu, K.; Fei, J.; Hu, S. Simultaneous determination of dopamine and serotonin on a glassy carbon electrode coated with a film of carbon nanotubes. *Anal Biochem* **2003,** *318* (1), 100-6.

122. Zhuang, Q. K.; Gan, Z. H.; Zhao, Q.; Gu, Z. N. Electrochemical studies of single-wall carbon nanotubes as nanometer-sized activators in enzyme-catalyzed reaction. *Anal Chim Acta* **2004,** *511* (2), 239-247.

123. Li, H.; Wen, H.; Barton, S. C. NADH Oxidation Catalyzed by Electropolymerized Azines on Carbon Nanotube Modified Electrodes. *Electroanalysis* **2011,** *24*, 398-406.

124. Tran, T. O.; Lammert, E. G.; Chen, J.; Merchant, S. A.; Brunski, D. B.; Keay, J. C.; Johnson, M. B.; Glatzhofer, D. T.; Schmidtke, D. W. Incorporation of single-walled carbon nanotubes into ferrocene-modified linear polyethylenimine redox polymer films. *Langmuir* **2011,** *27* (10), 6201-10.

125. Joshi, P. P.; Merchant, S. A.; Wang, Y.; Schmidtke, D. W. Amperometric biosensors based on redox polymer-carbon nanotube-enzyme composites. *Anal Chem* **2005,** *77* (10), 3183-8.

126. Joshi, P. P.; Merchant, S. A.; Wang, Y. D.; Schmidtke, D. W. Amperometric biosensors based on redox polymer-carbon nanotube-enzyme composites. *Anal. Chem.* **2005,** *77* (10), 3183-3188.

127. Merchant, S. A.; Meredith, M. T.; Tran, T. O.; Brunski, D. B.; Johnson, M. B.; Glatzhofer, D. T.; Schmidtke, D. W. Effect of Mediator Spacing on Electrochemical and Enzymatic Response of Ferrocene Redox Polymers. *J. Phys. Chem. C* **2010,** *114*, 11627-11634.

128. Tan, Y. Q.; Resasco, D. E. Dispersion of single-walled carbon nanotubes of narrow diameter distribution. *J Phys Chem B.* **2005,** *109* (30), 14454-60.

129. Green, A. A.; Hersam, M. C. Nearly Single-Chirality Single-Walled Carbon Nanotubes Produced via Orthogonal Iterative Density Gradient Ultracentrifugation. *Adv. Mater.* **2011,** *23*, 5.

130. Blanch, A. J.; Lenehan, C. E.; Quinton, J. S. Optimizing surfactant concentrations for dispersion of single-walled carbon nanotubes in aqueous solution. *J Phys Chem B* **2010,** *114* (30), 9805-11.

131. Katakis, I.; Ye, L.; Heller, A. Electrostatic control of the electron-transfer enabling binding of recombinant glucose oxidase and redox polyelectrolytes. *J. Am. Chem. Soc.* **1994,** *116*, 3617-3618.

132. Marcozzi, G.; Di Domenico, C.; Spreti, N. Effects of surfactants on the stabilization of the bovine lactoperoxidase activity. *Biotechnol Progr* **1998,** *14* (4),

653-656.

133. Cachile, M.; Schneemilch, M.; Hamraoui, A.; Cazabat, A. M. Films driven by surface tension gradients. *Adv Colloid Interface Sci* **2002,** *96* (1-3), 59-74.

134. Degani, Y.; Heller, A. Electrical Communication Between Redox Centers of Glucose Oxidase and Electrodes Via Electrostatically and Covalently Bound Redox Polymers. *J Am Chem Soc* **1989,** *111* (6), 2357-2358.

135. Antiochia, R.; Vinci, G.; Gorton, L. Rapid and direct determination of fructose in food: a new osmium-polymer mediated biosensor. *Food chemistry* **2013,** *140* (4), 742-7.

136. Spricigo, R.; Richter, C.; Leimkuhler, S.; Gorton, L.; Scheller, F. W.; Wollenberger, U. Sulfite biosensor based on osmium redox polymer wired sulfite oxidase. *Colloids and Surfaces A* **2010,** *354* (1-3), 314-319.

137. Niculescu, M.; Frebort, I.; Pec, P.; Galuszka, P.; Mattiasson, B.; Csoregi, E. Amine oxidase based amperometric biosensors for histamine detection. *Electroanal* **2000,** *12* (5), 369-375.

138. Muresan, L.; Valera, R. R.; Frebort, I.; Popescu, I. C.; Csoregi, E.; Nistor, M. Amine oxidase amperometric biosensor coupled to liquid chromatography for biogenic amines determination. *Microchmica Acta* **2008,** *163* (3-4), 219-225.

139. Ishikawa, M.; Schmidtke, D. W.; Raskin, P.; Quinn, C. A. Initial evaluation of a 290-microm diameter subcutaneous glucose sensor: glucose monitoring with a biocompatible, flexible-wire, enzyme-based amperometric microsensor in diabetic and nondiabetic humans. *Journal of diabetes and its complications* **1998,** *12* (6), 295-301.

140. Weinstein, R. L.; Schwartz, S. L.; Brazg, R. L.; Bugler, J. R.; Peyser, T. A.; McGarraugh, G. V. Accuracy of the 5-day FreeStyle Navigator Continuous Glucose Monitoring System: comparison with frequent laboratory reference measurements. *Diabetes care* **2007,** *30* (5), 1125-30.

141. Revzin, A. F.; Sirkar, K.; Simonian, A.; Pishko, M. V. Glucose, lactate, and pyruvate biosensor arrays based on redox polymer/oxidoreductase nanocomposite thin-films deposited on photolithographyically patterned gold microelectrodes. *Sensor Actuat B-Chem* **2002,** *81* (2-3), 359-368.

142. Katakis, I.; Heller, A. L-alpha-glycerophosphate and L-lactate electrodes based on the electrochemical "wiring" of oxidases. *Anal Chem* **1992,** *64* (9), 1008-13.

143. Belay, A.; Collins, A.; Ruzgas, T.; Kissinger, P. T.; Gorton, L.; Csoregi, E. Redox hydrogel based bienzyme electrode for L-glutamate monitoring. *Journal of pharmaceutical and biomedical analysis* **1999,** *19* (1-2), 93-105.

144. Kulagina, N. V.; Shankar, L.; Michael, A. C. Monitoring glutamate and ascorbate in the extracellular space of brain tissue with electrochemical microsensors. *Anal Chem* **1999,** *71* (22), 5093-100.

145. Calvo, E. J.; Danilowicz, C.; Lagier, C. M.; Manrique, J.; Otero, M. Characterization of self-assembled redox polymer and antibody molecules on thiolated gold electrodes. *Biosens Bioelectron* **2004,** *19* (10), 1219-28.

146. Campbell, C. N.; de Lumley-Woodyear, T.; Heller, A. Towards immunoassay in whole blood: separationless sandwich-type electrochemical immunoassay based on in-situ generation of the substrate of the labeling enzyme. *Fres. J Anal. Chem.* **1999,** *364*, 165-169.

147. Lu, B.; Iwuoha, E. I.; Smyth, M. R.; OKennedy, R. Development of an amperometric immunosensor for horseradish peroxidase (HRP) involving a non-diffusional osmium redox polymer co-immobilised with anti-HRP antibody. *Analytical Communications* **1997,** *34*, 21-24.

148. Kavanagh, P.; Leech, D. Redox polymer and probe DNA tethered to gold electrodes for enzyme-amplified amperometric detection of DNA hybridization. *Analytical Chemistry* **2006,** *78* (8), 2710-2716.

149. Chen, T.; Barton, S. C.; Binyamin, G.; Gao, Z.; Zhang, Y.; Kim, H. H.; Heller, A. A miniature biofuel cell. *J Am Chem Soc* **2001,** *123* (35), 8630-1.

150. Hudak, N. S.; Gallaway, J. W.; Barton, S. C. Mediated Biocatalytic Cathodes Operating on Gas-Phase Air and Oxygen in Fuel Cells. *J Electrochem. Soc.* **2009,** *156* (2), B9-B15.

151. MacAodha, D.; P, O. C.; Egan, B.; Kavanagh, P.; Leech, D. Membraneless glucose/oxygen enzymatic fuel cells using redox hydrogel films containing carbon nanotubes. *Chemphyschem : a European journal of chemical physics and physical chemistry* **2013,** *14* (10), 2302-7.

152. Minson, M.; Meredith, M. T.; Shrier, A.; Giroud, F.; Hickey, D.; Glatzhofer, D. T.; Minteer, S. D. High Performance Glucose/O2 Biofuel Cell: Effect of Utilizing Purified Laccase with Anthracene-Modified Multi-Walled Carbon Nanotubes. *J Electrochem. Soc.* **2012,** *159* (12), G166-G170.

153. Mano, N.; Kim, H. H.; Heller, A. On the relationship between the characteristics of bilirubin oxidases and O-2 cathodes based on their "wiring". *Journal of Physical Chemistry B* **2002,** *106* (34), 8842-8848.

154. Gregg, B. A.; Heller, A. Cross-linked redox gels containing glucose oxidase for amperometric biosensor applications. *Anal Chem* **1990,** *62* (3), 258-63.

155. Ye, L.; Hammerle, M.; Olsthoorn, A. J. J.; Schuhmann, W.; Schmidt, H. L.; Duine, J. A.; Heller, A. High Current Density "Wired" Quinoprotein Glucose Dehydrogenase Electrode. *Anal Chem* **1993,** *65*, 238-241.

156. Barton, S. C.; Kim, H. H.; Binyamin, G.; Zhang, Y. C.; Heller, A. Electroreduction of O-2 to water on the "Wired" laccase cathode. *Journal of Physical Chemistry B* **2001,** *105* (47), 11917-11921.

157. Scodeller, P.; Carballo, R.; Szamocki, R.; Levin, L.; Forchiassin, F.; Calvo, E. J. Layer-by-layer self-assembled osmium polymer-mediated laccase oxygen cathodes for biofuel cells: the role of hydrogen peroxide. *J Am Chem Soc* **2010,** *132* (32), 11132-40.

158. Vreeke, M. S.; Yong, K. T.; Heller, A. A Thermostable Hydrogen Peroxide Sensor Based on "Wiring" of Soybean Peroxidase. *Anal Chem* **1995,** *67*, 4247-4249.

159. Narvaez, A.; Suarez, G.; Popescu, I. C.; Katakis, I.; Dominguez, E. Reagentless Biosensors Based on Self-Deposited Redox Polyelectrolyte-Oxidoreductases Architectures. *Biosens Bioelectron* **2000,** *15*, 43-52.

160. Dominguez, E.; Suarez, G.; Narvaez, A. Electrostatic Assemblies of Bioelectrocatalytic and Bioelectronic Applications. *Electroanal* **2006,** *18* (19-20), 1871-1878.

161. Hickey, D. P.; Giroud, F.; Schmidtke, D. W.; Glatzhofer, D. T.; Minteer, S. D. Enzyme Cascade for Catalyzing Sucrose Oxidation in a Biofuel Cell. *ACS Catalysis* **2013,** *3*, 2729-2737.

162. Merchant, S. A.; Tran, T. O.; Meredith, M. T.; Cline, T. C.; Glatzhofer, D. T.; Schmidtke, D. W. High-sensitivity amperometric biosensors based on ferrocene-modified linear poly(ethylenimine). *Langmuir* **2009,** *25* (13), 7736-42.

163. Merchant, S. A.; Meredith, M. T.; Tran, T. O.; Brunski, D. B.; Johnson, M. B.; Glatzhofer, D. T.; Schmidtke, D. W. Effect of Mediator Spacing on Electrochemical and Enzymatic Response of Ferrocene Redox Polymers. *J Phys Chem C* **2010,** *114* (26), 11627-11634.

164. Chen, J.; Tran, T. O.; Ray, M. T.; Brunski, D. B.; Keay, J. C.; Hickey, D.; Johnson, M. B.; Glatzhofer, D. T.; Schmidtke, D. W. Effect of surfactant type and redox polymer type on single-walled carbon nanotube modified electrodes. *Langmuir* **2013,** *29* (33), 10586-95.

165. Katakis, I.; Ye, L.; Heller, A. Electrostatic Control of the Electron Transfer Enabling Binding of Recombinant Glucose Oxidase and Redox Polyelectrolytes. *J Am Chem Soc* **1994,** *116*, 3617-3618.

166. Ameyama, M.; Shinagawa, E.; Matsushita, K.; Adachi, O. Solubilization, Purification and Properties of Membrane-Bound Glycerol Dehydrogenase from Gluconobacter-Industrius. *Agr Biol Chem Tokyo* **1985,** *49* (4), 1001-1010.

167. Prado, F. E.; Sampietro, A. R. A Method for the Determination of Fructose Using a Single Enzyme - Production and Properties of Fructose Dehydrogenase from Gluconobacter-Industrius. *Biotechnology and Applied Biochemistry* **1994,** *19*, 361-368.

168. Weyts, K. F.; Goethals, E. J. Back Titration of Linear Polyethylenimine-Decrease of pH by Addition of Sodium-Hydroxide. *Makromoleculare Chemie-Rapid Communications* **1989,** *10* (6), 299-302.

169. Kokufuta, E.; Suzuki, H.; Yoshida, R.; Yamada, K.; Hirata, M.; Kaneko, F. Role of hydrogen bonding and hydrophobic interaction in the volume collapse of a poly(ethylenimine) gel. *Langmuir* **1998,** *14* (4), 788-795.

170. Merchant, S. A.; Glatzhofer, D. T.; Schmidtke, D. W. Effects of electrolyte and pH on the behavior of cross-linked films of ferrocene-modified poly(ethylenimine). *Langmuir* **2007,** *23* (22), 11295-302.

171. Ikeda, T.; Matsushita, F.; Senda, M. D-Fructose Dehydrogenase-Modified Carbon Paste Electrode Containing Para-Benzoquinone as a Mediated Amperometric

Fructose Sensor. *Agricultural and Biological Chemistry* **1990,** *54* (11), 2919-2924.

172. Kinnear, K. T.; Monbouquette, H. G. An amperometric fructose biosensor based on fructose dehydrogenase immobilized in a membrane mimetic layer on gold. *Anal Chem* **1997,** *69* (9), 1771-1775.

173. Garcia, C. A. B.; de Oliveira Neto, G.; Kubota, L. T.; Grandin, L. A. A new amperometric biosensor for fructose using a carbon paste electrode modified with silica gel coated with Meldola's Blue and fructose 5-dehydrogenase. *J Electroanal Chem* **1996,** *418*, 147-151.

174. Trivedi, U. B.; Lakshminarayana, D.; Kothari, I. L.; Patel, P. B.; Panchal, C. J. Amperometric Fructose Biosensor Based on Fructose Dehydrogenase Enzyme. *Sensor Actuat B-Chem* **2009,** *136* (1), 45-51.

175. Antiochia, R.; Gorton, L. A new osmium-polymer modified screen-printed graphene electrode for fructose detection. *Sensor Actuat B-Chem* **2014,** *195*, 287-293.

176. McEuen, P. L.; Fuhrer, M. S.; Park, H. K. Single-walled carbon nanotube electronics. *Ieee T Nanotechnol* **2002,** *1* (1), 78-85.

177. Zhao, Y. D.; Zhang, W. D.; Chen, H.; Luo, Q. M. Direct electron transfer of glucose oxidase molecules adsorbed onto carbon nanotube powder microelectrode. *Anal Sci* **2002,** *18* (8), 939-941.

178. Kong, J.; Franklin, N. R.; Zhou, C. W.; Chapline, M. G.; Peng, S.; Cho, K. J.; Dai, H. J. Nanotube molecular wires as chemical sensors. *Science* **2000,** *287* (5453), 622-625.

179. Staii, C.; Johnson, A. T. DNA-decorated carbon nanotubes for chemical sensing. *Nano Lett* **2005,** *5* (9), 1774-1778.

180. Shim, M.; Kam, N. W. S.; Chen, R. J.; Li, Y. M.; Dai, H. J. Functionalization of carbon nanotubes for biocompatibility and biomolecular recognition. *Nano Lett* **2002,** *2* (4), 285-288.

181. Besteman, K.; Lee, J. O.; Wiertz, F. G. M.; Heering, H. A.; Dekker, C. Enzyme-coated carbon nanotubes as single-molecule biosensors. *Nano Lett* **2003,** *3* (6), 727-730.

182. Nguyen, C. V.; Delzeit, L.; Cassell, A. M.; Li, J.; Han, J.; Meyyappan, M. Preparation of nucleic acid functionalized carbon nanotube Arrays. *Nano Lett* **2002,** *2* (10), 1079-1081.

183. Barisci, J. N.; Tahhan, M.; Wallace, G. G.; Badaire, S.; Vaugien, T.; Maugey, M.; Poulin, P. Properties of carbon nanotube fibers spun from DNA-stabilized dispersions. *Adv Funct Mater* **2004,** *14* (2), 133-138.

184. Shim, B. S.; Chen, W.; Doty, C.; Xu, C. L.; Kotov, N. A. Smart Electronic Yarns and Wearable Fabrics for Human Biomonitoring made by Carbon Nanotube Coating with Polyelectrolytes. *Nano Lett* **2008,** *8* (12), 4151-4157.

185. Zhao, P.; Wang, P. J.; Zhang, Z.; Fang, C. F.; Wang, Y. M.; Zhai, Y. X.; Liu, D. S. Electronic transport properties of a diarylethene-based molecular switch with single-walled carbon nanotube electrodes: The effect of chirality. *Solid State Commun* **2009,** *149* (23-24), 928-931.

186. Meredith, M. T.; Hickey, D. P.; Redemann, J. P.; Schmidtke, D. W.; Glatzhofer, D. T. Effects of ferrocene methylation on ferrocene-modified linear poly(ethylenimine) bioanodes. *Electrochim Acta* **2013,** *92*, 226-235.

187. HICKEY, D. P. FERROCENE-MODIFIED LINEAR POLY(ETHYLENIMINE) BIOELECTRODE MATERIALS FOR USE IN GLUCOSE/O2 BIOFUEL CELLS. Ph.D, UNIVERSITY OF OKLAHOMA2014.

188. Chen, R. S.; Xiao, H.; Huang, W. H.; Tong, H.; Wang, Z. L.; Cheng, J. K. High sensitive carbon fiber nanoelectrodes modified by single-walled carbon nanotubes. *Chem J Chinese U* **2003,** *24* (5), 808-810.

189. Wang, L.; Yuan, Z. B. Direct electrochemistry of glucose oxidase at a gold electrode modified with single-wall carbon nanotubes. *Sensors* **2003,** *3* (12), 544-554.

190. Huang, Y. X.; Zhang, W. J.; Xiao, H.; Li, G. X. An electrochemical investigation of glucose oxidase at a CdS nanoparticles modified electrode. *Biosens Bioelectron* **2005,** *21* (5), 817-821.

191. Wang, H. C.; Wang, X. S.; Zhang, X. Q.; Qin, X.; Zhao, Z. X.; Miao, Z. Y.; Huang, N.; Chen, Q. A novel glucose biosensor based on the immobilization of glucose oxidase onto gold nanoparticles-modified Pb nanowires. *Biosens Bioelectron* **2009,** *25* (1), 142-146.

192. Tsai, Y. C.; Li, S. C.; Chen, J. M. Cast thin film biosensor design based on a nafion backbone, a multiwalled carbon nanotube conduit, and a glucose oxidase function. *Langmuir* **2005,** *21* (8), 3653-3658.

193. Swoboda, B. E.; Massey, V. Purification and Properties of the Glucose Oxidase from Aspergillus Niger. *J Biol Chem* **1965,** *240*, 2209-15.

194. Asuri, P.; Karajanagi, S. S.; Yang, H. C.; Yim, T. J.; Kane, R. S.; Dordick, J. S. Increasing protein stability through control of the nanoscale environment. *Langmuir* **2006,** *22* (13), 5833-5836.

195. Kim, J. B.; Grate, J. W.; Wang, P. Nanobiocatalysis and its potential applications. *Trends Biotechnol* **2008,** *26* (11), 639-646.

196. Addo, P. K.; Arechederra, R. L.; Minteer, S. D. Evaluating Enzyme Cascades for Methanol/Air Biofuel Cells Based on NAD(+)-Dependent Enzymes. *Electroanal* **2010,** *22* (7-8), 807-812.

197. Wang, S. C.; Yang, F.; Silva, M.; Zarow, A.; Wang, Y. B.; Iqbal, Z. Membrane-less and mediator-free enzymatic biofuel cell using carbon nanotube/porous silicon electrodes. *Electrochem Commun* **2009,** *11* (1), 34-37.

198. Luo, H. X.; Shi, Z. J.; Li, N. Q.; Gu, Z. N.; Zhuang, Q. K. Investigation of the electrochemical and electrocatalytic behavior of single-wall carbon nanotube film on a glassy carbon electrode. *Anal Chem* **2001,** *73* (5), 915-920.

199. Wang, J. X.; Li, M. X.; Shi, Z. J.; Li, N. Q.; Gu, Z. N. Direct electrochemistry of cytochrome c at a glassy carbon electrode modified with single-wall carbon nanotubes. *Anal Chem* **2002,** *74* (9), 1993-1997.

200. Ye, J. S.; Wen, Y.; Zhang, W. D.; Cui, H. F.; Xu, G. Q.; Sheu, F. S. Electrochemical biosensing platforms using phthalocyanine-functionalized carbon nanotube electrode. *Electroanal* **2005,** *17* (1), 89-96.

201. Yang, H. P.; Zhu, Y. F.; Chen, D. C.; Li, C. H.; Chen, S. G.; Ge, Z. C. Electrochemical biosensing platforms using poly-cyclodextrin and carbon nanotube composite. *Biosens Bioelectron* **2010,** *26* (1), 295-298.

202. Gao, F.; Viry, L.; Maugey, M.; Poulin, P.; Mano, N. Engineering hybrid nanotube wires for high-power biofuel cells. *Nat Commun* **2010,** *1*.

203. Mano, N.; Mao, F.; Heller, A. Characteristics of a miniature compartment-less glucose-O-2 biofuel cell and its operation in a living plant. *J Am Chem Soc* **2003,** *125* (21), 6588-6594.

204. Willner, I.; Baron, R.; Willner, B. Integrated nanoparticle-biomolecule systems for biosensing and bioelectronics. *Biosens Bioelectron* **2007,** *22* (9-10), 1841-1852.

205. Katz, E.; Willner, I. Biomolecule-functionalized carbon nanotubes: Applications in nanobioelectronics. *Chemphyschem* **2004,** *5* (8), 1085-1104.

206. Akers, N. L.; Moore, C. M.; Minteer, S. D. Development of alcohol/O-2 biofuel cells using salt-extracted tetrabutylammonium bromide/Nafion membranes to immobilize dehydrogenase enzymes. *Electrochim Acta* **2005,** *50* (12), 2521-2525.

207. Mano, N.; Heller, A. A miniature membraneless biofuel cell operating at 0.36 V under physiological conditions. *J Electrochem Soc* **2003,** *150* (8), A1136-A1138.

208. Riklin, A.; Katz, E.; Willner, I.; Stocker, A.; Buckmann, A. F. Improving Enzyme-Electrode Contacts by Redox Modification of Cofactors. *Nature* **1995,** *376* (6542), 672-675.

209. Zayats, M.; Willner, B.; Willner, I. Design of amperometric biosensors and biofuel cells by the reconstitution of electrically contacted enzyme electrodes. *Electroanal* **2008,** *20* (6), 583-601.

210. Willner, B.; Katz, E.; Willner, I. Electrical contacting of redox proteins by nanotechnological means. *Curr Opin Biotech* **2006,** *17* (6), 589-596.

211. Tang, H.; Yan, F.; Lin, P.; Xu, J. B.; Chan, H. L. W. Highly Sensitive Glucose Biosensors Based on Organic Electrochemical Transistors Using Platinum Gate Electrodes Modified with Enzyme and Nanomaterials. *Adv Funct Mater* **2011,** *21* (12), 2264-2272.

212. Ajayan, P. M.; Iijima, S. Capillarity-Induced Filling of Carbon Nanotubes. *Nature* **1993,** *361* (6410), 333-334.

213. Britto, P. J.; Santhanam, K. S. V.; Ajayan, P. M. Carbon nanotube electrode for oxidation of dopamine. *Bioelectroch Bioener* **1996,** *41* (1), 121-125.

214. Yang, J. A.; Zhang, W. D.; Gunasekaran, S. An amperometric non-enzymatic glucose sensor by electrodepositing copper nanocubes onto vertically well-aligned multi-walled carbon nanotube arrays. *Biosens Bioelectron* **2010,** *26* (1), 279-284.

215. Villarrubia, C. W. N.; Rincon, R. A.; Radhakrishnan, V. K.; Davis, V.; Atanassov, P. Methylene Green Electrodeposited on SWNTs-Based "Bucky" Papers for NADH and L-Malate Oxidation. *Acs Appl Mater Inter* **2011,** *3* (7), 2402-2409.

216. Kwon, C. H.; Lee, S. H.; Choi, Y. B.; Lee, J. A.; Kim, S. H.; Kim, H. H.; Spinks, G. M.; Wallace, G. G.; Lima, M. D.; Kozlov, M. E.; Baughman, R. H.; Kim, S. J. High-power biofuel cell textiles from woven biscrolled carbon nanotube yarns. *Nat Commun* **2014,** *5*.

217. Merchant, S. A.; Tran, T. O.; Meredith, M. T.; Cline, T. C.; Glatzhofer, D. T.; Schmidtke, D. W. High-Sensitivity Amperometric Biosensors Based on Ferrocene-Modified Linear Poly(ethylenimine). *Langmuir* **2009,** *25* (13), 7736-7742.

218. Hudak, N. S.; Gallaway, J. W.; Barton, S. C. Mediated Biocatalytic Cathodes Operating on Gas-Phase Air and Oxygen in Fuel Cells. *J Electrochem Soc* **2009,** *156* (1), B9-B15.

219. Gellett, W.; Schumacher, J.; Kesmez, M.; Le, D.; Minteer, S. D. High Current Density Air-Breathing Laccase Biocathode. *J Electrochem Soc* **2010,** *157* (4), B557-B562.

220. Kim, B. C.; Zhao, X. Y.; Ahn, H. K.; Kim, J. H.; Lee, H. J.; Kim, K. W.; Nair, S.; Hsiao, E.; Jia, H. F.; Oh, M. K.; Sang, B. I.; Kim, B. S.; Kim, S. H.; Kwon, Y.; Ha, S.; Gu, M. B.; Wang, P.; Kim, J. Highly stable enzyme precipitate coatings and their electrochemical applications. *Biosens Bioelectron* **2011,** *26* (5), 1980-1986.

221. Biercuk, M. J.; Llaguno, M. C.; Radosavljevic, M.; Hyun, J. K.; Johnson, A. T.; Fischer, J. E. Carbon nanotube composites for thermal management. *Appl Phys Lett* **2002,** *80* (15), 2767-2769.

APPENDIX A: Estimation of the proportion of surface area of MWCNTs electrochemically accessible

A.1 Estimation of electrochemical area of MWCNTs array by cyclic voltammetry

Randles-Sevcik equation:

$$i_p = 0.4463 * n * F * A * C(n * F * \upsilon * \frac{D}{R * T})^{1/2}$$

At room temperature:

$$i_p = 268600 * n^{3/2} * A * D^{1/2} C \upsilon^{1/2}$$

Where i_P is peak current, n is the number of electrons appearing in the half-reaction of the redox couple, which is equal to 1 in this case, υ is the scan rate, which is equal to 0.001 v/s in this case; F is Faraday's constant (96485 C/mol), A is the area of electrode area (cm^2), C is the concentration for the redox couple, which is equal to 0.97 $*10^{-6}$ mol/cm^3, R is the universal gas constant (8.314 J/(mol·K)), D is the analyte's diffusion coefficient for potassium ferrocyanide in dilute aqueous solution at 298.15K ($1.2*10^{-5}$ cm^2/s).

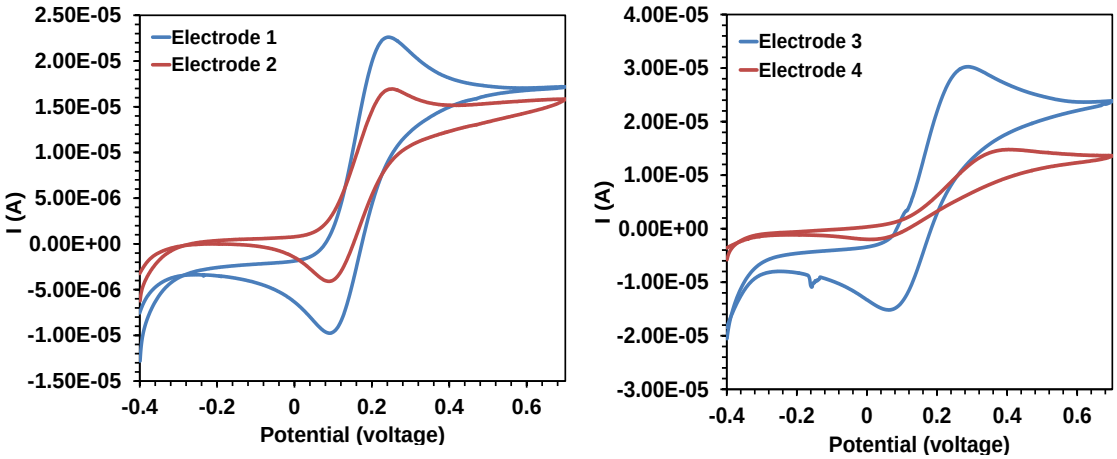


Figure A-1 CV curves of burned MWCNTs array electrodes without redox polymer hydrogel film in aqueous solution with 0.97 mM $[K_4Fe(CN)_6]\bullet 3H_2O$ and 50.94 mM NaCl.

$$i_p = 268600 * n^{3/2} * A * D^{1/2} C \upsilon^{1/2}$$

Parameters:

n=1; $D=1.2*10^{-5}$ cm^2/s; $C=0.97*10^{-6}$ mol/cm^3; υ=0.001 v/s

$$A_1 = \frac{i_p}{268600 * n^{3/2} * D^{1/2} * C * \upsilon^{1/2}} = \frac{2.3044 * 10^{-5}}{268600 * 1 * \sqrt{1.2 * 10^{-5}} * 0.97 * 10^{-6} * \sqrt{0.001}} = 0.807 \text{cm}^2$$

$$A_2 = \frac{i_p}{268600 * n^{3/2} * D^{1/2} * C * \upsilon^{1/2}} = \frac{1.4974 * 10^{-5}}{268600 * 1 * \sqrt{1.2 * 10^{-5}} * 0.97 * 10^{-6} * \sqrt{0.001}} = 0.524 cm^2$$

$$A_3 = \frac{i_p}{268600 * n^{3/2} * D^{1/2} * C * \upsilon^{1/2}} = \frac{2.648 * 10^{-5}}{268600 * 1 * \sqrt{1.2 * 10^{-5}} * 0.97 * 10^{-6} * \sqrt{0.001}} = 0.927 \text{cm}^2$$

$$A_4 = \frac{i_p}{268600 * n^{3/2} * D^{1/2} * C * \upsilon^{1/2}} = \frac{1.04 * 10^{-5}}{268600 * 1 * \sqrt{1.2 * 10^{-5}} * 0.97 * 10^{-6} * \sqrt{0.001}} = 0.364 cm^2$$

Table A.1 Estimation of electrochemical surface area of MWCNTs array electrode by cyclic voltammetry or measurement

Electrode	i_p (μA)	Calculated (cm^2)	measured(cm^2)
Electrode 1	23.044	0.807	0.662
Electrode 2	14.974	0.524	0.47
Electrode 3	26.48	0.927	0.457
Electrode 4	10.40	0.364	0.673
Average		0.6555	0.5655

A.2 Calculation of theoretical surface area of MWCNTs array

Diameter of MWCNTs: 30 nm

Height of MWCNTs forest: 20 um

Surface area of one nanotube:

$$S_{one} = \pi dl = 3.14 \times 30 \times 10^{-9} \times 20 \times 10^{-6} m^2 = 1884 \times 10^{-15} m^2 = 1.884 \times 10^{-12} m^2 = 1.884 \times 10^{-8} cm^2$$

Cross-section area of one nanotube:

$$A_{one} = \frac{\pi d^2}{4} = \frac{3.14 \times (3 \times 10^{-8})^2}{4} = 7.065 \times 10^{-16} m^2 = 7.065 \times 10^{-12} cm^2$$

Weight of nanotube per cm^2 of substrate: 1 mg/cm^2

The apparent density of MWCNTs array per square centimeter of substrate:

$$\rho_1 = \frac{m}{v_{apparent}} = \frac{1 \times 10^{-3} g}{1 cm^2 \times h} = \frac{1 \times 10^{-3} g}{1 cm^2 \times 20 \times 10^{-4} cm} = 0.5 g / cm^3$$

The real density of MWCNTs array per square centimeter of substrate:

$$\rho_2 = \frac{m}{v} = \frac{m}{n \times \left[\pi (\frac{d}{2})^2 h \right]} = \frac{m}{n \times A_{one} h} = \frac{1 \times 10^{-3} g}{n \times 7.065 \times 10^{-12} cm^2 \times 20 \times 10^{-4} cm} = 7.077 \times 10^{10} \Big/ n \; g / cm^3$$

Where n is the total number of MWCNTs on one cm^2 silicon substrate

According to references[221], the real density of MWCNTs per square centimeter of substrate was 1.8 g/cm^2.

$$\rho_2 = \frac{m}{v} = \frac{m}{n \times \pi(\frac{d}{2})^2 h} = \frac{m}{n \times A_{one} h} = \frac{1 \times 10^{-3} g}{n \times 7.065 \times 10^{-12} cm^2 \times 20 \times 10^{-4} cm} = 7.077 \times 10^{10} / n \; g/cm^3 = 1.8 g/cm^3$$

The total number of MWCNTs on one cm^2 silicon substrate is estimated to:

$n=3.932\times10^{10}\ g/cm^3$

$$\frac{\rho_1}{\rho_2} = \frac{\frac{m}{1cm^2 \times h}}{\frac{m}{n \times \pi(\frac{d}{2})^2 h}} = \frac{n \times \pi(\frac{d}{2})^2 h}{1cm^2 \times h} = \frac{n \times \pi(\frac{d}{2})^2}{1cm^2} = \frac{0.5}{1.8} = 0.2778$$

$$n = 0.2778 \times \frac{4}{\pi d^2} = 0.2778 \times \frac{4}{3.14 \times (30 \times 10^{-7})^2} = 0.2778 \times \frac{4}{3.14 \times (3 \times 10^{-6})^2}$$

$$= 0.0393 \times 10^{12} = 3.93 \times 10^{10}$$

The total surface area of MWCNTs on one square centimeter silicon substrate is:

$$S_{total} = n\pi dl = 3.93 \times 10^{10} \times 1.884 \times 10^{-8} cm^2 = 7.404 \times 10^2 cm^2 = 740.4 cm^2$$

There the total surface area of MWCNTs array on Si substrate in the experiment is :

Table A.2 Estimation of the ratio of electrochemical surface area to theoretical surface area

Electrode	Electrochemical effective surface area calculated (cm^2)	Theoretical effective Surface area (cm^2)	Ratio of electrochemical surface area to theoretical surface area
Electrode 1	0.807	490.14	0.165%
Electrode 2	0.524	347.99	0.151%
Electrode 3	0.927	338.37	0.27%
Electrode 4	0.364	499.23	0.073%
Average			0.165%